AN ABSTRACT OF THE THESIS OF

Huan Lin for the degree of Doctor of Philosophy in Civil Engineering presented on December 2, 1994. Title: Stochastic Analysis of a Nonlinear Ocean Structural System.

Redacted for Privacy

Abstract approved: _____

Solomon C.S. Yim

Stochastic analysis procedures have been recently applied to analyze nonlinear dynamical systems. In this study, nonlinear responses, stochastic and/or chaotic, are examined and interpreted from a probabilistic perspective. A multi-point-moored ocean structural system under regular and irregular wave excitations is analytically examined via a generalized stochastic Melnikov function and Markov process approach. Time domain simulations and associated experimental observations are employed to assist in the interpretation of the analytical predictions.

Taking into account the presence of random noise, a generalized stochastic Melnikov function associated with the corresponding averaged system, where a homoclinic connection exists near the primary resonance, is derived. The effects of random noise on the boundary of regions of possible existence of chaotic response is demonstrated via a mean-squared Melnikov criterion.

The random wave field is approximated as random perturbations on regular and nearly regular (with very narrow-band spectrum) waves by adding a white noise component, or using a filtered white noise process to fit the JONSWAP spectrum. A Markov process approach is then applied explicitly to analyze the response.

The evolution of the probability density function (PDF) of nonlinear stochastic response under the Markov process approach is characterized by a deterministic partial differential equation called the Fokker-Planck equation, which in this study is solved by a path integral solution procedure. Numerical evaluation of the path integral solution is based on path sum, and the short-time propagator is discretized accordingly. Short-time propagation is performed by using a fourth order Runge-Kutta scheme to calculate the most probable (i.e. mean) position in the phase space and to establish the fact that discrete contributions to the random response are locally Gaussian. Transient and steady-state PDF's can be obtained by repeat application of the short-time propagation.

Based on depictions of the joint probability density functions and time domain simulations, it is observed that the presence of random noise may expedite the occurrence of "noisy" chaotic response. The noise intensity governs the transition among various types of stochastic nonlinear responses and the relative strengths of coexisting response attractors. Experimental observations confirm the general behavior depicted by the analytical predictions.

STOCHASTIC ANALYSIS OF A NONLINEAR OCEAN STRUCTURAL SYSTEM

by

Huan Lin

A THESIS

submitted to

Oregon State University

in partial fulfillment of
the requirements for the
degree of

Doctor of Philosophy

Completed December 2, 1994
Commencement June 1995

Doctor of Philosophy thesis of Huan Lin presented on December 2, 1994

APPROVED:

Redacted for Privacy

Major Professor, representing Civil Engineering

Redacted for Privacy

Head of Department of Civil Engineering

Redacted for Privacy

Dean of Graduate School

I understand that my thesis will become part of the permanent collection of Oregon State University libraries. My signature below authorizes release of my thesis to any reader upon request

Redacted for Privacy

Huan Lin, Author

ACKNOWLEDGEMENT

Gratitude is expressed toward my thesis major advisor Prof. Solomon C.S. Yim, for his guidance and assistance on my graduate study at Oregon State University.

Appreciation is also given to other members of my committee: Prof. Robert M. Burton, Prof. John W. Leonard, Prof. Ron B. Guenther, Prof. Alan G. Hernried, Prof. Charles E. Smith, and Prof. Timothy C. Kennedy, for their interest and support.

Thanks are also extended to the staff, faculty and fellow students of the Ocean Engineering program at Oregon State University.

The financial support on this work from United States Office of Naval Research (Grant No. N00014-92-J-1221).

I would like to express my deepest gratitude toward my God for His faithfulness and blessings, to my mother Show-Jing for her continuous support, and to my wife Irene for her love and patience.

TABLE OF CONTENTS

TABLE OF CONTENTS (continued)

TABLE OF CONTENTS (continued)

LIST OF FIGURES

LIST OF FIGURES (continued)

LIST OF FIGURES (continued)

STOCHASTIC ANALYSIS OF A NONLINEAR OCEAN STRUCTURAL SYSTEM

1. INTRODUCTION

Complex responses including chaos of nonlinear deterministic compliant offshore structures have been demonstrated by many recent investigations (e.g. Thompson, 1983; Papoulias and Bernitsas, 1988; Sharma et al., 1988; Bishop and Virgin, 1988; Bernitsas and Chung, 1990; Gottlieb, 1991). Nonlinearities of these models includes restoring force (induced by geometry or discontinuity) and coupled hydrodynamic effects induced by quadratic fluid-structure interaction viscous drag. These fluid-structure models are often considered as single- or multi-degree-of-freedom (SDOF or MDOF) nonlinear dissipative dynamical systems (Gottlieb, 1991). The system response behavior may become further complicated when coupled nonlinear convective parametric excitation is significant.

The richness of the deterministic nonlinear moored structural response has been demonstrated analytically and numerically via period doubling cascade and the (co-) existence of harmonic, sub-harmonic and super-harmonic responses (Gottlieb, 1991). The underlying superstructure of these responses facilitates numerical search of quasi-periodic, and chaotic responses (Gottlieb and Yim, 1992). Under the same system parameters with different initial conditions, coexisting (and competing) nonlinear moored structural responses have been found near resonances where local bifurcations occur. The cascade of local bifurcations (and in some cases sudden explosions) often leads to chaotic responses (Gottlieb, 1991). These chaotic responses, which seem highly irregular and show no repetition in their time histories, possess a complex attractor structure and

are sensitive to initial conditions. The complexity and unpredictability of these nonlinear responses, if confirmed in field situations, need to be incorporated in future structural design.

The sensitivity and unpredictability of the deterministic chaotic response in dissipative nonlinear dynamical systems have been investigated theoretically and observed experimentally (Thompson and Stewart, 1986; Moon, 1987). From a structural engineer's point of view, this irregular (chaotic) motion may impede critical operations and induce structural instability. Chaotic response can be identified by modern quantitative measures such as Lyapunov exponents (Wolf *et al.*, 1985) and fractal (Farmer *et al.*, 1983; Grassberger and Procaccia, 1983) or multi-fractal (Feder, 1989) dimensions. Local stability analysis (local bifurcation) of a deterministic nonlinear system has been carried out by applying approximate perturbation techniques such as averaging (Sander and Verhulst, 1985), harmonic balance (Hayashi, 1964) and multiple-scales (Nayfeh, 1973). Global stability analysis can be conducted by employing the Melnikov function (Melnikov, 1963), which measures the distance between the stable and unstable manifolds in a system exhibiting homoclinicity or heteroclinicity (Guckenheimer and Holmes, 1983; Wiggins, 1988, 1990). Chaotic response (Smale horseshoe type) may be observed in regions where the stable and unstable manifolds intersect transversely.

Different moored structural models have been derived to isolate the effects of each nonlinear term (restoring, drag and convective parametric excitation) on the response behavior (Gottlieb and Yim, 1992, 1993). For example, under small amplitude motion

assumption, the nonlinear hydrodynamic exciting force is simplified (Thompson *et al.*, 1984; Virgin, 1987; Bishop and Virgin, 1988; Witz *et al.*, 1989; Choi and Lou, 1991) so that the effects of nonlinear restoring force on moored structural response can be analyzed. By the same token, the nonlinear hydrodynamic effects can be emphasized by linearizing the restoring force.

All the analysis techniques introduced above have been employed to analyze the moored structural system under (deterministic) periodic excitations (Gottlieb, 1991). However, ocean field environment including wind, waves and current often contain a significant random (noise) component. Thus the nonlinear response of a compliant offshore structure should be examined from a stochastic perspective. The presence of random noise adds another degree of coupling of excitation and structural response and necessitates a stochastic analysis of the perturbed nonlinear responses.

Nonlinear (possibly chaotic) stochastic behavior may be important for safety and reliability analysis of structures. Thus an important goal for studying noisy nonlinear response is to incorporate this irregular response into structure design. In the deterministic case, criteria for occurrence of chaotic response in simple nonlinear systems have been developed. In the stochastic case, probabilistic properties of random (no deterministic driving component) system response, both linear and nonlinear, can be analyzed. However, the gap between purely deterministic chaotic response and purely random response needs to be bridged. Thus, an immediate goal of this study is to investigate the structural response, even for the designed deterministic system, from a

stochastic perspective to gain a better understanding of the characteristics of the behavior of noisy chaotic response.

The moored structural system subjected to monochromatic regular waves with random noise perturbation will be used to demonstrate the characteristics of noisy chaos which may provide a link between deterministic and random dynamics. The structural response in more appropriate environmental models, e.g., JONSWAP random waves, will be examined. Experimental results will be also employed to qualitatively confirm the analytical predictions. Some recent developments in characterizing the relationship between deterministic and stochastic nonlinear (possible chaotic) dynamics are particularly useful in providing a basic understanding of the noise effects.

1.1 Literature Review

Analytical, numerical and experimental investigations of the deterministic (possible chaotic) response of nonlinear systems have been conducted in both engineering and science fields (e.g., Nayfeh and Mook, 1979; Ruelle, 1980; Thompson and Stewart, 1986; Moon, 1987). Standard perturbation techniques including averaging, harmonic balance and multiple scales have been employed to predict the loss of response stability and bifurcations. Through a bifurcation cascade, the nonlinear system may exhibit chaotic response.

Modern topological techniques, e.g. Melnikov function, have been developed to predict the possible occurrence of chaotic responses in periodically driven deterministic nonlinear low-degree-of-freedom systems (Guckenheimer and Holmes, 1983; Wiggins,

1988 and 1990). The Melnikov function measures the distance between stable and unstable manifolds through a first-order approximation. The lower boundary for a possible chaotic domain in the parameter space can be derived, when stable and unstable manifolds intersect transversely (the Melnikov function equals zero).

Identification of chaotic responses in practical engineering systems has been investigated recently. Examples include rocking block system (Wang and Tso, 1989; Hogan, 1989; Yim and Lin, 1991a,b) and compliant mooring system (Thompson and Stewart, 1986; Gottlieb and Yim, 1992 and 1993) among others. The characteristics of chaotic response were examined via techniques such as Poincaré map, phase plane, Lyapunov exponent, and spectral density. The Poincaré map can exhibit the embedded fractal structure of chaotic response by sampling at integer multiples of the forcing period (Thompson and Stewart, 1986; Moon, 1987). The phase plane can demonstrate the sub-space where the chaotic response resides and the non-repetition in the response trajectory (Moon, 1987). By estimating the averaged divergence rate of a perturbed response trajectory, the Lyapunov exponent can be computed. The Lyapunov exponent quantitatively measures the sensitivity of response to perturbations and a positive exponent indicate the existence of chaos (Wolf *et al.*, 1985). In the frequency domain, a chaotic response is characterized by a broad-band spectrum (Moon, 1987).

Examples of applying deterministic chaos theories to stability analysis of engineering systems have been carried out by Thompson *et al.* (1990) and Falzarano *et al.* (1991) on ship roll motion. Thompson *et al.* (1990) generated invariant manifolds and simulated roll responses with various initial conditions in a fine grid phase space.

Detailed pictures of the basin boundaries between bounded and escaping (divergent and hence capsize) motions were constructed. Numerical results illustrated the manner in which systems that are inherently safe when unforced become unsafe as periodic excitation is applied. Falzarano *et al.* also generated the invariant manifolds and employed the concept of lobe dynamics, which reflects the transport of dynamics in the phase space, to demonstrate the mechanism of "unexpected capsizing".

For systems under pure stochastic excitations, systematic analysis techniques in the frequency domain are well established for the analysis of linear systems (Lin, 1967; Ochi, 1990; Roberts and Spanos, 1990). However, when the system is nonlinear, linear analysis techniques can no longer apply and specific (and often ad hoc) methods are developed to analyze its response behavior. Among these methods are equivalent linearization (Lyon, 1960; Crandall, 1962, 1964), time domain simulations (Bathe and Wilson, 1976), and Markov process approach (Fokker-Planck equation) (Fuller, 1970; Risken, 1984; Gardiner, 1985).

The stochastic linearization technique reduces a weakly nonlinear system to a linear system by approximating the nonlinear component with an equivalent linear counterpart. The constant coefficients of the linear terms are determined by minimizing the errors of the approximation with respect to a certain error norm in a stochastic sense (e.g., minimum square value). In this manner, linear analysis techniques can be applied to the linearized system to estimate stochastic properties of the response. However, the nonlinear nature of the system behavior is lost.

Time domain simulations can be implemented by numerically integrating the nonlinear governing equation with respect to time. A large number of sample response realizations is necessary to derive the response statistics (Rubinstein, 1981). There are no limitations on the nonlinearity of the system for the application of this technique. However, due to the large number of sample responses required, application of this technique is often computationally involved and time-consuming.

The Markov process approach can be applied to nonlinear systems with excitations modeled as white noise or filtered white noise. The conditional PDF of the system behavior is determined by the knowledge of the most recent condition (Gardiner, 1985). The PDF of the system response can be represented by a statistically equivalent deterministic partial differential equation called the Fokker-Planck equation (FPE). The degree of nonlinearity in the system is not limited by this approach, however, no closed-form solution is available in general.

Using the above stochastic nonlinear analysis techniques, characteristics of the responses and some highly nonlinear phenomena of noise-driven nonlinear dynamical systems have been investigated. Early work about the noise effect on the bifurcation phenomenon was carried out by Crutchfield *et al.* (1982), who examined the noise effect on period doubling of a discrete system. The noise was found to introduce a scaling behavior at the chaotic threshold, in the critical Lyapunov exponent. Similar work was carried out by Svensmark and Samuelson (1987) on the Josephson junction. They found that, in the presence of noise, the bifurcation points are shifted by an amount proportional to the square of the perturbation amplitude. Recent work by Wiesenfeld and

McNamara (1985, 1986) demonstrated that the amplification of a small resonant periodic perturbation in the presence of noise, near the periodic doubling threshold. The role of bridging different basins of attraction was numerically demonstrated by Arecchi *et al.* (1985). Meunier and Verga (1988) investigated the behavior of a first order nonlinear system driven by Gaussian white noise. The FPE was derived and solved for the stationary PDF as an invariant measure. Through this probabilistic representation, they observed a shift and broadening of the region of the bifurcation transition. They concluded that in noisy systems topological concepts become less useful and the bifurcation phenomenon should be delineated by a probabilistic representation. Just (1989) performed a Gaussian approximation to the noisy response distribution and quantitatively showed the shift of the bifurcation point in a mean sense.

The phenomenon of stochastic resonance was discussed by Nicolis *et al.* (1993). They suggested that chaotic dynamical systems characterized by intermittent jumps between two preferred regions of the phase space display an enhanced sensitivity to weak periodic forcings through a stochastic-like mechanism. The residence time in each region was studied numerically to carry out the intermittent behavior. Similar work was carried out by Anishchenko *et al.* (1993).

To examine the effects of various weak noise perturbations (finite-mean and zero-mean) on the existence of chaotic responses, two possible stochastic extensions of the corresponding deterministic Melnikov function have been carried out by Bulsara *et al.* (1990) and Frey and Simiu (1992). Bulsara *et al.* (1990) introduced a generalized Melnikov function to take into account the presence of finite-mean noise. The noise is

embedded to form a pair of noisy homoclinic orbits, and they inferred that, on the average, the threshold for the chaos is elevated by the presence of finite-mean noise. In a parallel investigation, Frey and Simiu (1992) adopted Shinozuka's zero-mean and banded-limited noise as perturbation to the homoclinic orbits. By applying the concept of average flux, which measures the phase space transport for possible jumps (Wiggins, 1990), the strength of the chaotic attractor and the frequency of jumps can be examined. They concluded that the presence of weak zero-mean noise can not suppress chaotic motion.

Results of computer experiments on deterministic chaotic systems have suggested a wealth of phenomena of nonlinear system behaviors. Interdependence between the deterministic and stochastic properties of these systems including the existence of invariant measures and densities, statistical stability and periodicity, the influence of stochastic perturbations, and the formation of attractors have been observed. Thus, concepts from stochastic processes and ergodic theory can be applied to chaotic systems.

To gain a good understanding of the relationships between deterministic and stochastic systems, knowledge of advanced mathematical theory is required (Lasota and Mackey, 1994). While the Markov operator is an efficient tool in studying the evolution and asymptotic behavior of densities of stochastic systems, its deterministic restriction, the Frobenius-Perron operator, is useful in studying the evolution of densities under the operation of deterministic systems. Most concepts concerning the asymptotic behavior of densities are equally well formulated for both deterministic and stochastic systems. Many results for the Frobenius-Perron operator concerning the behavior evolving under

the influence of deterministic systems are special cases of the general results for the Markov operator corresponding to stochastic systems. There are three levels of irregular behavior a deterministic (measure-preserving) transformation can achieve -- ergodicity, mixing, and exactness. The Frobenius-Perron operator can be used to discern these behaviors in a nonlinear system. Preservation of an initial measure by a nonlinear transformation corresponds to the fact that the constant density is a stationary density of the Frobenius-Perron operator. Ergodicity requires that the constant density is the unique stationary density of the Frobenius operator, while mixing and exactness correspond to two different kinds of stability of the stationary density.

In the presence of random noise, the response of a nonlinear system can be described by a system of stochastic differential equations. The response behavior can be examined via the evolution of the density governed by the FPE. Solutions of the FPE is equivalent to a flow of densities governed by a semi-group of Markov operators. Under certain smoothness conditions, when the stochastic perturbation in the excitation reduces to zero, the FPE reduces to the Liouville equation and the semi-group of Markov operators reduces to the semi-group of Frobenius-Perron operators. Thus, deterministic properties can be obtained as the special cases of stochastic results.

Examples of deterministic chaotic response exhibiting definitive stochastic properties have been shown by Yang *et al.* (1991), Yim and Lin (1992) and Lin and Yim (1994). The marginal amplitude probability density function (MAPDF) has been used to demonstrate the first order statistics of a deterministic chaotic response (Yim and Lin, 1992). It is found that the MAPDF is periodic in time and characterized by a multi-

maxima curve (Kapitaniak, 1988; Yim and Lin, 1992). Sequence of Poincaré points (which are sample points at the interval of the forcing period) of a chaotic response are shown to exhibit ergodicity (Yim and Lin, 1992).

This interdependence between deterministic and stochastic systems have also been indicated by the existence of noisy chaos through a vast of numerical studies. Kapitaniak (1988) solved the FPE to demonstrate the behavior of the marginal probability densities of second order nonlinear systems driven by periodic plus random noise excitation. He observed that the noisy chaotic response is characterized by a multi-maxima curve in the marginal probability density function (MPDF) which is non-stationary in time. The corresponding Lyapunov exponent is a random number, and the mean of which approaches zero as the noise strength increases. Bulsara and Jacobs (1990) investigated the noise effect on the behavior of nonlinear systems through Lyapunov exponent and PDF. The smoothing effect on the chaotic attractor and the noise-induced chaos have been demonstrated via numerical simulations. Kunert and Pfeiffer (1991) employed an alternating-direction finite difference method procedure to solve the FPE. The resulting stationary state of the joint probability density function (JPDF) can depict the corresponding chaotic attractor on the Poincaré section. Finally, the invariant measure of noisy chaos has been examined. Kifer (1989) provided a mathematical support for the existence of invariant measure of attractors under weak noisy disturbance. Jung and Hänggi (1990) proposed the time-averaged PDF, which can suppress the periodicity of the PDF by taking the time average of the PDF over a long duration of time. The time-

averaged PDF can be defined as the ubiquitous invariant measure applicable to deterministic, noisy chaotic, as well as stochastic dynamics.

1.2 Thesis Outline

The major objective of this investigation is to examine both the deterministic and stochastic nonlinear (possible chaotic) moored structural system behaviors from a stochastic perspective. A stochastic extension of the deterministic moored structural system analyzed by Gottlieb (1991) is performed. The random noise effects on the nonlinear moored structural responses (regular and chaotic) and their interactive relationship are examined through transient and steady-state PDF's, which are obtained by solving the associated FPE using path integral solution (PIS) (Markov process approach). Considering the random noise as a perturbation to the Hamiltonian moored structural system, a generalized stochastic Melnikov function under the presence of noise is developed. A mean square representation of the stochastic Melnikov criterion is derived and the possible chaotic domain in the parameter space is defined. Various random wave fields are approximated by filtered white noise processes. From a stochastic perspective, the incident flow considered in this study includes monochromatic regular waves, monochromatic regular waves with white noise, narrow-band random waves and JONSWAP random waves. Experiments conducted in 1992 at the Hinsdale Wave Research Lab at OSU are analyzed, and the experimental observations are explained based on the analytical predictions. A detailed description of thesis Chapters incorporating objectives, methodology and analysis summary is given as follows.

1.2.1 System Considered

The multi-point moored structural system considered is formulated as a two-degree-of-freedom (2DOF, surge and heave) submerged rigid body, hydrodynamically damped and excited nonlinear oscillator. Although the mooring lines are linearly elastic, depending on the mooring angles, the restoring force is geometrically nonlinear. The elastic mooring cables are assumed to be taut and the associated restoring force continuous. The degree of nonlinearity of the restoring force depends on the geometric configuration (mooring angle), and the exciting force takes into account both nonlinear drag and inertia effects on a submerged axis-symmetric small body (Gottlieb, 1991).

Random perturbations in the wave field can be included by a generalized representation of the equation of motion. The randomness in the wave profile is approximated by additive Gaussian white noise (Risken, 1984) which induces the perturbations in drag and inertia exciting forces. The random perturbations in narrow-band random waves can also be described by a white noise approximation. When the spectral bandwidth is very narrow, the wave spectrum can be approximated by a delta function located at the peak frequency with background noise. In the limit as bandwidth approaches zero, the wave field can be described by deterministic monochromatic regular waves. An arbitrary random wave field can be also approximated by a filtered white noise process, and the JONSWAP spectrum is a sample spectrum for examination.

Nonlinearities (restoring and hydrodynamic) in the moored structural system are isolated via auxiliary models. The noise-induced transition among responses in each model are examined in later Chapters to shed some light on the stochastic fully-nonlinear

moored structural behavior. The auxiliary models include SDOF model with linearized drag and nonlinear restoring forces, SDOF model with nonlinear drag and two-term polynomial restoring force, SDOF fully nonlinear model with white noise approximation, 2DOF model to monochromatic waves with random perturbations, and SDOF model with linearized drag and nonlinear moored structure subjected to JONSWAP random waves.

1.2.2 Methods of Analysis

The stochastic analysis procedures considered include generalized Melnikov function, Markov process approach, and time domain simulations. The moored structural system is of single-well potential and there exists no homoclinicity or heteroclinicity, thus the Melnikov function can not directly apply. However, a homoclinic connection can be found near the primary resonance in its associated averaged system, which indicates the asymptotic response behavior (Gottlieb, 1991). Using the Rice's noise representation (Kapitaniak, 1988), the effective noise component is projected onto the averaged system and thus its influence in the formulation of the generalized stochastic Melnikov function is demonstrated, and a possible chaotic domain can be identified. The Markov process approach is applied to depict the global information of response via transient and steady-state PDF's. Due to the very weak chaotic attraction of the structural response, the standard (Euler) numerical evaluation of the PIS in the Markov process approach needs to be modified. The modified procedure preserves the Gaussian approximation for random response but incorporates a higher order numerical scheme (a Runge-Kutta fourth order procedure) to compute the most probable position. Accordingly, even very weak chaotic attractor of the structural response can be represented via the JPDF on the

Poincaré section. Shinozuka's simulation method is used to provide a zero-mean and band-limited noise representation, thus time domain simulations can be implemented to validate the analytical predictions.

1.2.3 Stochastic Nonlinear System Response

In various stochastic wave fields, the moored structural response is examined using the analysis procedures introduced. The effects of randomness in the wave field on the nonlinear moored structural responses are investigated. The wave fields considered include monochromatic regular waves with random perturbations, narrow-banded random waves, and JONSWAP random waves. The noise effects on the nonlinear moored structural response, e.g., chaos, are examined from a stochastic perspective. The narrow band and JONSWAP random wave spectra are approximated by filtered white noise, and with the bandwidth as a parameter the moored structural responses subjected to random waves are also investigated.

1.2.4 Experiment

To validate the analytical investigation on the nonlinear stochastic phenomena in SDOF and 2DOF moored structural systems, an experiment characterizing the response behavior of a submerged spherical body was conducted (Yim *et al.*, 1993). The excitation considered includes both monochromatic and random waves. However, due to the inevitability of the presence of noise in the wave flume, the incident waves are always considered randomly perturbed, even for the designed regular waves, and the experimental observations are interpreted in a stochastic sense. The experimental setup

and configuration for the SDOF model (a submerged sphere with a rod confining its movement in surge direction) and the MDOF model (a free-play-allowed submerged sphere) are described. Hydrodynamic calibrations including return current, wave kinematics and reflection, and instrument locations are also considered. Damping mechanism of the model is separated into linear structural damping and hydrodynamic quadratic drag. In a test under wave excitation, the structural damping component is assumed the same as that in still water. The hydrodynamic damping component can be approximated analytically when the hydrodynamic drag coefficient is determined. The movement of the sphere is measured by attached string pots for both SDOF and MDOF models, and the sphere response is analyzed accordingly. Due to symmetry the MDOF model moves essentially in a 2-D fashion. Thus the measurements can be converted into surge and heave motions. To avoid instrument-induced calibration errors, all biases in the measurements are removed for further analysis. Techniques to analyze the response of sphere include time history and spectrum plots, and marginal amplitude PDF. Experimental observations of the structural response, even for that under designed monochromatic regular wave excitation, are interpreted from a stochastic perspective based on the analytical predictions.

2. STOCHASTIC MODELS OF MOORED STRUCTURAL SYSTEM

The multi-point moored structural system considered is formulated as a two-degree-of-freedom (2DOF, surge and heave) submerged rigid body, hydrodynamically damped and excited nonlinear oscillator (Figs.2.1a and b). Although the mooring lines are linearly elastic, depending on the mooring angles, the restoring force is geometrically nonlinear. Various types (slack, pre-tensioned and taut) of nonlinearities in the restoring force (stiffness) have been discussed by Gottlieb (1991). In this study, the elastic mooring cables are assumed to be taut and the associated restoring force is continuous (Figs.2.2a and b). The degree of nonlinearity of the restoring force depends on the geometric configuration (mooring angle). The exciting force takes into account both nonlinear drag and inertia effects on a submerged axis-symmetric small body (Gottlieb, 1991) using the relative motion Morison formulation (Isaacson, 1979, Gottlieb, 1991). Through an appropriate transformation, the randomness in the wave field are incorporated into the hydrodynamic forcing terms.

2.1 Governing Equations

By considering displacements (surge and heave) as the generalized coordinates, the drag and inertia components as the generalized forces, and employing the Lagrange approach, the equation of motion of the moored structural system subjected to regular (sinusoidal) wave field is derived (Gottlieb, 1991). Numerically, a random wave field can be approximated as the sum an infinite number of regular (sinusoidal) waves with random phase shifts. The amplitudes of those sinusoidal waves are modulated according

a)

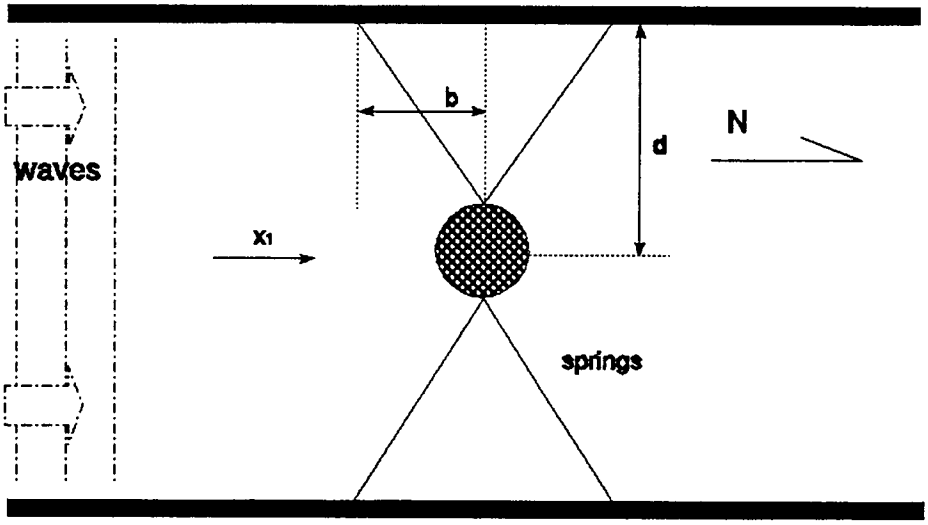

Plan View

b)

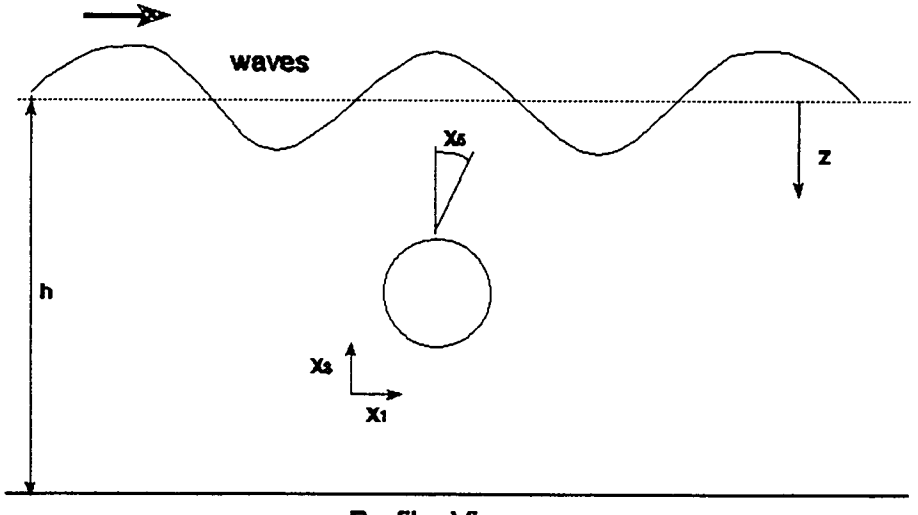

Profile View

Figure 2.1 Definition sketch of a submerged, hydrodynamically damped and excited nonlinear ocean structural system

a)

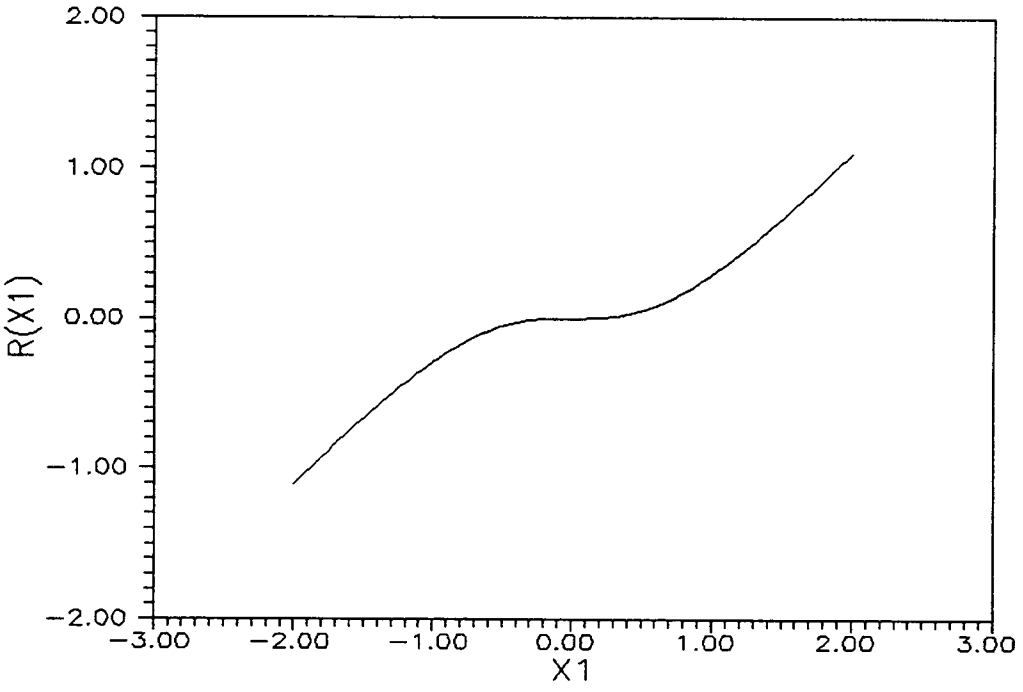

b)

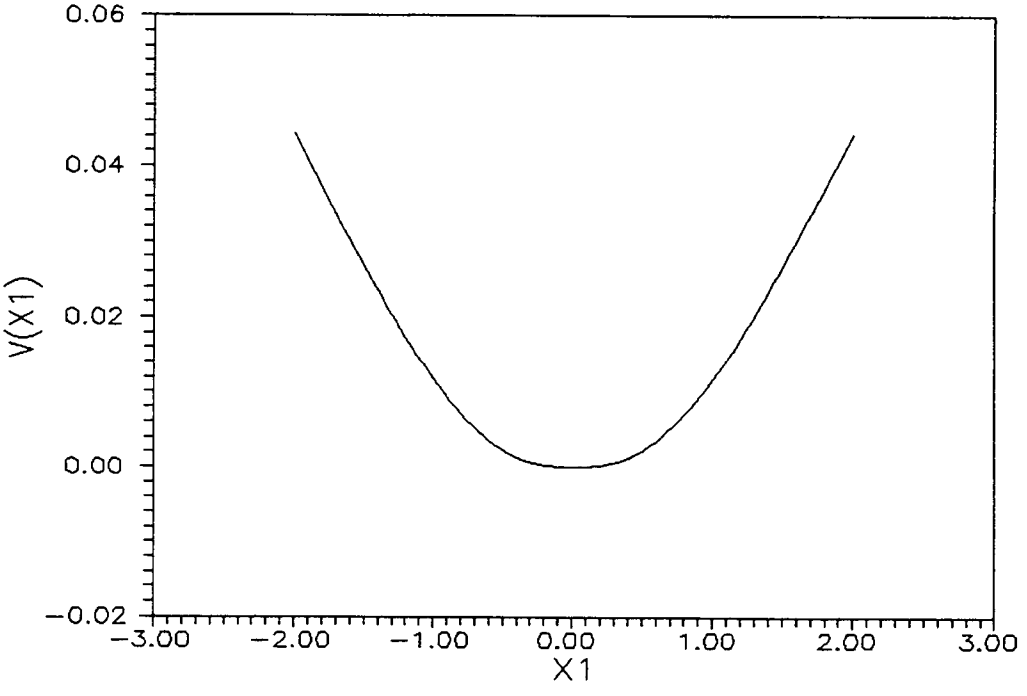

Figure 2.2 Restoring force and potential of ocean structural system: a) restoring force; b) potential

to the random wave spectrum, the associated frequencies are located within the spectral range, and the phase shifts are random variables with uniform distribution over $[0,2\pi]$. The stochastic nature of the wave field can be included by a generalized representation of the equation of motion. The generalized governing equations for a 2DOF moored structural system in a regular or irregular wave field become

$$\begin{aligned}
\dot{x}_1 &= x_2 \\
\dot{x}_2 &= -R_1(x_1,x_3)-\gamma_1 x_2+F_{D1}(x_1,x_2,x_3,x_4,\theta_1,\ldots,\theta_J)+F_{I1}(x_1,x_2,x_3,x_4,\theta_1,\ldots,\theta_J) \\
\dot{x}_3 &= x_4 \\
\dot{x}_4 &= -R_3(x_1,x_3)-\gamma_3 x_4+F_{D3}(x_1,x_2,x_3,x_4,\theta_1,\ldots,\theta_J)+F_{I3}(x_1,x_2,x_3,x_4,\theta_1,\ldots,\theta_J) \\
\dot{\theta}_j &= \omega_j
\end{aligned} \tag{2.1}$$

with $j=1,2,\ldots,J$ $(J\to\infty)$, x_1 and x_3 are nondimensionalized surge and heave displacements (Gottlieb, 1991), respectively, and

$$\begin{aligned}
R_1 &= \alpha\left[x_1-\tau\left[\frac{l_1+l_2}{l_1 l_2}x_1-\beta\frac{l_1-l_2}{l_1 l_2}\right]\right] \\
R_3 &= \alpha\left[(1+\delta)x_3-\tau\left[\frac{l_1+l_2}{l_1 l_2}x_3\right]\right] \\
l_{1,2} &= [1+(\beta\pm x_1)^2+x_3]^{1/2}
\end{aligned} \tag{2.2}$$

$$\begin{aligned}
F_{D1} &= \mu_1\delta_1\left[u_1-\frac{x_2}{\omega}\right]\left|u_1-\frac{x_2}{\omega}\right| \\
F_{D3} &= \mu_3\delta_3\left[u_3-\frac{x_4}{\omega}\right]\left|u_3-\frac{x_4}{\omega}\right|
\end{aligned} \tag{2.3}$$

$$F_{I1} = \mu_1\omega^2\left[\frac{\partial u_1}{\partial\theta} + \left(u_1 - \frac{x_2}{\omega}\right)\frac{\partial u_1}{\partial x_1}\right] + \mu_3\omega^2\left(u_3 - \frac{x_4}{\omega}\right)\frac{\partial u_3}{\partial x_1}$$

$$F_{I3} = \mu_3\omega^2\left[\frac{\partial u_3}{\partial\theta} + \left(u_3 - \frac{x_4}{\omega}\right)\frac{\partial u_3}{\partial x_3}\right] + \mu_1\omega^2\left(u_1 - \frac{x_2}{\omega}\right)\frac{\partial u_1}{\partial x_3} \qquad (2.4)$$

(see Gottlieb (1991) for expressions for parameters α, β, γ, δ, $\mu_{1,3}$, and τ), and

$$\theta_j = k_j x_1 - \omega_j t + \phi_j, \qquad j = 1,2,\ldots,J \ (J\to\infty) \qquad (2.5)$$

where ω_j is the j^{th} frequency component in the wave and ϕ_j is the associated phase shift (monochromatic regular waves: $J=1$ with a fixed phase shift; random waves: $J\gg 1$ with random phase shifts). A sample realization of the wave profile can be obtained by summing up contributions of all frequencies.

The random wave fields considered here include slightly randomly perturbed regular waves, very narrow-band random waves, and JONSWAP type random waves. Variations in the wave profile can be approximated by additive Gaussian white noise (Risken, 1984). Under wind waves in a deep water, the wave spectrum is narrow-banded. If the spectral bandwidth is very narrow, the spectrum can be approximated by a delta function located at the peak frequency with adequate amount of background noise. In the limit as the spectral bandwidth approaches zero, the exciting force can be approximated by a deterministic harmonics with driving frequency at the spectral peak. Moreover, an arbitrary random wave spectrum can be also approximated by a filtered white noise, and the JONSWAP spectrum is a sample for investigation in this study.

When the rigid body is submerged beneath the water surface, under linear wave condition, the surge displacement is of the greatest importance. To demonstrate the behavior of the system response in the surge direction, the moored structural system (equation (2.1)) may be approximated by a lower DOF model. Assume that the displacements (surge and heave) are uncoupled such that the characteristics of the surge motion can be singled out by examining a SDOF moored structural model, i.e., x_3 is equal to zero in equations (2.1-4). Using a least square approach, the nonlinear restoring force can be approximated by a polynomial consisting of odd order terms only. Good agreement between the taut mooring restoring force and a two-term polynomial approximation has been demonstrated (Gottlieb, 1991). The quadratic drag force can be linearized under small amplitude kinematics. Thus, for demonstration, SDOF models with nonlinear drag and polynomial restoring force, and with linearized drag and nonlinear restoring force will be used.

2.2 Exciting Forces

Randomness in the exciting hydrodynamic forces (drag and inertia) induced by random perturbations in a regular wave profile and by a random narrow-band wave field are discussed in this study as follows.

2.2.1 Regular Waves with Random Perturbations

A randomly perturbed regular wave field can be formulated by a sinusoidal function with white noise perturbations. Thus, the wave profile is described by

$$\eta_r(t) = \frac{H}{2}\cos(k x_1 - \omega t + \phi) + \xi(t) \tag{2.6}$$

$\xi(t)$ is a zero-mean, delta-correlated white noise i.e.,

$$\begin{aligned} \langle \xi(t) \rangle &= 0 \\ \langle \xi(t)\xi(t') \rangle &= q\delta(t-t') \end{aligned} \tag{2.7}$$

where q denotes the noise intensity. The associated particle velocities in the x_1 and x_3 directions are

$$\begin{aligned} u_1 &= a_0 + a_1\cos(k x_1 - \omega t + \phi) + \zeta_1(t) \\ u_3 &= a_3\sin(k x_1 - \omega t + \phi) + \zeta_3(t) \end{aligned} \tag{2.8}$$

with

$$\begin{aligned} a_0 &= \frac{U_0}{\omega d} \\ a_1 &= \frac{\omega H}{2}\frac{\cosh[k(x_3+h')]}{\sinh(kh')} \\ a_3 &= \frac{\omega H}{2}\frac{\sinh[k(x_3+h')]}{\sinh(kh')} \end{aligned} \tag{2.9}$$

The intensity of the randomness, $\zeta_{1,3}(t)$ in equation (2.8) can be computed based on the Shinozuka's representation $\xi_s(t)$ of the white noise $\xi(t)$ (equation (2.6)). The Shinozuka's noise is represented by the sum of harmonics of deterministic amplitudes, random frequencies and phase shifts

$$\xi(t) \cong \xi_s(t) = \sum_{k=1}^{N} a_k' \cos(\omega_k t + \phi_k) \tag{2.10}$$

where a_k''s are the amplitudes of the harmonics and given by

$$a_k' = \sqrt{2S_o(\omega_k)\Delta\omega} \tag{2.11}$$

with S_o the noise spectral intensity. ω_k's are the frequencies and given by

$$\omega_k = (k-0.5)\Delta\omega + \delta\omega_k + \omega_{\min} \tag{2.12}$$

where

$$\Delta\omega = \frac{\omega_{\max} - \omega_{\min}}{N} \tag{2.13}$$

and the $\delta\omega_k$'s are independent random variables uniformly distributed within the interval $[-\Delta\omega/2, \Delta\omega/2]$, and ϕ_k's are the random phase shifts uniformly distributed in $[0, 2\pi]$. Thus each individual harmonic in equation (2.10) contributes to the fluid particle velocity through the transformation in equation (2.9), i.e.,

$$\begin{aligned} \zeta_{s1}(t) &= \sum_{k=1}^{N} \omega_k a_k' \frac{\cosh[k(x_3+h')]}{\sinh(kh')} \cos(\omega_k t+\phi) \\ \zeta_{s3}(t) &= \sum_{k=1}^{N} \omega_k a_k' \frac{\sinh[k(x_3+h')]}{\sinh(kh')} \cos(\omega_k t+\phi) \end{aligned} \tag{2.14}$$

Taking the average of the amplitudes of the sinusoidal functions over the frequency range $[\omega_{min}, \omega_{max}]$, randomness in the fluid particle velocity can be approximated by white noise

$$\zeta_1(t) = r_1\xi(t) = \frac{(\omega_{max}-\omega_{min})\cosh[k(x_3+h')]}{2\sinh(kh')}\xi(t)$$
$$\zeta_3(t) = r_3\xi(t) = \frac{(\omega_{max}-\omega_{min})\sinh[k(x_3+h')]}{2\sinh(kh')}\xi(t) \quad (2.15)$$

where $\zeta_{1,3}(t)$ are zero-mean and delta-correlated Gaussian white noises with re-scaled intensities r_1^2q and r_3^2q, respectively. Recall that q is the intensity of $\xi(t)$ (see equation (2.7)).

2.2.1.1 SDOF Model with Linear Drag

If the surge displacement is assumed the dominant motion and uncoupled with other DOF, the 2DOF model can be approximated as a SDOF moored structural model with surge motion only. When the hydrodynamic forces in this SDOF model are described by a linear drag and nonlinear restoring force, the randomness in the wave profile can be incorporated into the exciting force via a linear transformation resulting in a modulated intensity but preserving the (Gaussian) distribution. Combining the linear drag effect and structural damping force, a new damping coefficient γ^* is derived, and the corresponding equation of motion can be obtained

$$\dot{x}_1 = x_2$$
$$\dot{x}_2 = -\gamma^* x_2 - R(x_1) + F_1 + \nu(t) \quad (2.16)$$

where

$$F_I = \mu\omega^2 a_1' \cos(\omega t+\phi)$$

$$R(x_1) = \alpha\left[x_1 - \tau\left[\frac{\beta+x_1}{\sqrt{1+(\beta+x_1)^2}} - \frac{\beta-x_1}{\sqrt{1+(\beta-x_1)^2}} \right] \right] \tag{2.17}$$

$\nu(t)$ is a zero-mean white noise approximation for the random perturbation in hydrodynamic exciting forces.

2.2.1.2 SDOF Model with Nonlinear Drag

When nonlinear quadratic drag is considered, the influence of random noise becomes highly nonlinear and no simple expressions of the equation of motion corresponding to equation (2.16) can be obtained in general. However, for systems with small surge velocity response relative to that of the fluid particle, i.e. $|x_2| \ll |u|$, and assuming the higher order random effect is negligible, the random perturbations in the hydrodynamic drag exciting forces can be approximated by an additive white noise. The drag force on a submerged rigid body induced by regular wave with random perturbation is given by

$$\begin{aligned} F_D &= \mu\delta\left[u - \frac{x_2}{\omega}\right] |u - \frac{x_2}{\omega}| \\ &= F_D^d + F_D^r \end{aligned} \tag{2.18}$$

where superscripts d and r denote the deterministic and random components of drag force, respectively. Consider the fluid velocity, u, over a positive half period and neglecting higher order random effects, i.e. $\zeta_1^2(t)$, equation (2.18) becomes

$$\begin{aligned} F_D &= F_D^d + F_D^r = \mu \delta u^2 \\ &= \left(u^d\right)^2 + 2\zeta_1(t) u^d \end{aligned} \tag{2.19}$$

It is noted in equation (2.19), the random perturbations are modulated by the periodic motion of the fluid field, thus a parametric noise. The multiplicative randomness can be approximated by an additive form by averaging the fluid particle motion over a half period. Thus the nonlinear drag can be written as

$$\begin{aligned} F_D &= F_D^d + 2\mu\delta\zeta_1(t) \int_{-\frac{\pi}{2}}^{\frac{\pi}{2}} \frac{a_1}{\omega} \cos\theta \, d\theta \\ &= F_D^d + \frac{4\mu\delta a_1}{\omega} \zeta_1(t) \end{aligned} \tag{2.20}$$

The randomness in the hydrodynamic exciting forces can be obtained by adding up the perturbations in the inertia and drag forces (equations (2.16) and (2.20)). The equation of motion becomes

$$\begin{aligned} \dot{x}_1 &= x_2 \\ \dot{x}_2 &= -\gamma x_2 - R(x_1) + F_D^d(x_1, x_2, t) + F_I^d(x_1, x_2, t) + \nu(t) \end{aligned} \tag{2.21}$$

where $F_D{}^d$ and F_I^d are represented in equations (2.20) and (2.16), and $\nu(t)$ is a zero-mean Gaussian white noise.

2.2.1.3 2DOF Model Subjected to Regular Waves with Random Perturbations

Using the white noise approximation to the randomness in the exciting forces (equation (2.8)), the equations of motion for a 2DOF moored structural model are

$$\begin{aligned} \dot{x}_1 &= x_2 \\ \dot{x}_2 &= -R_1 - \gamma_1 x_2 + F_{D1}^d + F_{I1}^d + \nu_1(t) \\ \dot{x}_3 &= x_4 \\ \dot{x}_4 &= -R_3 - \gamma_3 x_4 + F_{D3}^d + F_{I3}^d + \nu_3(t) \end{aligned} \tag{2.22}$$

where x_1 and x_3 denote the displacements in surge and heave directions (see equations (2.1-9)). White noise components, $\nu_1(t)$ and $\nu_3(t)$, approximate the combined random effects in the particle velocity through nonlinear drag (see equations (2.16) and (2.20)).

2.2.2 Narrow-Band Random Waves

In deep water with limited fetch, wind waves possess a narrow-band spectrum (Sarpkaya and Isaacson, 1983). This spectrum can be approximated by a filtered white noise process (with white noise spectral intensity S_0)

$$S_{nb}(f) = \frac{S_0}{[-(2\pi f)^2 + f_0]^2 + \beta_n^2 f^2} \tag{2.23}$$

where β_n ($\ll 1$) is a spectral bandwidth parameter and f_0 is the peak frequency. Numerically, a narrow-band excitation can be represented by an infinite number of sinusoidal functions with uniformly distributed random phase shifts

$$\eta_{nb}(t) = \sum_{j=1}^{N} a_{nj} \cos(k_j x_1 - \omega_j t + \phi_j), \quad \text{with } N \text{ large} \tag{2.24}$$

where N is a large number, a_{nj}'s are the amplitudes modulated according to the spectrum, ω_j's represent the frequencies within the spectral range considered, and ϕ_j's are the uniformly distributed random phase shifts.

For convenience of analysis, this narrow-band random excitation can also be approximated by a sum of a finite number (much smaller than N) of frequencies within the frequency range with background noise (zero-mean and delta-correlated)

$$\eta'_{nb}(t) = \sum_{j=1}^{J} a_{nj}\cos(k_j x_1 - \omega_j t + \phi_j) + \xi(t) \tag{2.25}$$

The corresponding fluid particle velocities in x_1 and x_3 directions are given by

$$\begin{aligned} u_1 &= a_0 + \sum_{j=1}^{J} a_{1j}\cos(k_j x_1 - \omega_j t + \phi_j) + \zeta_1(t) \\ u_3 &= \sum_{j=1}^{J} a_{3j}\sin(k_j x_1 - \omega_j t + \phi_j) + \zeta_3(t) \end{aligned} \tag{2.26}$$

where a_0 is given by equation (2.9) and

$$\begin{aligned} a_{1j} &= \omega_j a_{nj}\frac{\cosh[k_j(x_3+h')]}{\sinh(k_j h')} \\ a_{3j} &= \omega_j a_{nj}\frac{\sinh[k_j(x_3+h')]}{\sinh(k_j h')} \\ \zeta_1(t) &= r_1\xi(t) \\ \zeta_3(t) &= r_3\xi(t) \end{aligned} \tag{2.27}$$

The background noise in the spectra are approximated by $\zeta_{1,3}(t)$, which represent zero mean, delta correlated white noises with modulated intensities. Note that when the bandwidth is narrow, the system response closely follows its deterministic counterpart (with peak frequency as the driving frequency) with slow variations in the amplitude and frequency (Davis and Liu, 1990). Thus when the spectral bandwidth is very narrow, the narrow-band excitation characteristics can be described by a deterministic component

with driving frequency at the peak frequency with white noise which approximates the slow variation in the response (Fig.2.3a). In the limit as bandwidth approaches zero, the narrow band spectrum degenerates to a delta function at the peak frequency ω_p, which represents a deterministic periodic time series with period of $2\pi/\omega_p$.

For convenience of demonstration, the SDOF model with linear hydrodynamic excitation and nonlinear restoring force is examined. When very narrow-band random waves are considered, based on the assumed linear relationship between the wave profile and the wave forces, the corresponding hydrodynamic exciting forces are also very narrow-banded. Thus the force spectrum can be approximated by a dominant frequency and background noise. The equations of motion is then given by

$$\begin{aligned} \dot{x}_1 &= x_2 \\ \dot{x}_2 &= -\gamma^* x_2 - R(x_1) + F_I + \nu(t) \end{aligned} \tag{2.28}$$

where

$$F_I = \mu \omega_p a_1 \cos(kx_1 - \omega_p t + \phi) \tag{2.29}$$

2.2.3 JONSWAP Random Waves

The simple spectra considered above are designed for convenience of analysis, under practical field conditions, the wave spectral density is often described by the JONSWAP spectrum (Sarpkaya and Isaacson, 1983)

$$S(f) = \frac{\alpha_J g^2}{(2\pi)^4 f^5} \exp\left[-\frac{5}{4}\left[\frac{f}{f_p}\right]^{-4}\right] \gamma_J^a \tag{2.30}$$

where

$$a = \exp\left[-\frac{(f-f_p)}{2\sigma^2 f_p^2}\right] \tag{2.31}$$

with

$$\sigma = \begin{cases} \sigma_a = 0.07 & \text{for } f \le f_p \\ \sigma_b = 0.09 & \text{for } f > f_p \end{cases} \tag{2.32}$$

where f_p is the peak frequency and is found to be related to the fetch parameter by $f_p = 2.84(gF/U^2)^{-0.33}$; σ_a and σ_b relate to respectively to the widths of the left and right sides of the spectral peak; α_J is equivalent to the Phillips' constant but is now taken to depend on the fetch parameter: $\alpha_J = 0.066(gF/U^2)^{-0.22}$; and γ_J is the ratio of the maximum spectral density to that of the corresponding Pierson-Moskowitz spectrum (Sarpkaya and Isaacson, 1983). Because of its narrow bandwidth, the JONSWAP spectrum can be approximated by filtered Gaussian white noise. The governing equation of the filter is given by

$$\ddot{\zeta} + \beta_n \dot{\zeta} + (2\pi f_0)^2 \zeta = \eta(t) \tag{2.33}$$

The transfer function and spectral density function of the output of the filtered white noise are

$$|H(f)|^2 = \frac{1}{[-(2\pi f)^2 + (2\pi f_0)]^2 + (2\pi\beta_n f)^2} \tag{2.34}$$

and

$$S_\zeta(f) = \frac{S_0}{[-(2\pi f)^2 + (2\pi f_0)^2]^2 + (2\pi\beta_n f)^2} \tag{2.35}$$

respectively (Newland, 1984), where S_0 is the white noise spectral intensity, β_n is the spectral bandwidth parameter, and f_0 is the natural frequency. In this approximation there are three controlling variables, f_e, S_0 and β_n. The best fit is determined by equating: (i) the total energy, (ii) the magnitude of the maximum spectral density, and (iii) the value of the frequency where the peak occur for both JONSWAP and the approximate spectra. That is,

$$\int_{-\infty}^{\infty} S_\zeta(f)df = \int_{-\infty}^{\infty} S(f)df \tag{2.36}$$

$$S(f_p) = \frac{\alpha\gamma g^2 e^{-1.25}}{(2\pi)^4 f_p^5} = S_\zeta(f_e) = \frac{S_0}{[-(2\pi f_e)^2 + (2\pi f_0)^2]^2 + (2\pi\beta_n f_e)^2} \tag{2.37}$$

$$f_p = f_e = \sqrt{f_o^2 - \frac{\beta_n^2}{8\pi^2}} \tag{2.38}$$

The three filter parameters f_e, S_0 and β_n are determined by solving the three nonlinear algebraic equations iteratively. Damping parameter β_n serves as a parameter for the degree of randomness. Sample JONSWAP and the filtered-white-noise spectra are compared in Fig.2.3b. The approximation is a little off the mark in the low frequency

range, however, a good approximation is observed in general. The JONSWAP random waves will be used for numerical simulations, and the filtered-white-noise model will be used to analyze the response behavior of the nonlinear system analytically.

By adopting the model with linearized drag and nonlinear restoring forces, the wave force spectrum $S_{FI}(f)$ can be determined. Thus the equation of motion for the nonlinear moored structural system subjected to filtered-white-noise random waves is

$$\ddot{x} + \gamma^* \dot{x} + R(x) = F_I(t) \tag{2.39}$$

where $F_I(t)$ has a spectrum (Sarpkaya and Isaacson, 1983) as

$$S_{F_I}(f) = \frac{8}{\pi} \mu^2 \delta^2 \sigma_u^2 S_u(f) + \mu^2 \omega^4 S_a(f) \tag{2.40}$$

and

$$\begin{aligned} S_u(f) &= 4\pi^2 f^2 \frac{\cosh^2(k(z+d))}{\sinh^2(kd)} S_\zeta(f) \\ S_a(f) &= 16\pi^4 f^4 \frac{\cosh^2(k(z+d))}{\sinh^2(kd)} S_\zeta(f) \end{aligned} \tag{2.41}$$

where $S_u(f)$ and $S_a(f)$ are evaluated according to the filtered-white-noise spectrum $S_\zeta(f)$ (equation (2.35)).

a)

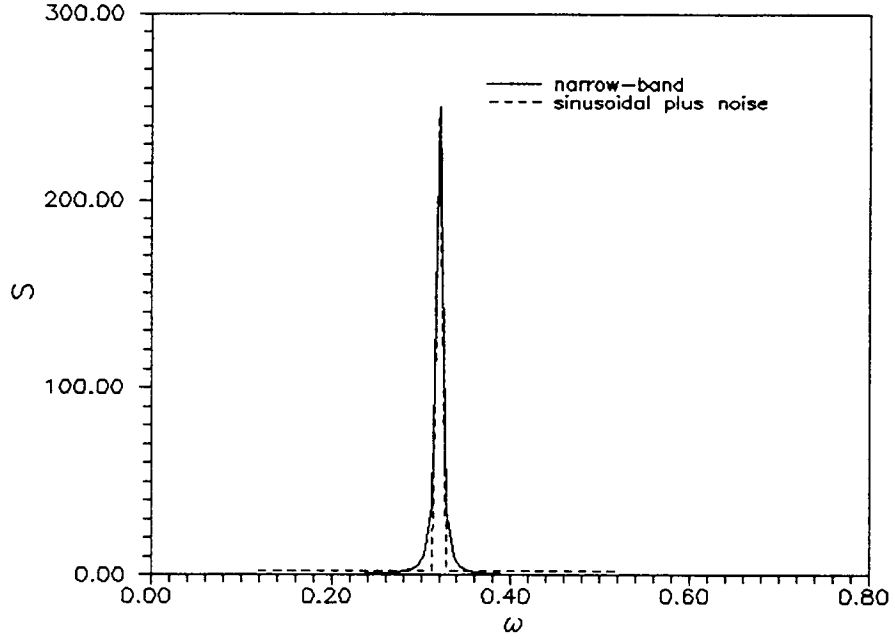

b)

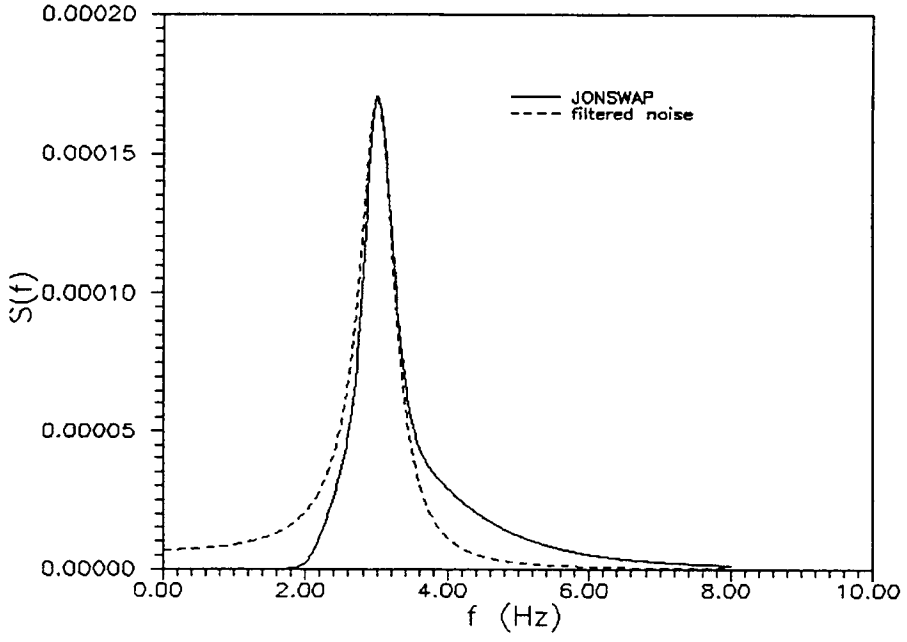

Figure 2.3 Actual and approximated spectra: a) sinusoidal plus noise approximation to narrow-band spectrum ($\sigma^2=0.03^2$); b) filtered white noise to JONSWAP spectrum

3. METHODOLOGY

Methods developed in this study to analyze nonlinear stochastic response include generalized stochastic Melnikov function, Markov process approach, and time domain simulations. Assuming slow variations in the response amplitude and phase angle, an associated averaged system can be obtained by integrating with respect to the action angle and dividing by the total action. In the averaged system, existence of homoclinic connections near the primary resonance is proved. Thus the generalized stochastic Melnikov function can be applied to identify possible chaotic domains. With the white noise approximation discussed in Chapter 2, the Markov process approach can be used to examine probabilistic response properties. The resulting transient and steady-state of JPDF can depict global information about the response behavior. Numerical simulation is employed to confirm the analytic predictions of the responses in the time domain.

3.1 Melnikov Approach

The Hamiltonian of the SDOF model has only one fixed point, a center, and no homoclinic or heteroclinic orbits. Nevertheless, homoclinic connections may exist near the primary resonance in the associated averaged system (Gottlieb, 1991). The averaged system derived is associated to the model of quadratic drag with polynomial restoring forces. Regarding the presence of random perturbations, a possible expansion of the Melnikov method applied to the averaged system can be derived. The effects of randomness on the stochastic Melnikov criterion are examined in a mean square sense.

For convenience of reference, the derivation of the averaged system and the existence of homoclinic orbits (Gottlieb, 1991) are summarized here.

3.1.1 Existence of Homoclinic Orbits

By treating time explicitly as a state variable, equation (2.21) can be rewritten in an autonomous form

$$\begin{aligned} \dot{x}_1 &= x_2 \\ \dot{x}_2 &= -\gamma x_2 - R(x_1) + F_I(\omega,\theta) + F_D(x_2,\omega,\theta) + \nu(\omega,\theta) \\ \dot{\theta} &= \omega \end{aligned} \tag{3.1}$$

where

$$\begin{aligned} R(x_1) &= \alpha_1 x_1 + \alpha_3 x_1^3 \\ F_I(\omega,\theta) &= -\mu\omega^2 a_1' \sin\theta \\ F_D(x_2,\omega,\theta) &= \mu\delta(u - \frac{x_2}{\omega})\,|u - \frac{x_2}{\omega}| \end{aligned} \tag{3.2}$$

The white noise component, $\nu(\omega,\theta)$, in equation (3.1) can be approximated by a Rice noise representation (Kapitaniak, 1988)

$$\nu(\omega,\theta) \cong \nu_r(\omega,\theta) = \sum_{j=1}^{N} a_j'' \cos(\omega_j t - \psi_j) \tag{3.3}$$

Defining the detuning parameter $\epsilon\Omega' = \omega^2 - (m/n)^2\alpha_1$ and the Van der Pol coordinate transformation

$$\begin{Bmatrix} u \\ v \end{Bmatrix} = \begin{bmatrix} \cos\frac{n}{m}\theta & -\frac{m}{n\omega}\sin\frac{n\theta}{m} \\ -\sin\frac{n}{m}\theta & -\frac{m}{n\omega}\cos\frac{n\theta}{m} \end{bmatrix} \begin{Bmatrix} x_1 \\ x_2 \end{Bmatrix} \tag{3.4}$$

then the governing equations of the moored structural model in u-v coordinates are

$$\begin{Bmatrix} \dot{u} \\ \dot{v} \end{Bmatrix} = \left\{ -\frac{\epsilon n}{m}[R(u,v,\theta) + C(u,v,\theta) + F_D(u,v,\theta) + F_I(\theta) + \nu(\omega,\theta)] \right\} \begin{Bmatrix} \sin\frac{n\theta}{m} \\ \cos\frac{n\theta}{m} \end{Bmatrix} \tag{3.5}$$

Expressions of R, C, F_D and F_I are in Gottlieb (1991). By integrating the right-hand side of equation (3.5) and averaging over period $2m\pi/n$, the averaged system is obtained

$$\dot{u} = -\frac{\epsilon n}{2m\omega}\left\{ -\Omega v + \frac{3}{4}(\frac{m}{n})^2\alpha_3'(u^2+v^2)v + \frac{m\omega}{n}\gamma' u + I_s - \mu\omega^2 a_1\delta_{r,1} + \frac{1}{2}(\frac{m}{n})^2 a'\sin\psi \right\} \tag{3.6}$$

$$\dot{v} = -\frac{\epsilon n}{2m\omega}\left\{ \Omega u - \frac{3}{4}(\frac{m}{n})^2\alpha_3'(u^2+v^2)u + \frac{m\omega}{n}\gamma' u + I_c + \frac{1}{2}(\frac{m}{n})^2 a'\cos\psi \right\} \tag{3.7}$$

and $\alpha_{n+2}=\epsilon\alpha'_{n+2}$, $\gamma=\epsilon\gamma'$, $\delta=\epsilon\delta'$, $a_1'=\epsilon a_1$, $a''=\epsilon a'$. Where $\delta_{r,1}$ is the Kronecker delta function: $\delta_{r,1}=1$ for $r=1$ and $\delta_{r,1}=0$ otherwise, $I_s(u,v)$ and $I_c(u,v)$ represent the averaged drag force over period $2n\pi/m$ (Gottlieb, 1991), and a' denotes the amplitude of the noise component, which is in tune with the dominant frequency. By employing a nonlinear polar transformation (Meirovitch, 1970), $J= 1/2(u^2+v^2)$ and $\Phi=\tan^{-1}(v/u)$, the averaged system (equations (3.6) and (3.7)) can be written as a perturbed ($\delta^*<1$) Hamiltonian system

$$\begin{Bmatrix} \dot{J} \\ \dot{\Phi} \end{Bmatrix} = \begin{Bmatrix} F_1(J,\Phi) \\ F_2(J,\Phi) \end{Bmatrix} + \delta^* \begin{Bmatrix} G_1(J,\Phi) \\ G_2(J,\Phi) \end{Bmatrix} \tag{3.8}$$

where

$$\begin{aligned} F_1(J,\Phi) &= \delta_{r,1} f^* \sqrt{2J}\cos\Phi \\ F_2(J,\Phi) &= -\Omega^* + 2J\alpha^* - \delta_{r,1}\frac{f^*}{\sqrt{2J}}\sin\Phi \end{aligned} \tag{3.9}$$

and

$$\begin{aligned} G_1(J,\Phi) &= -2J\gamma^* - \sqrt{2J}\left[I_s(J,\Phi)\cos\Phi + I_c(J,\Phi)\sin\Phi\right] \\ &\quad -A^*\sqrt{2J}\sin(\Phi+\psi) \\ G_2(J,\Phi) &= -\sqrt{2J}\left[I_c(J,\Phi)\cos\Phi - I_s(J,\Phi)\sin\Phi\right] \\ &\quad -A^*\sqrt{2J}\cos(\Phi+\psi) \end{aligned} \tag{3.10}$$

with $f^*=1/2\mu\omega a_1$ for $m=n=1$ and $f^*=0$ otherwise; $\Omega^*=n[\omega^2-(m/n)^2\alpha_1]/2m\omega$, $\alpha_3^*=3m\alpha_3/8n\omega$, $\delta^*=\mu\delta/\pi\omega$, $\gamma^*=\pi\omega\gamma'/2\mu\delta$, and $A^*=m\pi a'/4n\mu\gamma$. The associated Hamiltonian system is obtained by setting $\gamma^*=0$ with Hamiltonian

$$H(J,\Phi) = \Omega^* J - \alpha_3^* J^2 + \delta_{r,1}\sqrt{2J}\, f^* \sin\Phi \tag{3.11}$$

The corresponding fixed points $[(J_i,\Phi_i)_e=(j_i,\phi_i),\ i=1,2,3]$ are obtained by setting $F_1=F_2=0$ in equation (3.9). Moreover, by taking square of and adding up the expressions in equation (3.9) (with $F_1=F_2=0$), the characteristics equation can be obtained

$$(2j_i)^3 - 2\left[\frac{\Omega^*}{\alpha^*}\right](2j_i)^2 + \left[\frac{\Omega^*}{\alpha^*}\right]^2(2j_i) - \left[\frac{f^*}{\Omega^*}\right]^2 = 0 \qquad (3.12)$$

$$\cos\phi_i = 0$$

It is observed that the stability structures near resonance regions other than the primary resonance ($r=1$) are always governed by a unique center, whereas the stability of response is governed by either a unique center or two coexisting centers which are separated by a hyperbolic saddle point. A jump bifurcation defines the criterion for the existence of a unique center $[a_1 > \beta_c^H]$ or the coexistence of two centers and a saddle $[a_1 < \beta_c^H]$ (Gottlieb, 1991), where

$$\beta_c^H = \frac{16}{27}\frac{(\omega^2-\alpha_1)}{\mu\omega^2}\left[\frac{\omega^2-\alpha_1}{\alpha_3}\right]^{\frac{3}{2}} \qquad (3.13)$$

To determine the existence of a pairs of homoclinic orbits within the averaged system, the Bendixson criterion (Jordan and Smith, 1987) is employed. A closed path is determined to exist when a sign change occurs in $\partial[F_1(J,\Phi)+G_1(J,\Phi)]/\partial J + \partial[F_2(J,\Phi)+G_2(J,\Phi)]/\partial\Phi$. Consequently, for small structural damping ($\gamma < \delta^*$), the system near primary resonance contains homoclinic loops defined by the stable and unstable manifolds of the saddle (Gottlieb, 1991).

The pair of homoclinic orbits $(q_\pm^o(\gamma)) = (J_\pm(\theta), \Phi_\pm(\theta))$ is given by

$$\theta - \theta_o = \int_{J_\pm(\theta_o)}^{J_\pm(\theta)} \frac{dJ}{\sqrt{2Jf^{*2} - (H_o - \Omega^* J + \alpha_3^* J^2)^2}} \qquad (3.14)$$

and

$$\Phi = \sin^{-1}\frac{H_o - \Omega^* J + \alpha_3^* J^2}{\sqrt{2J}\, f^*} \tag{3.15}$$

where $J_{\pm}(\theta)$ and Φ are functions of θ and θ_o. Based on the existence of homoclinic connections, the generalized stochastic Melnikov function is formulated in the following section.

3.1.2 Generalized Stochastic Melnikov Function

The standard Melnikov method has been used in determining the criterion for chaos of nonlinear system subjected to periodic excitation (Guckenheimer and Holmes, 1983, Wiggins, 1988, 1990). The Melnikov function provides a quantitative representation of the existence of the transverse intersection of homoclinic orbit and hyperbolic periodic orbit in a two dimensional vector field. By considering the Poincaré map, based on theorems derived by Moser and Smale (Wiggins, 1990), the Melnikov criterion can be applied to conclude that the system possess chaotic dynamics. A generalized version of the Melnikov function for a system subjected to an excitation with multiple frequencies was introduced by Wiggins (1988). By taking one step further, a generalized stochastic Melnikov function applied to the averaged model with the presence of random noise is derived here.

With the presence of random perturbations, the distance between the stable and unstable manifolds is given by

$$M(\theta_o) = \int_{-\infty}^{\infty} F(q_{\pm}^0(\theta)) \wedge G(q_{\pm}^0(\theta), \theta+\theta_o)\, d\theta$$
$$= \int_{-\infty}^{\infty} (F_1 G_2 - F_2 G_1)\, d\theta \tag{3.16}$$

where

$$F_1 G_2 - F_2 G_1 = f^* \sqrt{2J_{\pm}} \cos\Phi_{\pm} \left[-\frac{4a_1 \cos\Phi_{\pm} \sqrt{\Gamma_{\pm}}}{\sqrt{2J_{\pm}}} - A^* \sqrt{2J_{\pm}} \cos(\Phi_{\pm}+\psi) \right]$$
$$- \left[-\Omega^* + 2J_{\pm}\alpha_3^* - \frac{f^* \sin\Phi_{\pm}}{\sqrt{2J_{\pm}}} \right] \left[-2J_{\pm}\gamma^* - \frac{4}{3}(2J_{\pm} + a_1\sqrt{2J_{\pm}} \sin\Phi_{\pm})\sqrt{\Gamma_{\pm}} \right.$$
$$\left. - A^* \sqrt{2J_{\pm}} \sin(\Phi_{\pm}+\psi) \right]$$

$$= 2\gamma^* J_{\pm} \left[-\Omega^* + 2\alpha_3^* J_{\pm} - \frac{f^* \sin\Phi_{\pm}}{\sqrt{2J_{\pm}}} \right] + \frac{4}{3}\sqrt{\Gamma_{\pm}} \left[2J_{\pm}^* (-\Omega^* + 2\alpha_3^* J_{\pm}) \left[1 + \frac{a_1 \sin\Phi_{\pm}}{\sqrt{2J_{\pm}}} \right] \right.$$
$$\left. - f^* \sqrt{2J_{\pm}} \sin\Phi_{\pm} - a_1 f^* \right] - 2J_{\pm} f^* A^* \cos\Phi_{\pm}(\theta) \cos[\Phi_{\pm}(\theta+\theta_o)+\psi]$$
$$+ \left[-\Omega^* + 2\alpha_3^* J_{\pm} - \frac{f^* \sin\Phi_{\pm}}{\sqrt{2J_{\pm}}} \right] [A^* \sqrt{2J_{\pm}} \sin(\Phi_{\pm}(\theta+\theta_o))] \tag{3.17}$$

and

$$\Gamma_{\pm} = a_1^2 + 2a_1\sqrt{2J_{\pm}} \sin\Phi_{\pm} + 2J_{\pm};\ J_{\pm} = J_{\pm}(\theta,\theta_0);\ \Phi_{\pm} = \Phi_{\pm}(\theta,\theta_0) \tag{3.18}$$

Note that, equation (3.16) represents the Melnikov function for an autonomous system, which does not depend on time explicitly. In this case the Melnikov function is a constant independent of time. For autonomous two-dimensional vector fields, either the

stable and unstable manifolds of a hyperbolic fixed point coincide or they do not intersect at all (Wiggins, 1990). Moreover, the presence of a fixed point in the averaged system indicates the existence of a periodic orbit in the original dynamical system. Thus, a zero (fixed point) in the autonomous Melnikov function implies the possible existence of a periodic (time-dependent) Melnikov function and infinite transverse intersections between stable and unstable manifolds in the original system. Thus, when $M(\theta_o)=0$ in equation (3.16), possible chaotic response may exist and stochastic Melnikov criterion can be identified.

The resulting Melnikov criterion is a function of γ^*, α^*, Ω^*, a_1, f^*, and A^* (equations (3.16-18)). Note that the Melnikov criterion identify a boundary of possible chaotic domain. Underneath the boundary the excitation can overcome the chaos threshold induced by the damping mechanism. Thus by isolating the damping term related to the chaos threshold and regrouping the perturbation effects into deterministic and random components, equation (3.16) can be rewritten as

$$\gamma^* \int_{-\infty}^{\infty} m_1^d d\theta = \int_{-\infty}^{\infty} m_2^d d\theta - A^* \int_{-\infty}^{\infty} m_1^r d\theta + A^* \int_{-\infty}^{\infty} m_2^r d\theta \tag{3.19}$$

where

$$m_1^d = 2J_{\pm}\left[-\Omega^* + 2\alpha_3^* J_{\pm} - \frac{f^* \sin\Phi_{\pm}}{\sqrt{2J_{\pm}}} \right] \tag{3.20}$$

$$m_2^d = \frac{4}{3}\sqrt{\Gamma_{\pm}}\left[2J_{\pm}(-\Omega^* + 2\alpha_3^* J_{\pm})\left[1 + \frac{a_1 \sin\Phi_{\pm}}{\sqrt{2J_{\pm}}} \right] - f^* \sqrt{2J_{\pm}} \sin\Phi_{\pm} - a_1 f^* \right] \tag{3.21}$$

$$m_1^r = 2J_{\pm} f^* \cos\Phi_{\pm}(\theta)\cos[\Phi_{\pm}(\theta+\theta_o)+\psi] \tag{3.22}$$

$$m_2^r = \left[-\Omega^* + 2\alpha_3^* J_{\pm} - \frac{f^* \sin\Phi_{\pm}}{\sqrt{2J_{\pm}}} \right] \sqrt{2J_{\pm}}\, \sin(\Phi_{\pm}(\theta+\theta_o)) \tag{3.23}$$

with superscripts d and r correspond to the deterministic and random perturbations, respectively. Due to the complexity of the integrant (see equation (3.17)), equation (3.19) is not explicitly solved here. However, the noise effects on the Melnikov criterion can be demonstrated qualitatively.

Perturbations m_1^r and m_2^r are Gaussian random variables, thus, the resulting generalized stochastic Melnikov function is also Gaussian distributed. The effects of random noise on the Melnikov criterion may be identified by examining the noise variance. Because the convolution integration in the Melnikov function (equations (3.16-19)), the homoclinic orbits $q^o_{\pm}$ can be considered as a linear filter (Lin and Yim, 1994). Thus the variance of the random component can be obtained by taking the Fourier transform of the convolution integrals. The Fourier transforms of m_1^r and m_2^r in equation (3.19) are given by

$$\begin{aligned} F_1(\omega) &= \int_{-\infty}^{\infty} [2J_{\pm} f^* \cos\Phi_{\pm}(\theta)][A^* \cos(\Phi_{\pm}(\theta+\theta_o)+\psi)] \\ &\quad \times \exp(-i\omega\theta)\, d\theta \\ F_2(\omega) &= \int_{-\infty}^{\infty} [-\Omega^* \sqrt{2J} + \alpha_3^* (2J)^{3/2} - f^* \sin\Phi_{\pm}(\theta)] \\ &\quad \times [A^* \sin(\Phi_{\pm}(\theta+\theta_o)+\psi)] \exp(-i\omega\theta)\, d\theta \end{aligned} \tag{3.24}$$

with corresponding variances

$$Var(M_1^r) = Var(A^* \int_{-\infty}^{\infty} m_1^r d\theta) = \int_{-\infty}^{\infty} F_1^2(\omega) S_1(\omega) d\omega$$
$$= \frac{A^{*2}}{2} \int_{-\infty}^{\infty} F_1^2(\omega) d\omega \tag{3.25}$$

and

$$Var(M_2^r) = Var(A^* \int_{-\infty}^{\infty} m_2^r d\theta) = \int_{-\infty}^{\infty} F_2^2(\omega) S_2(\omega) d\omega$$
$$= \frac{A^{*2}}{2} \int_{-\infty}^{\infty} F_2^2(\omega) d\omega \tag{3.26}$$

The Melnikov criterion provides a necessary condition for the existence of chaotic response (Yim and Lin, 1992). Because the random noise effects can be positive or negative, the Melnikov criterion (equation (3.19)) in the stochastic case should be represented in a mean square sense

$$\gamma^* \left\langle (\int m_1^d d\theta)^2 \right\rangle = \left\langle (\int m_2^2 d\theta)^2 \right\rangle + \sigma_{M_1^r}^2 + \sigma_{M_2^r}^2 + 2\left\langle \left(\int m_2^d d\theta \right) \left(A^* \int m_1^r d\theta \right) \right\rangle$$
$$+ 2\left\langle \left(\int m_2^d d\theta \right) \left(A^* \int m_2^r d\theta \right) \right\rangle + 2\left\langle \left(\int m_1^r d\theta \right) \left(\int m_2^r d\theta \right) \right\rangle \tag{3.27}$$

Because m_1^r and m_2^r are un-correlated, the noise effects represented via variance is

$$\gamma^* (\int m_1^d d\theta)^2 = (\int m_2^d d\theta)^2 + \sigma_{M_1^r}^2 + \sigma_{M_2^r}^2 \tag{3.28}$$

Positivity of the variance indicates that the presence of noise lowers the threshold for chaos and enlarges the possible chaotic domain (Melnikov sense) in the parameter space.

3.2 Markov Process Approach

By assuming the stochastic response is a function of only the most recent probability states, a Markov process approach can be applied to obtain the response PDF. The Markov process approach is used here to derive the Fokker Planck equation (FPE) and to develop a solution procedure based on the path integral solution (PIS). For demonstration, the FPE and a standard PIS procedure will be derived in detail on a general nonlinear system in the following section. Numerical evaluation of the PIS will be demonstrated. Modifications in the PIS and specific applications to the moored structural models will also be discussed.

3.2.1 Fokker-Planck Equation and Path Integral Solution

A general nonlinear stochastic system can be written as

$$\dot{X} = F(X) + G(X)\eta(t) \tag{3.29}$$

where

$$X = [x_1\ x_2 \ldots x_N]^T;\quad F(X,t) = [F_1\ F_2 \ldots F_N]^T;\quad G(X) = [G_1\ G_2 \ldots G_N]^T \tag{3.30}$$

Note that X denotes the N-dimensional state vector, and $\eta(t)$ denote a zero-mean, delta-correlated white noise.

The evolution of the response PDF is governed by a deterministic partial differential equation called the FPE. For equation (3.29), the associated FPE is

$$\frac{\partial f(X,t)}{\partial t} = Lf(X,t) \tag{3.31}$$

where the operator

$$L = \frac{1}{2}\frac{\partial^2}{\partial x_\nu \partial x_\mu} Q_{\nu\mu}(X) - \frac{\partial}{\partial x_\nu} K_\nu(X,t); \quad \nu,\mu = 1,2\ldots N \tag{3.32}$$

and

$$K_\nu = F_\nu(X); \quad Q_{\nu\mu} = \kappa G_\nu G_\mu \tag{3.33}$$

with $f(X,t)$ representing the PDF, K_ν's ($\nu=1,2,\ldots N$) are the entries in the drift vector **K**, and $Q_{\nu\mu}$ are the entries of the $N\times N$ diffusion matrix **Q**.

The PIS, which is a systematic semi-analytical procedure, has been developed to solve the FPE (Graham, 1978; Haken, 1976; Wissel, 1979). The PIS is well-known for solving for the PDF of Markov processes described by the linear Langevin equation with white noise or the statistically equivalent FPE. Extensions of nonlinear Gaussian process solutions of the FPE have been deduced in functional integral form yielding generalizations of the Onsager-Machlup function. The PIS procedure employed in this study, including time-varying drift coefficients (periodic excitation), is derived as follows.

The PIS can be represented by a (discrete) Riemann sum (Wissel, 1979)

$$f(X_n,t_n) = \lim_{\substack{n\to\infty \\ n\tau=t_0}} \prod_{i=0}^{n-1} (\mu_i dx_i) \exp\left[-\tau \sum_{j=0}^{n-1} L^*(X_{j+1}, X_j, \tau) \right] f(X_0,t_0) \tag{3.34}$$

where $\mu_i dx_i$ is the (Wiener) measure in the functional space, and L^* is the Lagrangian. A short-time transition can be obtained analytically using a first order approximation to equation (3.34)

$$f(X,t+\tau)=\left(1+\tau L+O(\tau^2)\right)f(X,t) \tag{3.35}$$

Thus the PDF at the n^{th} step is represented by

$$f(X,t_0+n\tau)\cong(1+\tau L)^n f(X_0,t_0)\cong\exp[(n\tau)L]f(X_0,t_0) \tag{3.36}$$

Convergence of equation (3.36) has been demonstrated by Wissel (1979), and the short-time propagator (Green's function) is given by

$$\begin{aligned}P_{t,\tau}(X'\,|\,X)&=[1+\tau L+O(\tau^2)]\delta(X'-X)\cong\delta(X'-X)\\&+\tau\{\frac{1}{2}\frac{\partial^2[Q_{\mu\nu}\delta(X'-X)]}{\partial x_\mu\partial x_\nu}-\frac{\partial}{\partial x_\nu}[K_\nu\delta(X'-X)]\}\end{aligned} \tag{3.37}$$

To handle the Dirac delta functions in equation (3.37), a coordinate transformation is introduced

$$U=X'-X;\quad V=V(X',X) \tag{3.38}$$

then the short-time propagator becomes

$$\begin{aligned}P_{t,\tau}(X'\,|\,X)=P_{t,\tau}(U,V)&=\delta(U)+\frac{\tau}{2}\delta(U)Q_{\nu\mu}^{(\nu\mu)}(X)-\tau\delta^{(\nu)}(U)Q_{\nu\mu}^{(\mu)}(X)\\&+\frac{\tau}{2}\delta^{(\nu\mu)}(U)Q_{\nu\mu}(X)-\tau\delta^{(\nu)}(U)K_\nu(X)+\tau\delta(U)K_\nu^{(\nu)}(X)\end{aligned} \tag{3.39}$$

where superscripts ν and μ denote the differentiations with respect to x_ν and x_μ, respectively. Equation (3.39) can be converted into a Fourier representation

$$P_{t,\tau}(U,V)=\int\frac{d\Omega}{(2\pi)^n}\exp(i\Omega U)\times\tilde{P}_{t,\tau}(\Omega,V) \tag{3.40}$$

where

$$\begin{aligned}\tilde{P}_{t,\tau}(\Omega, V) &= \int \exp(-i\Omega U) P_{t,\tau}(U, V)\, dU \\ &= 1 + \tau K_\nu^{(\nu)} + \frac{\tau}{2} Q_{\nu\mu}^{(\nu\mu)} + \frac{\tau}{2}\frac{\partial^2}{\partial x_\nu \partial x_\mu} Q_{\nu\mu} - \tau \frac{\partial}{\partial x_\nu} Q_{\nu\mu}^{(\mu)} - \tau \frac{\partial}{\partial x_\nu} K_\nu\end{aligned} \tag{3.41}$$

By adopting the approximation described in equation (3.36), equation (3.41) becomes

$$\begin{aligned}\tilde{P}_{t,\tau} e^{(i\Omega U)} \cong \exp\{&\frac{\tau}{2}\frac{\partial^2 Q_{\nu\mu}}{\partial x_\nu \partial x_\mu} - \frac{\partial}{\partial x_\nu}[\tau Q_{\nu\mu}^{(\mu)} + \tau K_\nu - U_\nu] \\ &+ \tau K_\nu^{(\nu)} + \frac{\tau}{2} Q_{\nu\mu}^{(\nu\mu)}\}\end{aligned} \tag{3.42}$$

Inserting equation (3.42) into equation (3.40) and integrating over Ω with help of the quadratic completion (Wissel, 1979), the short-time propagator is given by

$$\begin{aligned}P_{t,\tau}(X' \mid X) = (2\pi\tau)^{-\frac{n}{2}} Q^{-\frac{1}{2}} \exp\Bigg\{ &-\frac{\tau}{2}[Q_{\nu\lambda}^{(\lambda)} + K_\nu - \frac{x_\nu' - x_\nu}{\tau}] Q_{\nu\mu}^{-1} \\ &[Q_{\mu\rho}^{(\rho)} + K_\mu - \frac{x_\mu' - x_\mu}{\tau}] + \tau K_\nu^{(\nu)} + \frac{\tau}{2} Q_{\nu\mu}^{(\nu\mu)} \Bigg\}\end{aligned} \tag{3.43}$$

Note that the short-time propagator is in a form of multi-variate Gaussian distribution.

Using a multi-dimensional histogram representation for the PDF, the path sum (equation (3.34)) can be implemented numerically. The probability domain at time t is discretized into a finite number of elements represented by function π:

$$P(X, t) = \sum_{i=1}^{l} \pi(x_1 - x_{1i})\, \pi(x_2 - x_{2i}) \ldots \pi(x_N - x_{Ni}) f(X, t) \tag{3.44}$$

where

$$\pi(x_n - x_{ni}) = \begin{cases} 1 & \text{for } x_n - \dfrac{\Delta x_{n(i-1)}}{2} \le x \le x_{n(i)} + \dfrac{\Delta x_{n(i)}}{2} \\ 0 & \text{otherwise} \end{cases} \tag{3.45}$$

with $n=1,2,\ldots N$. The short-time propagator is also discretized into a short-time transition tensor $T_{kl}(\tau)$. Subscripts k,l represent the descritized probability domains at the pre- and post-state, respectively. The short-time propagation can be numerically implemented by determining the most probable (mean) position in the phase space and the local random response following a Gaussian distribution. The most probable phase position after a short-time propagation for each element is deterministically computed by the drift coefficients. The PDF at time $t+\tau$ can be obtained by summing all the probability mass propagated from time t (and normalizing afterward):

$$P_k(t+\tau) = T_{kl}(\tau) P_l(t) \tag{3.46}$$

the transition tensor is given by

$$T_{kl}(\tau) = \frac{2^N}{(\Delta x_{kl(i-1)} + \Delta x_{kl(i)}) \ldots (\Delta x_{kN(j-1)} + \Delta x_{kN(j)})} \int_{x_{kl(i)} - \frac{\Delta x_{kl(i-1)}}{2}}^{x_{kl(i)} + \frac{\Delta x_{kl(i)}}{2}} dx_{kl} \ldots \int_{x_{kN(j)} - \frac{\Delta x_{kN(j-1)}}{2}}^{x_{kN(j)} + \frac{\Delta x_{kN(j)}}{2}} dx_{kN} \int_{x_{ll(i)} - \frac{\Delta x_{ll(i-1)}}{2}}^{x_{ll(i)} + \frac{\Delta x_{ll(i)}}{2}} dx_{ll} \ldots \int_{x_{lN(j)} - \frac{\Delta x_{lN(j-1)}}{2}}^{x_{lN(j)} + \frac{\Delta x_{lN(j)}}{2}} dx_{lN} \; P_{t,\tau}(X_k \mid X_l) \tag{3.47}$$

The PDF at a desired time can be obtained by applying the short-time transition in equation (3.47) iteratively. Due to the fact that the MPDF of a chaotic response is

governed by a jagged curve (Kapitaniak, 1988), to avoid misinterpreting the fractal nature of the chaotic response, no interpolation techniques are used in this study.

To obtain accurate numerical results, the grid size of the discretized probability domain has to be sufficiently small. However, the computational time will increase geometrically proportional to the number of elements. To preserve the numerical accuracy and save computational time, the concept of moving boundary is employed.

For all numerical results in this study, the initial conditions are assumed deterministic, represented by the product of two Dirac delta functions

$$P(X,t_0) = \delta(x_1 - x_{10})\delta(x_2 - x_{20}) \tag{3.48}$$

which is represented by a point with area virtually zero in the phase space. Initially, the (pre-state) probability domain is set just large enough to enclose this spot, and the post-state domain after a short-time propagation is estimated based on the spreading behavior indicated by $Q_{r\mu}$ in equation (3.43). With the adjustment of the boundary for the probability domain, the numerical PIS procedure is computationally efficient.

Numerical errors could be introduced in discretizing time and the probability domain. These errors, which are functions of the size of time segment and the probability domain grid size, can be minimized by normalizing the transition tensor and PDF after each application

$$\sum_k T_{kl}(\tau)\frac{(\Delta X_k + \Delta X_{k-1})}{2} = \left[\frac{\Delta X_l + \Delta X_{l-1}}{2}\right] A_j(\Delta X_k, \tau); \quad T_{kl}^{new} \rightarrow \frac{T_{kl}^{old}}{A_l} \tag{3.49}$$

and

$$\sum_k P_k(X,t)\Delta X_k = 1 + \epsilon(\Delta X_k, \tau)$$
$$\Rightarrow P_k(X,t) = \frac{1}{1+\epsilon(\Delta X_k,\tau)} P_k(X,t) \tag{3.50}$$

By following the systematic approach described above, the FPE's and short-time propagators are obtained for the SDOF and 2DOF models in the following sections.

3.2.1.1 SDOF Model Subjected to Regular Waves with Random Perturbation

In Chapter 2, in a regular wave field with random perturbations, three governing equations are derived for the moored structural response with different approximations on the hydrodynamic and restoring forces. Among them, sensitivity of the moored structural response to the initial conditions was detected in the deterministic (no random perturbations) model with nonlinear drag and polynomial restoring force (Gottlieb, 1991). Furthermore, deterministic chaotic moored structural response was observed in the other two (linearized drag and nonlinear restoring force, and the fully nonlinear model (Gottlieb, 1991)) moored structural models. For demonstration, the moored structural model with linearized drag and nonlinear restoring force is examined in detail to determine the stochastic properties of its chaotic response behavior. Moreover, the same procedure is expanded to the fully nonlinear model as well. A generalized expression for the governing equation of the moored structural response in a slightly perturbed regular wave field is given by

$$\begin{aligned} \dot{x}_1 &= x_2 \\ \dot{x}_2 &= -R(x_1) - \gamma x_2 + F_D^d(x_2,t) + F_I^d(t) + \nu(t) \end{aligned} \tag{3.51}$$

and the associated FPE is given by

$$\begin{aligned} \frac{\partial P(x_1,x_2,t)}{\partial t} &= -\frac{\partial}{\partial x_1}[x_2 P(x_1,x_2,t)] - \frac{\partial}{\partial x_2}\Big[\Big(-R(x_1) - \gamma x_2 + F_D^d(x_2,t) \\ &\quad + F_I^d(t)\Big)P(x_1,x_2,t)\Big] + \frac{\kappa}{2}\frac{\partial^2 P(x_1,x_2,t)}{\partial x_2^2} \end{aligned} \tag{3.52}$$

where the same notations are used as those in Chapter 2. It is noted that when the linearized drag force is considered, the drag effect is included within the linear damping coefficient γ^* (see Chapter 2). For the fully nonlinear model, F_D and F_I are described by equation (2.21).

The corresponding short-time propagator $G(x_1',x_2',x_1,x_2,t;\tau)$ is given by

$$\begin{aligned} G(x_1',x_2',x_1,x_2,t;\tau) &= (2\pi\tau)^{-2}\kappa^{-\frac{1}{2}}\exp[-\frac{\tau}{2\kappa}(-R(x_1) - \gamma x_2 \\ &\quad + F_D^d(x_1,x_2,t) + F_I^d(x_1,x_2,t) - \frac{x_2' - x_2}{\tau})^2]\,\delta(x_2 - \frac{x_1' - x_1}{\tau}) \end{aligned} \tag{3.53}$$

where $[x_1',x_2']^T$ and $[x_1,x_2]^T$ represent the post-state and the pre-state, respectively.

3.2.1.2 SDOF Model Subjected to Narrow-Band Random Waves

As described in section 2.2.2, the surge response of moored structural model in a very narrow-band random wave field is governed by equation (2.26) and the energy in the spectral tails is approximated by white noise, thus, the FPE can be applied

$$\frac{\partial P(x_1,x_2,t)}{\partial t} = -\frac{\partial}{\partial x_1}[x_2 P(x_1,x_2,t)] - \frac{\partial}{\partial x_2}\{[-R(x_1)-\gamma^* x_2 + F_I^d(t)]P(x_1,x_2,t)\} + \frac{\kappa}{2}\frac{\partial^2 P(x_1,x_2,t)}{\partial x_2^2} \tag{3.54}$$

The corresponding short-time propagator is given by

$$G(x_1',x_2',x_1,x_2,t;\tau) = (2\pi\tau)^{-2}\kappa^{-\frac{1}{2}}\exp[-\frac{\tau}{2\kappa}(-R(x_1)-\gamma^* x_2 + F_I^d(t) - \frac{x_2'-x_2}{\tau})^2]\delta(x_2 - \frac{x_1'-x_1}{\tau}) \tag{3.55}$$

3.2.1.3 SDOF Model Subjected to JONSWAP Random Waves

As described in section 2.2.3, the JONSWAP wave spectrum can be approximated by a linearly filtered white noise process. As shown in equations (2.28) and (2.33), the filtering process adds two more state variables into the system. By setting

$$\begin{aligned} x_1 &= x\ ; \quad x_2 = \dot{x}\ ; \quad \eta_1 = \eta\ ; \quad \eta_2 = \dot{\eta} \\ \dot{x}_1 &= x_2\ ; \quad \dot{x}_2 = -\gamma^* x_2 - R(x_1) + \eta_1(t) \\ \dot{\eta}_1 &= \eta_2\ ; \quad \dot{\eta}_2 = -\beta_n \eta_2 - (2\pi f_0)^2 \eta_1 + \xi(t) \end{aligned} \tag{3.56}$$

then the FPE is given by

$$\frac{\partial P(x_1,x_2,\eta_1,\eta_2,t)}{\partial t} = -\frac{\partial[x_2 P]}{\partial x_1} - \frac{\partial\{[-R(x_1)-\gamma^* x_2+\eta_1]P\}}{\partial x_2} - \frac{\partial[\eta_2 P]}{\partial \eta_1} + \frac{\partial\{[-\beta_n\eta_2 - (2\pi f_0)^2\eta_1]P\}}{\partial \eta_2} + \frac{\kappa}{2}\frac{\partial^2 P}{\partial \eta_2^2} \tag{3.57}$$

and the associated sort-time propagator is given by

$$G(x_1',x_2',\eta_1',\eta_2',x_1,x_2,\eta_1,\eta_2,t;\tau) = (2\pi\tau)^{-4}\kappa^{-\frac{1}{2}}\exp\left[-\frac{\tau}{2\kappa}(\sigma^2\eta_2+\Omega_f^2\eta_1 + \frac{\eta_2'-\eta_2}{\tau})^2\right]\delta(-\gamma^* x_2 - R(x_1)+\eta_1-\frac{\eta_2'-\eta_2}{\tau}) \quad (3.58)$$
$$\delta(x_2-\frac{x_1'-x_1}{\tau})\delta(\eta_2-\frac{\eta_1'-\eta_1}{\tau})$$

Applying the discretization based on path sum (section 3.2.1) to the above short-time propagators, the associated transition tensors can be derived. The PDF at a desired time is obtained by repeated application of the transition tensor. The resulting PDF's will be used as an analytical tool to interpret experimental results.

3.2.1.4 2DOF Model Subjected to Regular Waves with Random Perturbations

Due to the complexity of the 2DOF model, only the hydrodynamic exciting forces induced by regular waves with random perturbations is considered here for demonstration. Using the white noise approximation to the randomness in the exciting forces (equation (2.9)), the equations of motion for a stochastic 2DOF moored structural model was derived in Chapter 2 (equation (2.24)). The associated FPE is obtained by adding two additional state variables x_3 and x_4 describing heave displacement and velocity, respectively

$$\frac{\partial P(x_1,x_2,x_3,x_4,t)}{\partial t} = -\frac{\partial}{\partial x_1}(x_2 P)-\frac{\partial}{\partial x_3}(x_4 P)-\frac{\partial}{\partial x_2}\left[(-R_1-\gamma_1 x_2+F_{D1}^d+F_{I1}^d)P\right] \quad (3.59)$$
$$-\frac{\partial}{\partial x_4}\left[(-R_3-\gamma_3 x_4+F_{D3}^d+F_{I3}^d)P\right]+\frac{\kappa_1}{2}\frac{\partial^2 P}{\partial x_2^2}+\frac{\kappa_3}{2}\frac{\partial^2 P}{\partial x_4^2}$$

The corresponding short-time propagator $G(x_1',x_2',x_3',x_4',x_1,x_2,x_3,x_4,t;\tau)$ is given by

$$G(X',X,t;\tau) = (2\pi\tau)^{-4}\sqrt{\kappa_1\kappa_3}\exp\left[-\frac{\tau}{2\kappa_1}(-R_1-\gamma_1 x_2+F_{D1}^d+F_{I1}^d-\frac{x_2'-x_2}{\tau})^2\right.$$
$$\left.-\frac{\tau}{2\kappa_3}(-R_3-\gamma_3 x_4+F_{D3}^d+F_{I3}^d-\frac{x_4'-x_4}{\tau})^2\right] \qquad (3.60)$$
$$\delta(x_2-\frac{x_1'-x_1}{\tau})\,\delta(x_4-\frac{x_3'-x_3}{\tau})$$

where X' and X represent $[x_1',x_2',x_3',x_4']^T$ and $[x_1,x_2,x_3,x_4]^T$, the post-state and the pre-state, respectively.

It is noted that in all the FPE's derived the drift vectors are periodic in time, thus the resulting PDF's are also periodic (Stratonovich, 1967). To suppress the periodicity and depict the evolution of PDF, the transient and steady states of PDF are sampled at integer multiples of the forcing period (Poincaré section). Invariant properties of the steady-state PDF on Poincaré section will be demonstrated in a later Chapter.

3.2.2 Notes on Numerical Evaluation of Path Integral Solution

As demonstrated previously, the PIS is a first order Euler approximation (Wissel, 1979), and one possible numerical evaluation based on lattice representation (path sum) (Wehner and Wolfer, 1983) can be applied to implement the PIS numerically. Using this standard numerical procedure, the results can demonstrate the evolution of JPDF and its steady state can depict the existing response attractors of strong attraction (i.e., even with small amount of uncertainty, the response trajectory is contained in the attractor and does not diverge; see Lin and Yim, 1994).

However, the chaotic response in the moored structural system is of weak stability, and a small amount of uncertainty may skew the numerical results. Figure 3.1a shows a sample deterministic chaotic moored structural response. Adding white noise perturbation to formulate the FPE and using the standard numerical evaluation as described in section 3.2.1 for the PIS the corresponding JPDF is shown in Fig.3.1b.

The obscurity in the JPDF implies a divergent numerical result (even with very weak white noise added). The diverging numerical result is caused by the combination of numerical error in the numerical evaluation (first order iteration as described in Lin and Yim, 1994) and the weak stability of chaotic moored structural response. In order to depict the existing chaotic attractor via the JPDF, improvement over the first order Euler approximation is needed for the numerical evaluation of the PIS. In this study, a fourth-order Runge-Kutta integration procedure is employed to compute the deterministic response trajectory more precisely for the mean of each propagation. Applying the same iterative procedure as described previously, more accurate numerical results are obtained for the JPDF.

3.3 Time Domain Simulations

Time domain simulations can be implemented by numerically integrating the governing equation (2.29) with respect to time. Realizations of the moored structural response subjected to monochromatic regular waves with white noise are obtained using a Runge-Kutta fourth order integration scheme. The numerical representation of Gaussian white noise selected here is based on the Shinozuka's method (1977), which characterizes a Gaussian noise of zero mean, limited frequency bandwidth $[\omega_{min}, \omega_{max}]$,

a)

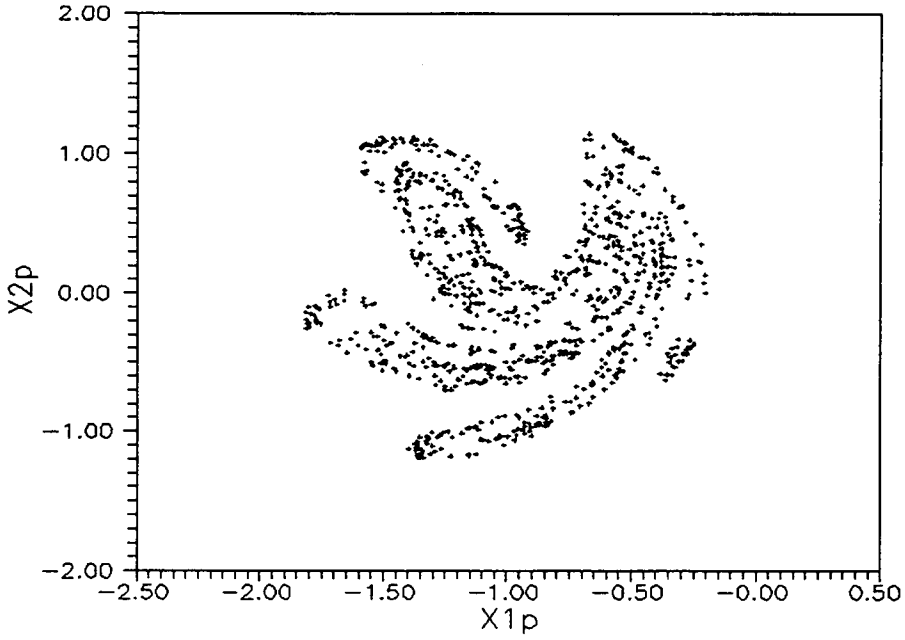

b)

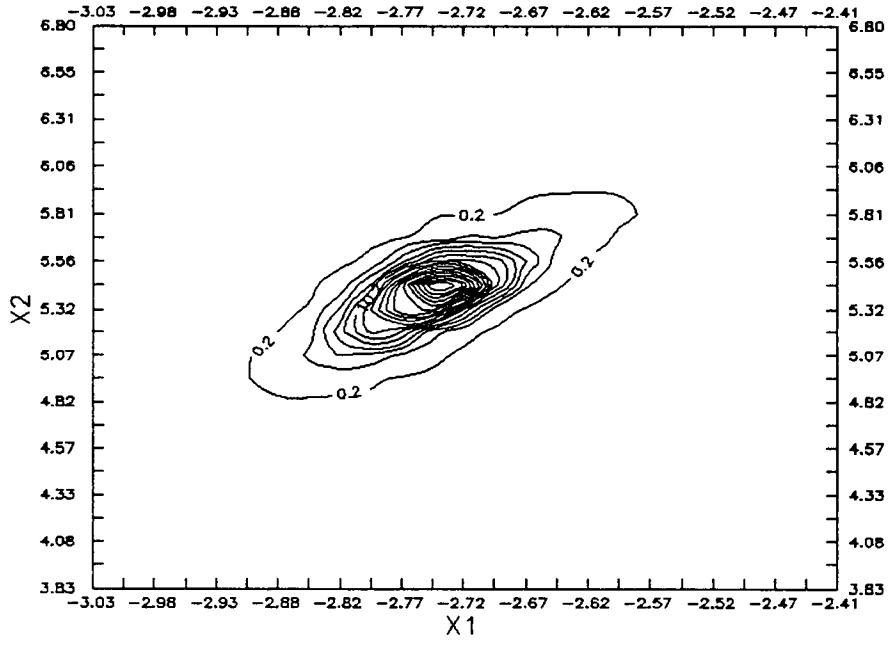

Figure 3.1 Standard numerical evaluation of PIS for system response: a) deterministic chaotic attractor in Poincaré map; b) associated JPDF on Poincaré section (numerical result diverges after 24 seconds)

and finite variance (See Chapter 2 for details). In order to achieve a good approximation, the number of harmonics in equation (2.10) must be sufficiently large (e.g., $N > 30$ according to Kapitaniak (1988)). The number of harmonics in equation (2.10) is chosen 50 for an adequate representation of Shinozuka's Gaussian noise in this investigation.

Numerical representations of the narrow-band and JONSWAP random waves can be implemented following the above procedure. For both wave spectra, the frequency range is equally divided into small segments and the corresponding strips are formed in the spectrum. The area of each strip denotes the input energy, which is equivalent to a sinusoidal excitation with a random phase shift and a random frequency with mean located at the center of the frequency segment. The total energy due to a narrow-band spectrum imposed to the moored structural system is equivalent to the sum of all sinusoidal excitations. Thus a single realization of the narrow-band random waves can be represented by

$$\xi_{nb}(t) = \sum_{k=1}^{N_s} A_k \cos(\omega_k t + \phi_k) \tag{3.61}$$

where the A_k's are the amplitudes of the harmonics, which are modulated by the shape of the narrow-band spectrum

$$A_k = \sqrt{2 S_{nb}(\omega_k) \Delta\omega} \tag{3.62}$$

the ω_k's represent the central frequency for each strip, and

$$\omega_k = (k-0.5)\Delta\omega + \delta\omega_k + \omega_{\min} \tag{3.63}$$

where

$$\Delta\omega = \frac{\omega_{\max} - \omega_{\min}}{N} \tag{3.64}$$

The $\delta\omega_k$'s are independent random variables uniformly distributed in the interval $[-\Delta\omega/2, \Delta\omega/2]$, and ϕ_k's are the random phase shifts, which are uniformly distributed in $[0, 2\pi]$. The number of harmonics N_s is selected as 100 in this study for an appropriate description.

Note that, in the Markov approach, a narrow-band spectrum may be approximated by a dominant periodic excitation with an appropriate amount of noise. For the purpose of comparison, the energy contribution from the peak frequency of the narrow-band spectrum in the simulations and that from the dominant frequency of the Markov approach is held identical. Thus, the tails of the narrow-band spectrum can be approximated by the white noise perturbation.

3.4 Mean Poincaré Map

It is well known that the fractal structure of a chaotic attractor can be depicted on the Poincaré map (Thompson and Stewart, 1986). However, this structure is obscured by the presence of noise. As proposed by Kapitaniak (1988), the noise-induced obscurity can be minimized and the fractal structure can be clarified by introducing the mean Poincaré map, which is defined as

$$M_k = \{(<x_1(t)>, <x_2(t)>) \mid t = kT,\ k = 1, 2, \ldots\} \tag{3.65}$$

where T is the forcing period. M_k represents the mean Poincaré point at the k^{th} cycle of forcing period; x_1 and x_2 are the displacement and velocity obtained from equation (2.14). $<x_1>$ and $<x_2>$ represent the ensemble averages of x_1 and x_2, respectively, with realizations obtained through direct numerical simulations. Thus, the mean Poincaré map takes the ensemble average after each mapping as initial condition for the next iteration. This mapping technique can average out the noise effect and amplify the structure of the existing chaotic attractor.

4. STOCHASTIC ANALYSIS OF NONLINEAR SYSTEM RESPONSE

Nonlinear responses of a periodically driven deterministic moored structure have been examined via stability analysis, and the underlying super-structure in the bifurcations indicates possible existence of chaotic response (Gottlieb, 1991). Nonlinear responses including sub-harmonic, super-harmonic, and chaos were found in corresponding numerical simulations. In this study, the effects of the randomness of waves on the nonlinear structural responses will be investigated from a probabilistic perspective. The wave fields considered include regular waves with white-noise random perturbations, narrow-banded random waves, and JONSWAP random waves. Theoretical predictions based on a generalized stochastic Melnikov function (see Chapter 3 for details) are confirmed by numerical results. The PIS procedure based on the Markov process approach using FPE is implemented numerically. Numerical predictions from the PIS procedure are also compared with time domain simulations.

4.1 Regular Waves with Random Perturbations

As discussed in Chapter 2, imperfect monochromatic regular waves can be characterized by a sinusoidal function with additive random perturbations (noise). Lin and Yim (1994) demonstrated the presence of noise bridges the domains of attraction for (co-) existing response attractors, and provides a scale for the relative strengths of coexisting response attractors. With noise intensity as the controlling parameter, highly nonlinear phenomena (e.g., coexisting attractors and chaos) relating to the instability of responses are examined in the following sections.

4.1.1 Coexisting Attractors

Bifurcations in deterministic moored structural response have been examined via stability analysis (Gottlieb, 1991). The associated backbone curve showing possible coexisting attractors of a typical nonlinear moored structural system is shown in Fig.4.1. By fixing the system parameters and varying the initial conditions, coexisting periodic responses may be obtained. Figure 4.2 shows two coexisting periodic responses (small- and large-amplitude) in the phase plane with initial conditions at (0,0) and (1,-2) respectively, where symbol "*" denotes the corresponding Poincaré points.

By following the Markov process approach presented in Chapter 3, the PDF of the nonlinear stochastic moored structural response can be obtained. Coexisting response attractors can be demonstrated in the probability domain using the PDF. The evolution of PDF is depicted by repeatedly sampling its transient and steady state on a Poincaré section (integer multiple of excitation period).

Near the bifurcation point with weak random noise present (κ=0.007), the transient (Figs.4.3a-c) and the steady-state (Fig.4.3d) PDF's are shown. When the system is excited under quiescent initial conditions, i.e. (0,0) (see Fig.4.3a), the response trajectories reside in a periodic attractor (small amplitude) after four cycles of the forcing period (Fig.4.3b). The response trajectories start to shift from the attractor (small amplitude) to the coexisting attractor (large amplitude) after 8 cycles of the forcing period (Fig.4.3c). The probability of the trajectories to stay in the coexisting attractor (large amplitude) increases after 12 cycles of the forcing period (Fig.4.3d). The steady-state PDF is observed after 16 cycles of the forcing periods (Figs.4.3e and f) and it

clearly depicts coexisting periodic responses. Thus with noise present, the precision of the initial conditions becomes less significant to observe the coexisting responses, and the associated PDF provides a global information about the system behavior.

The noise effects on the coexisting nonlinear responses are examined in Figs.4.4 a-f. When the intensity of the noise present is very low (κ=0.003), the PDF is concentrated at the domain of small-amplitude response (Fig.4.4a), indicating its stronger attracting strength relative to the coexisting large response attractor. Thus the moored structural system oscillator mainly (most of the time) with small motions with a small probability of excursion to large amplitude motions (i.e. rarely visits the large amplitude domain). When the noise intensity increases (κ=0.007), the domains of attraction of the coexisting responses begin to bridge as shown in Fig.4.4b. Characteristics of both attractors (small and large amplitudes) may exhibit in the moored structural response behavior. When the noise intensity is moderate (κ=0.02), the attractors further emerge into a single attraction domain (Fig.4.4c), in which no obvious periodic response can be distinguished. The variation the boundary of the emerged attraction domain is stabilized when the noise intensity further increases (Figs.4.4d-f). The "orderness" still can be observed in the PDF with κ=0.1 (Fig.4.4d), which indicates that the periodicity may exhibit in the system response. The smooth curve and the stationary boundary of the PDF (Figs.4.4e and f) implies strong randomness in the system behavior.

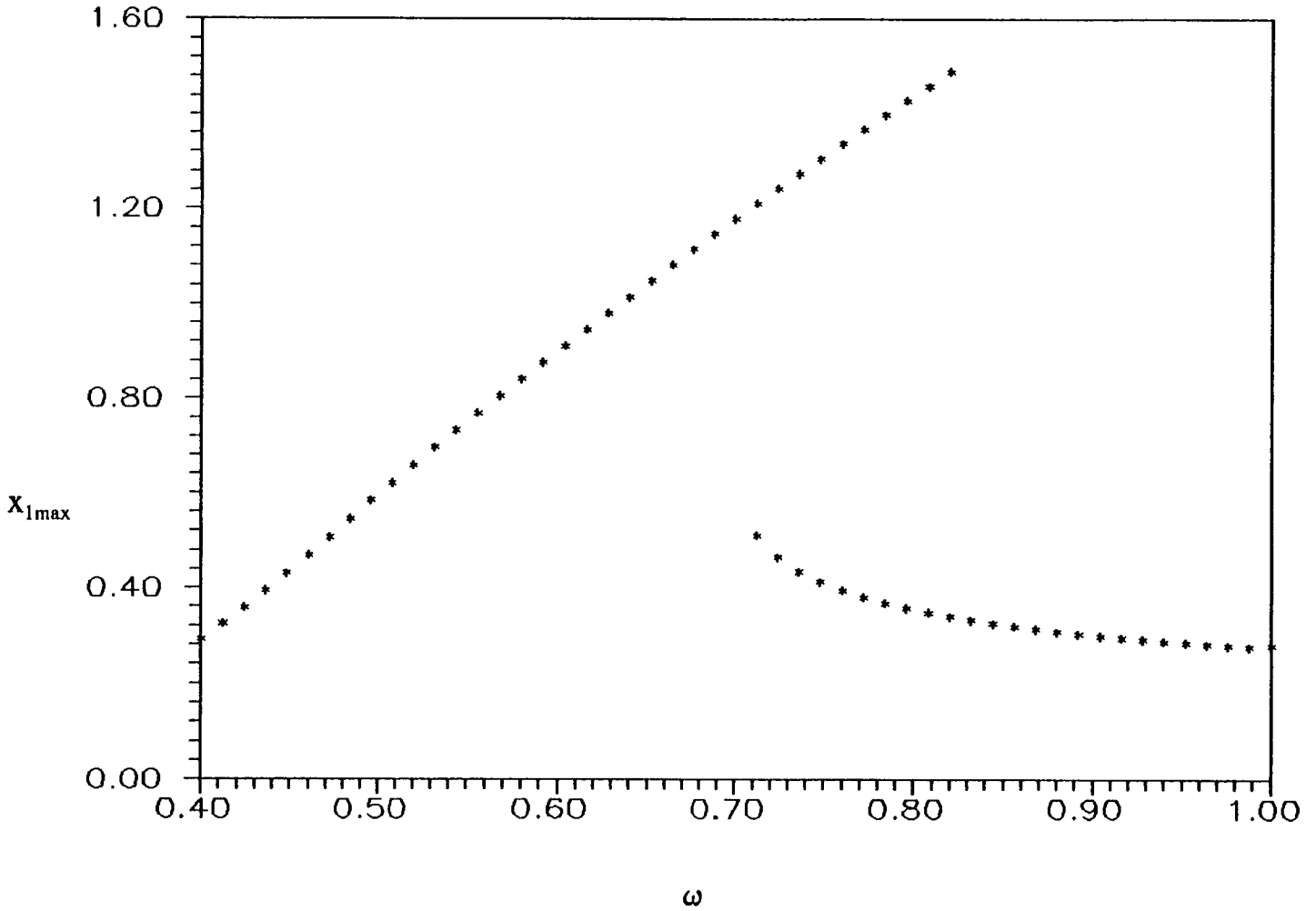

Figure 4.1 Backbone curve (model with nonlinear drag and polynomial restoring force); $(k_1,k_3,\gamma,\delta,\mu,A)=$ (0.25,0.3,0.01,0.05,1.0,0.2)

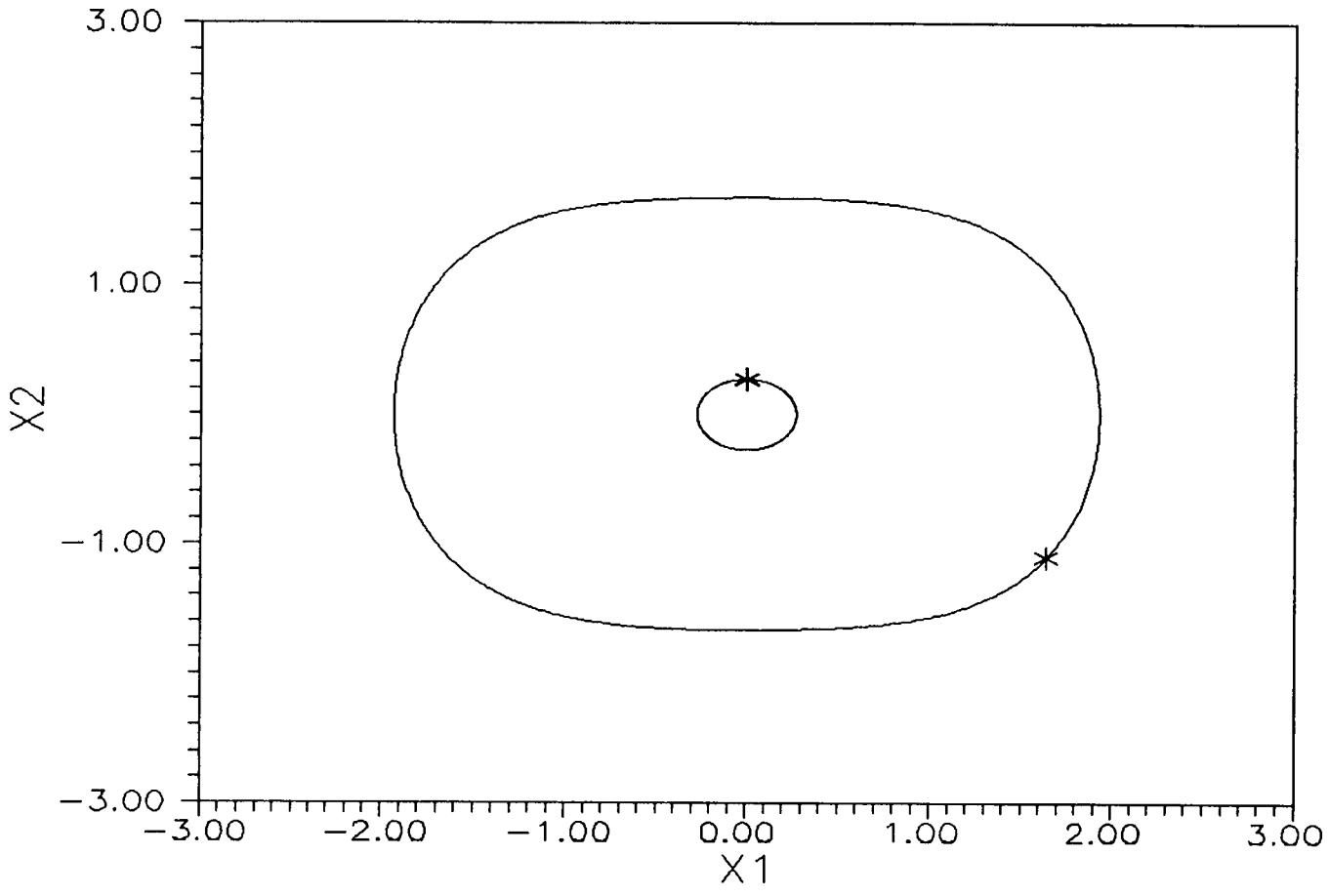

Figure 4.2 Phase trajectories and corresponding Poincaré points (*) of coexisting periodic responses; $(k_1,k_3,\gamma,\delta,\mu,A)=$ (0.25,0.3,0.01,0.05,1.0,0.2)

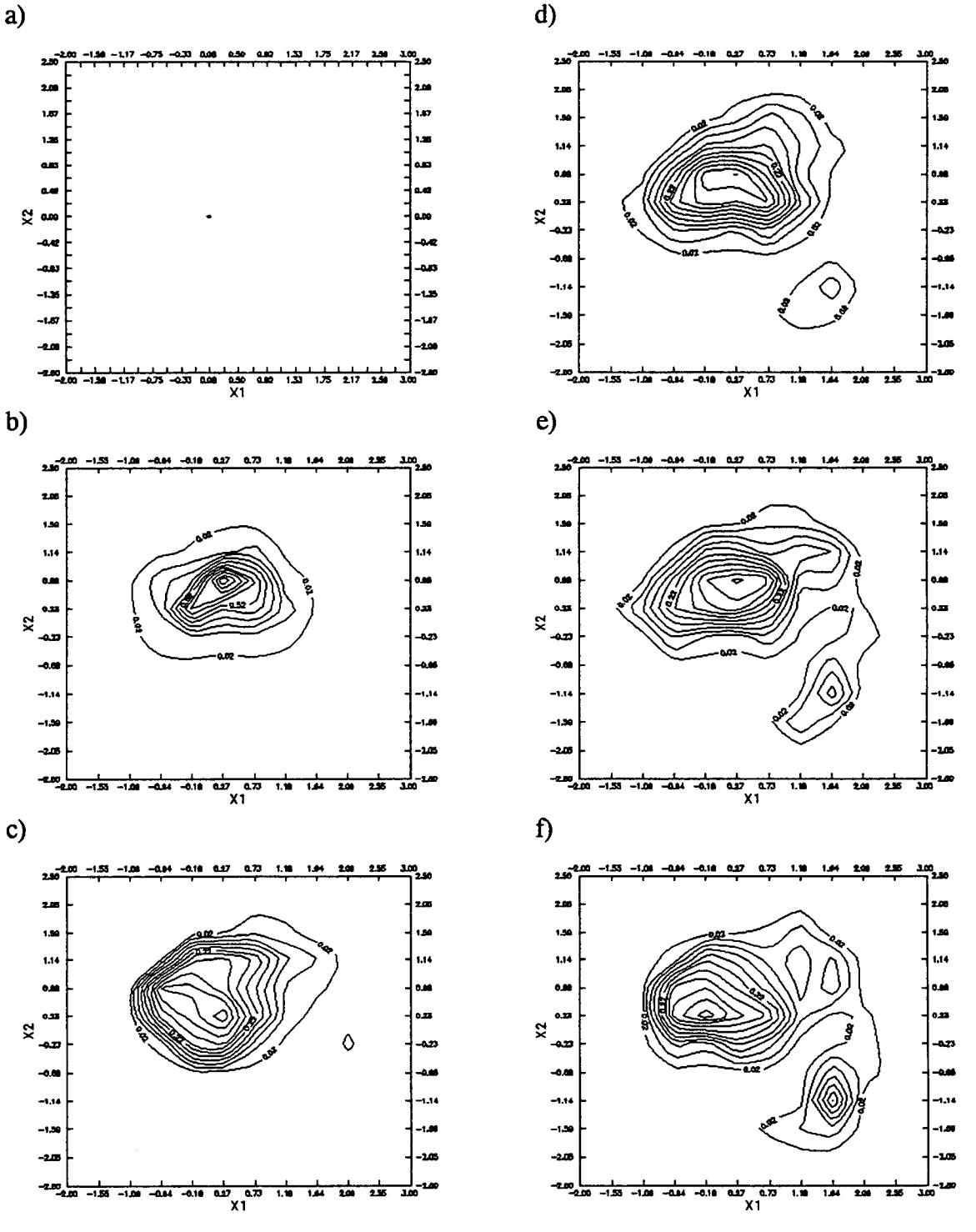

Figure 4.3 Evolution of PDF of coexisting periodic responses: a) initial condition, b) 4th cycle, c) 8th cycle d) 12th cycle, e) 16th cycle and f) 20th cycle; $(\alpha,\beta,\gamma,\delta,\mu,A,\omega,\kappa)=(0.25,0.3,0.01,0.05,1.0,0.2,1.0,0.007)$

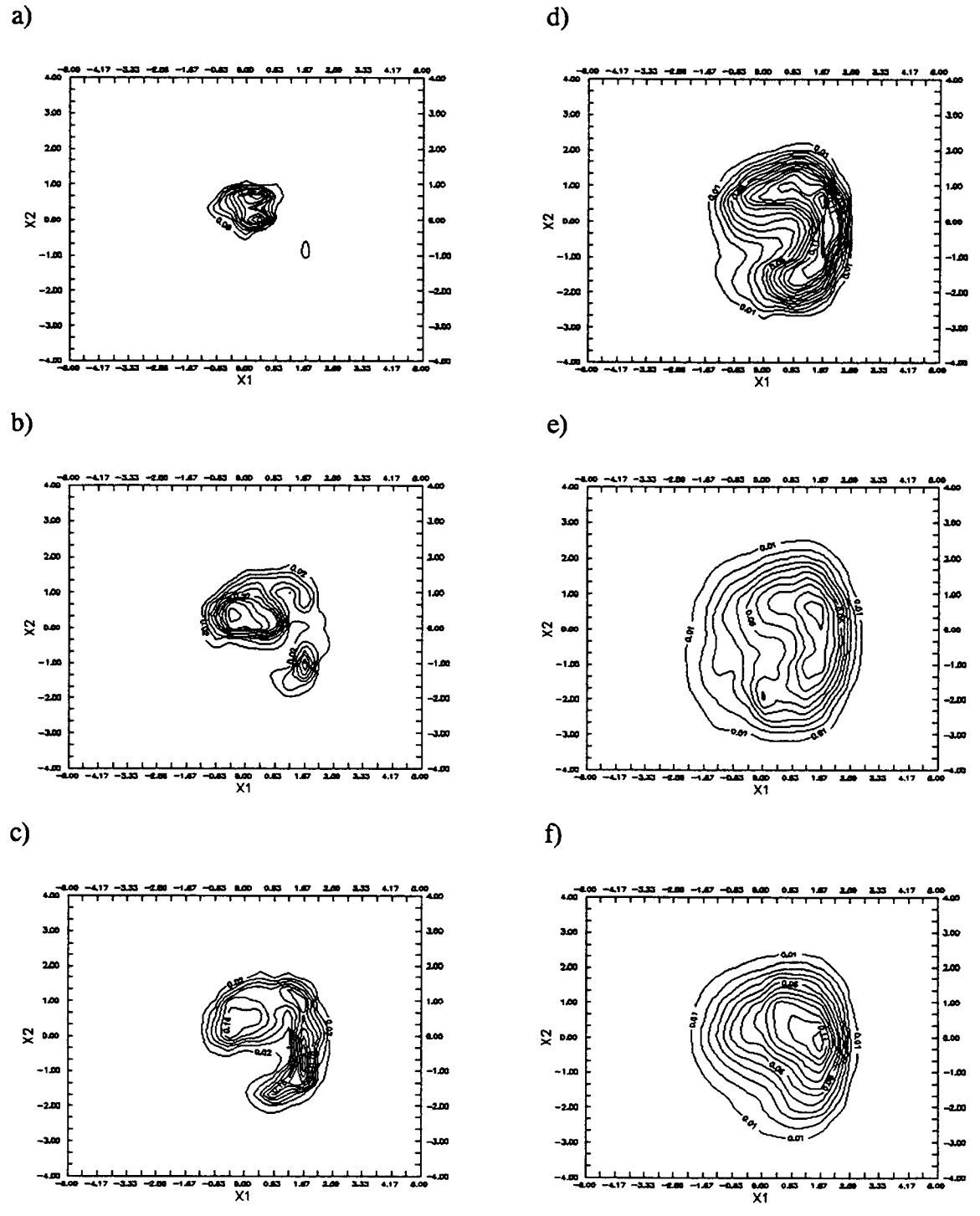

Figure 4.4 Coexisting periodic responses with increasing noise intensity (JPDF's); κ=a) 0.003, b) 0.007, c) 0.02, d) 0.1, e) 0.3 and f) 0.4; $(\alpha,\beta,\gamma,\delta,\mu,A,\omega)=(0.25,0.3,0.01,0.05,1.0,0.2,1.0)$

4.1.2 Noise-Induced Chaotic Response

It is well-known that, by varying system parameters, a deterministic nonlinear response may shift from one attractor to another, even to chaos (Moon, 1985; Thompson and Stewart, 1986). On the other hand, the presence of weak noise may expedite the occurrence of chaotic response in the parameter space (based on the generalized stochastic Melnikov criterion in Chapter 3). Transitions in response from one attractor to another caused by the variation of the excitation amplitude and of the noise strength are demonstrated and compared in this chapter.

As an example, for the parameters specified in Fig.4.5 in the deterministic moored structural system, by increasing the excitation amplitude, the response shifts from a period-2 sub-harmonics, to a higher order sub-harmonics, to a chaotic attractor, and then to another chaotic attractor (Figs.4.5a-d, respectively). In a stochastic environment, with the same parameters as its deterministic counterpart specified in Fig.4.5a, a similar transition among response attractors can be observed when the noise intensity is increased (Figs.4.6a-d). Figure 4.6a (which is identical to Fig.4.5a) shows a deterministic period-2 sub-harmonic response ($\sigma^2 = 0.0$), and under the same system parameters, the moored structural response becomes chaotic with the presence of weak noise ($\sigma^2 = 0.01^2$) (Fig.4.6b). When the noise intensity is further increased ($\sigma^2 = 0.02^2$), the response shifts to another chaotic attractor (Fig.4.6c). When the noise intensity is relatively strong, increasing noise intensity in the excitations increases the randomness in the response ($\sigma^2 = 0.07^2$) (Fig.4.6d).

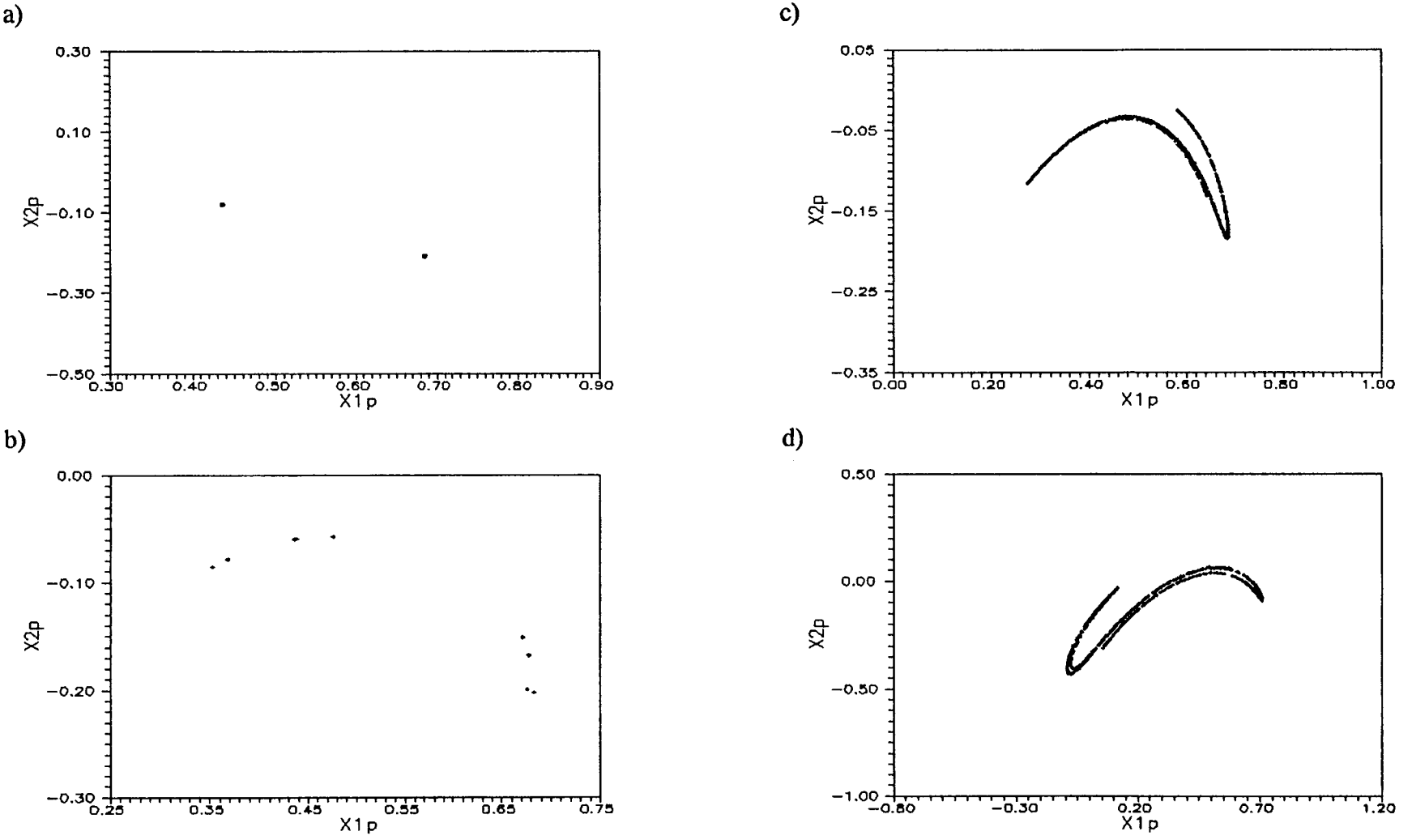

Figure 4.5 Transition of system response with increasing excitation amplitude: A = a) 15, b) 16, c) 17 and d) 20; $(\alpha,\beta,\gamma,\delta,\mu,\omega)=(4.0,0.0,0.001,0.01,1.0,0.32)$

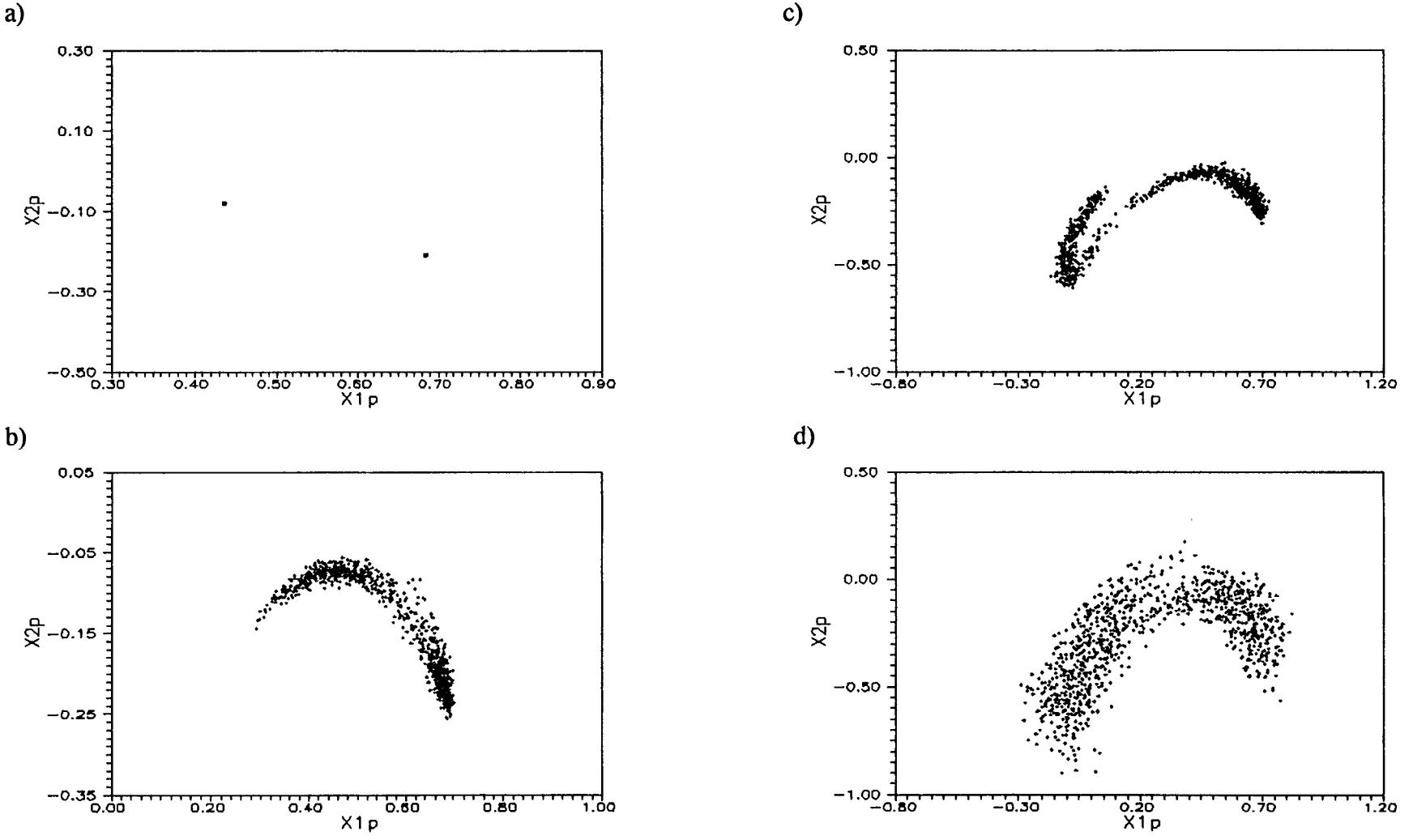

Figure 4.6 Noise-induced transition of system response; σ^2 = a) 0.0^2, b) 0.01^2, c) 0.02^2 and d) 0.07^2; $(\alpha,\beta,\gamma,\delta,\mu,A,\omega)$= (4.0,0.0,0.001,0.01,1.0,15.0,0.32)

Note that the chaotic attractors observed via Poincaré map in both cases (deterministic (Figs.4.5b and c) and stochastic (Figs.4.6b and c) are of the same shape, indicating transitions induced by both deterministic and stochastic parameter variations follow the same route. Thus the noise intensity can also be considered as a controlling parameter between different response attractors in the parameter space.

4.1.3 Nonlinear Stochastic Response

The occurrence of deterministic chaotic response of the moored structural system has been predicted by Gottlieb (1991). With the presence of noise, the probabilistic properties of this nonlinear response and the corresponding noise-induced transition to a random state are examined here via transient and steady-state PDF's.

Figures 4.7a and c show two sample deterministic chaotic moored structural response on Poincaré maps (obtained by sampling data-points from the response time history at integer multiples of the forcing period). The corresponding JPDF's (Figs.4.7b and d) can be obtained by adding a low intensity random noise (κ=0.001) to the system and solving the associated FPE using the PIS procedure. It is observed that the steady-state JPDF's can portray the fractal details of the deterministic chaotic attractors on the Poincaré section.

The evolutions of the PDF's in Figs.4-7b and d are demonstrated in Figs.4.8a-d and 4.8a-d, respectively. For both cases, the moored structural system response starts with deterministic quiescent conditions, i.e. a delta function at (0,0) in the probability domain (Figs.4.8a and 4.9a). Initially, the JPDF's spread with time (Figs.4.8b and 4.9b), and move toward the chaotic attractors and begin to cover the attracting domains

(Figs.4.8c and 4.9c). After 10 cycles of the forcing period, the PDF's reach their steady states (Figs.4.8d and 4.9d) and indicate probabilistic information of the corresponding strange attractors.

The noise effects on a sample chaotic attractor are examined by varying the noise intensities (Figs.4.10a-d). The fractal details of the chaotic attractor is preserved (Fig.4.10a) when the additive noise is of low intensity (κ=0.0003). The boundary of the chaotic attractor becomes obscured as the noise intensity increases to 0.001 (Fig.4.10b). When the noise intensity κ is further increased to 0.007, the domain of the attractor becomes more obscured and the fractal details of the boundary of the attractor diminish. In fact, it becomes difficult to identify the chaotic attractor from the shape of the observed boundary (Fig.4.10c). Randomness in the response increases further as the noise intensity increases to 0.02 (Fig.4.10d). It is noted that the structure of the attracting domain is smoothed even with very low noise intensity ($\kappa \geq 0.001$), which indicates the strong sensitivity to the random noise and the weak stability of the chaotic attractor.

The noise intensity effects on the chaotic response is demonstrated next via time domain simulations. Figures 4.11a-f show Poincaré maps of system responses with increasing noise intensity. Note that the structure of the strange attractor becomes obscured when the noise variance is 0.05^2 or higher (Figs.4.11c-f). These numerical results again indicate that the chaotic system response is of weak stability, and with low intensity random perturbations the fractal structure deteriorates. However, it is clear

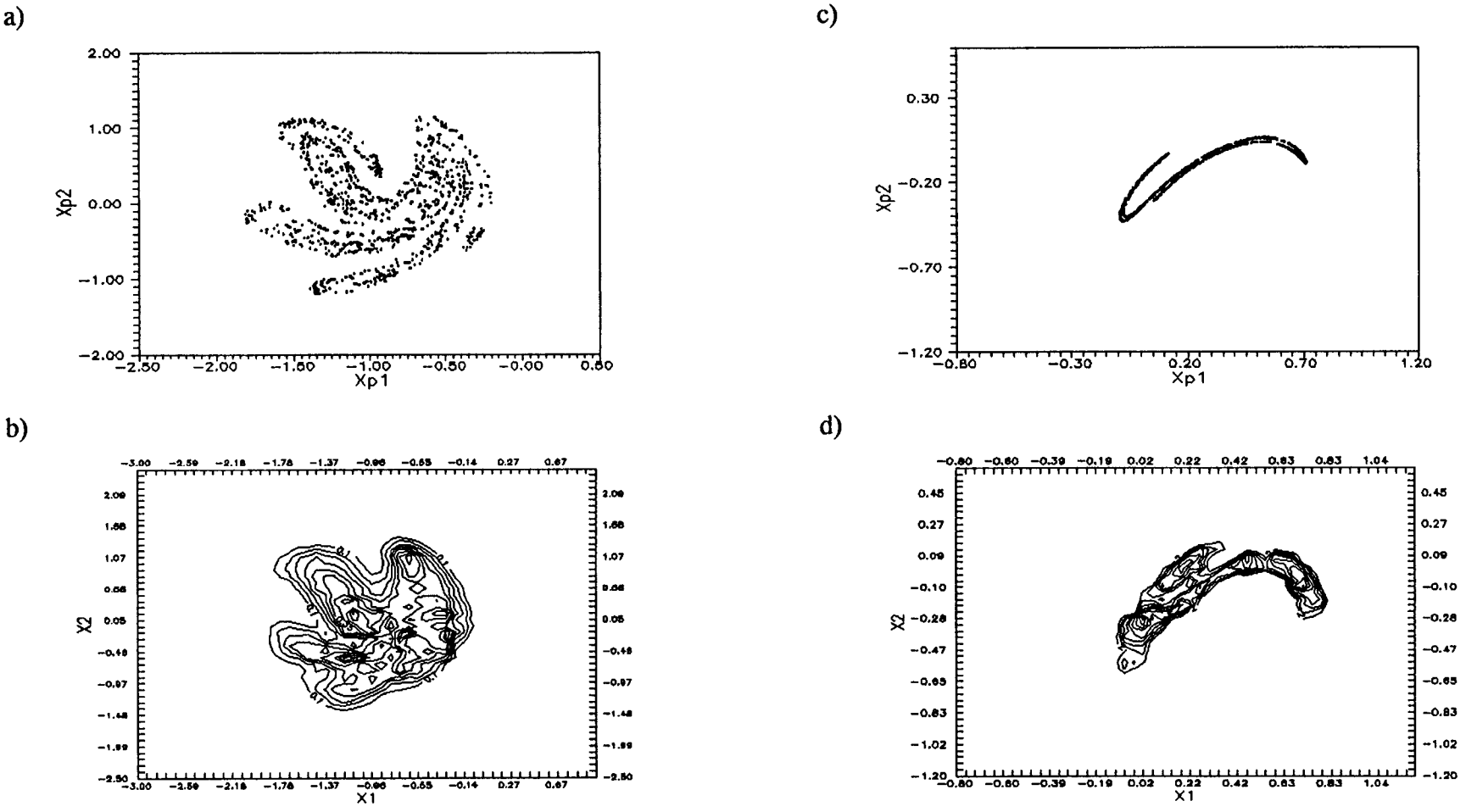

Figure 4.7 Chaotic responses (Poincaré maps and JPDF's): a) simulation, b) JPDF (κ=0.001) and (α,β,γ^*,μ,A,ω) =(4.0,0.0,0.01,1.0,2.0,0.32); and c) simulation, d) JPDF (κ=0.0003) and (α,β,γ,δ,μ,A,ω) =(4.0,0.0,0.001,0.01,1.0,20.0,0.32)

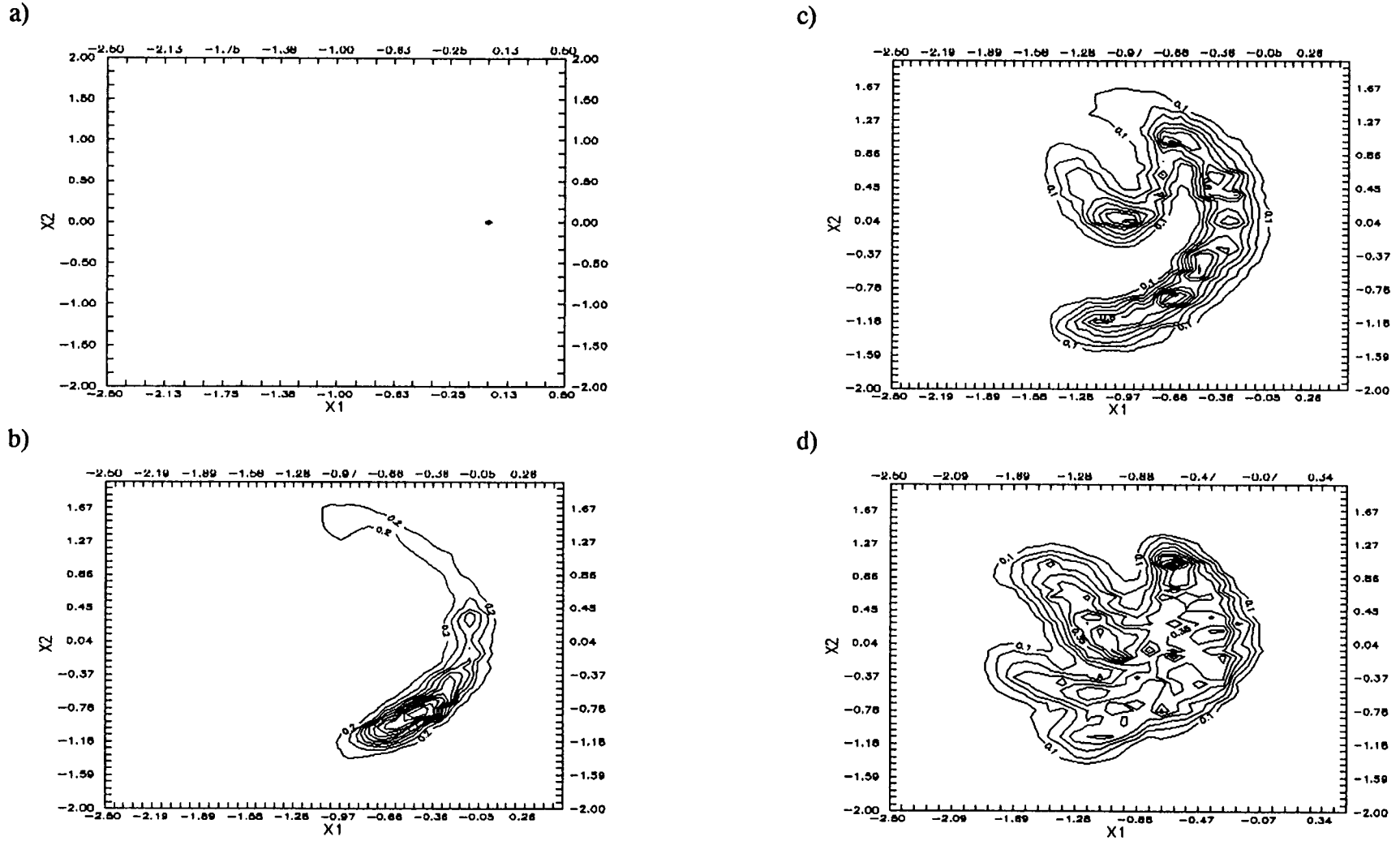

Figure 4.8 Evolution of PDF of chaotic response: a) initial conditions, b) 2nd cycle, c) 4th cycle and d) 10th cycle of the forcing period; $(\alpha,\beta,\gamma^*,\mu,A,\omega,\kappa)=(4.0,0.0,0.01,1.0,2.0,0.32,0.001)$

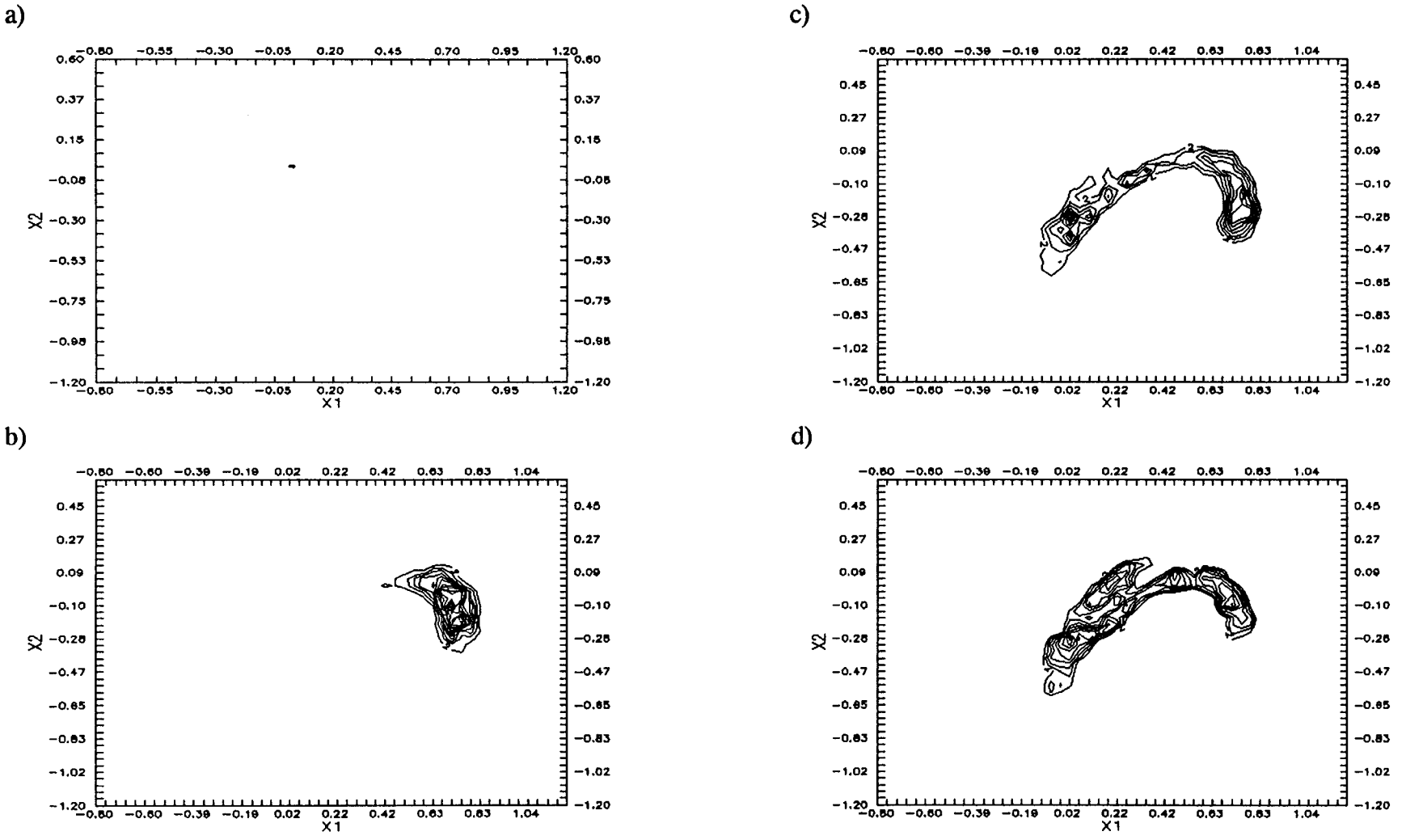

Figure 4.9 Evolution of PDF of chaotic response with weak attraction: a) initial conditions, b) 2nd cycle, c) 5th cycle and d) 10th cycle of the forcing period; $(\alpha,\beta,\gamma,\delta,\mu,A,\omega)=(4.0,0.0,0.001,0.01,1.0,20.0,0.32)$

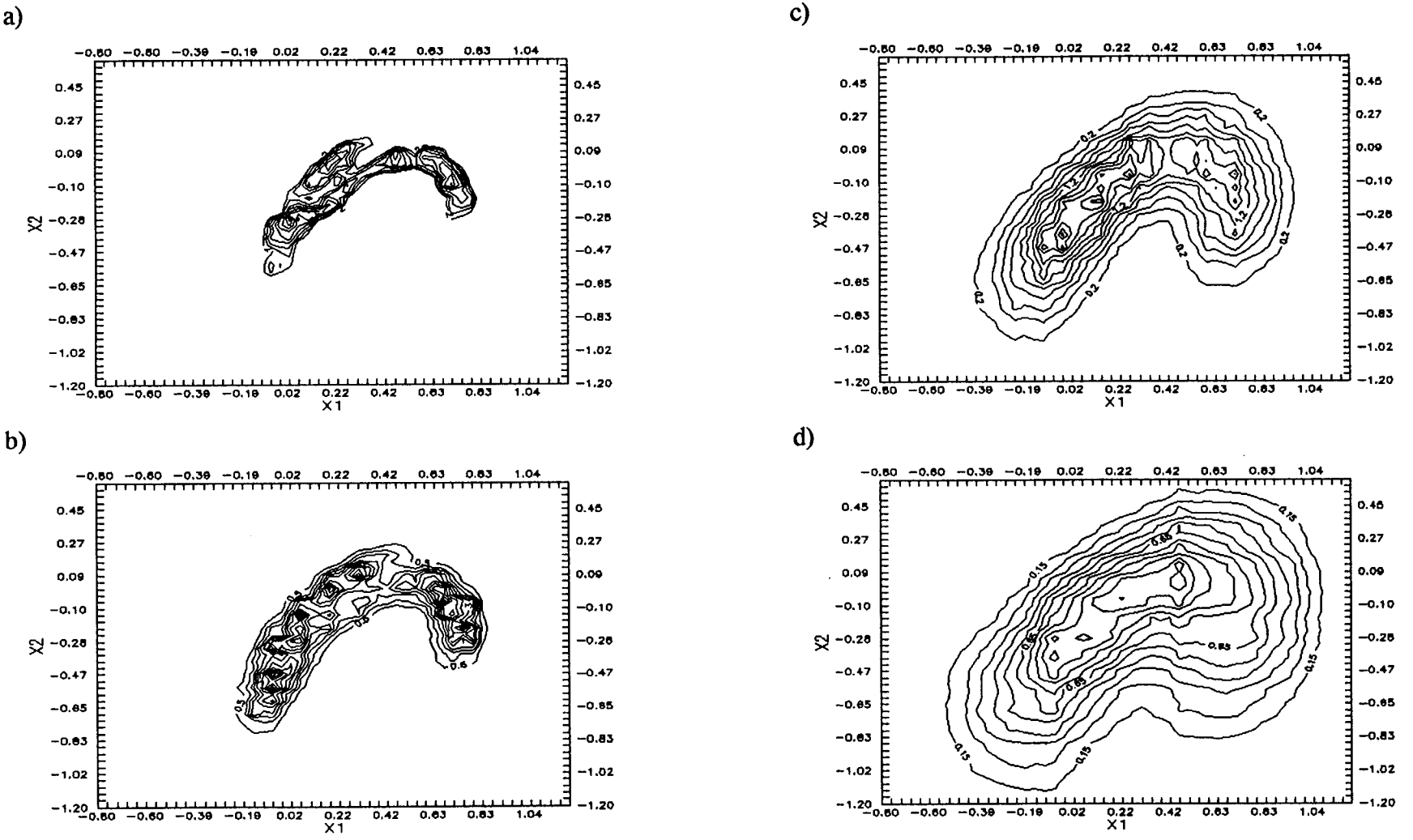

Figure 4.10 Transition of PDF with increasing noise intensity: κ=a) 0.0003, b) 0.001, c) 0.007 and d) 0.02; $(\alpha,\beta,\gamma,\delta,\mu,A,\omega)$= (4.0,0.0,0.001,0.01,1.0,20.0,0.32)

that, except for the case with high random noise intensity (Fig.4.11f), the chaotic attractor is still embedded in the noisy environment.

To enhance the analysis of the chaotic behavior of a nonlinear system, the technique of mean Poincaré map, which is used to reconstruct the embedded strange attractor, has been employed in the literature. This mapping technique (see Chapter 3 for details) averages out the noise effect at each Poincaré sampling, and then use the averaged Poincaré point as the initial condition for the next mapping. The capability of this mapping technique to identify potential chaotic response depends upon the intensity of randomness and the stability of the attractor.

Figures 4.11a-f show a single chaotic system response perturbed by noise with different intensities in the Poincaré map. Figures 4.11a and b show a purely deterministic chaotic response and a weakly perturbed chaotic response, respectively, while Figs.4.11c, d, e and f exhibit increasingly strongly perturbed chaotic responses. No strange attractor can be observed in Figs.4.11d, e and f. However, the perturbed attractors may be reconstructed by applying the mean Poincaré map technique (Kapitaniak, 1988). The capability of this technique is indicated by Figs.4.12a-d. When σ^2 is less than 0.05^2, the fractal details of the embedded strange attractor can be reconstructed. When σ^2 is larger than 0.05^2, even the mean Poincaré map fails to trace and reconstruct the attractor, which indicates that the chaotic attractor is weakly stable and its structure is destroyed by the presence of noise.

Thus, in general, in the analysis of observed (experimental or simulated) time series, the presence of random noise in the system can obscure the existence of chaotic

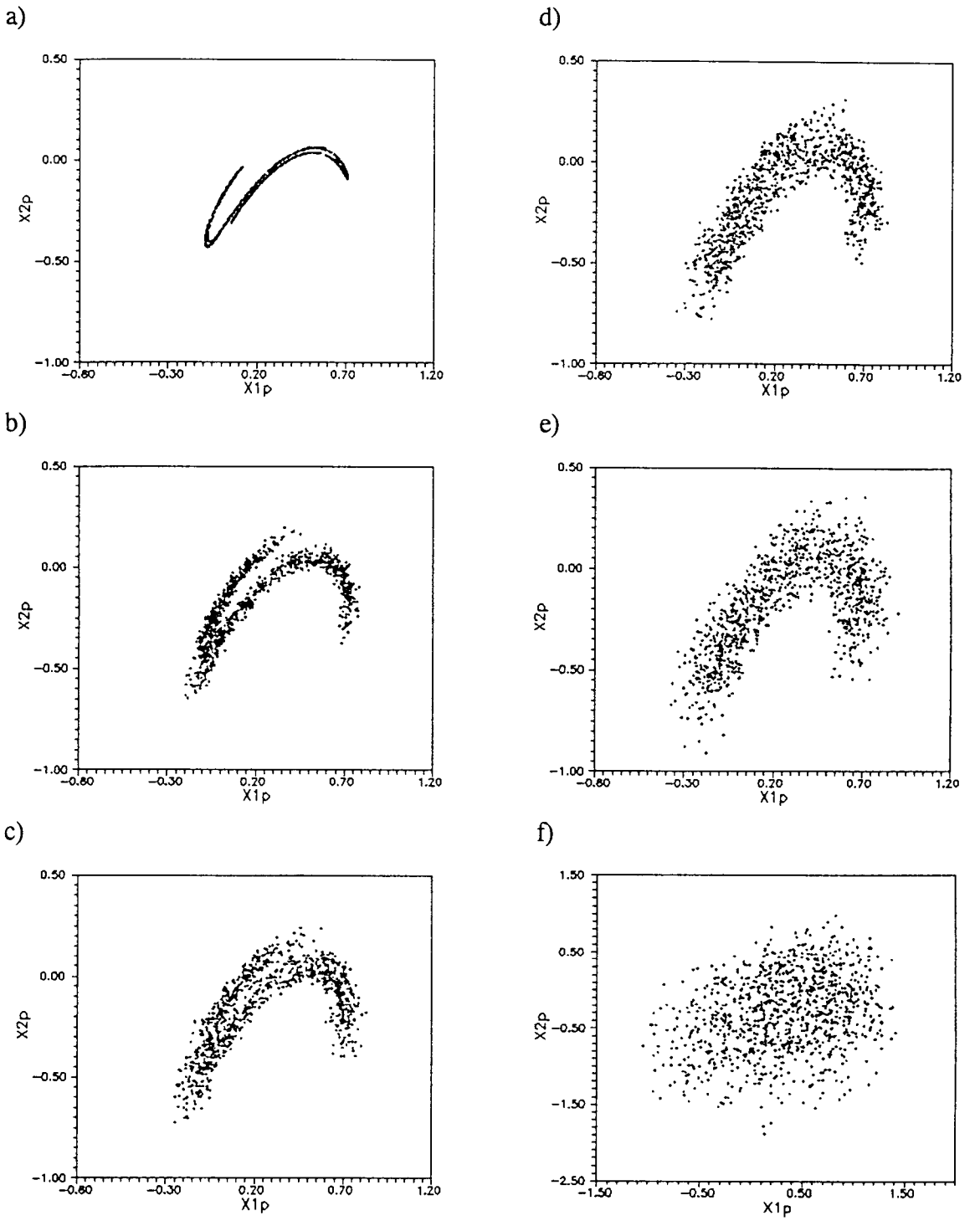

Figure 4.11 Noise effects on system response (Poincaré map): σ^2 = a) 0.0^2, b) 0.03^2, c) 0.05^2, d) 0.07^2, e) 0.10^2 and f) 0.40^2; $(\alpha,\beta,\gamma,\delta,\mu,A,\omega)$= (4.0,0.0,0.001,0.01,1.0,20.0,0.32)

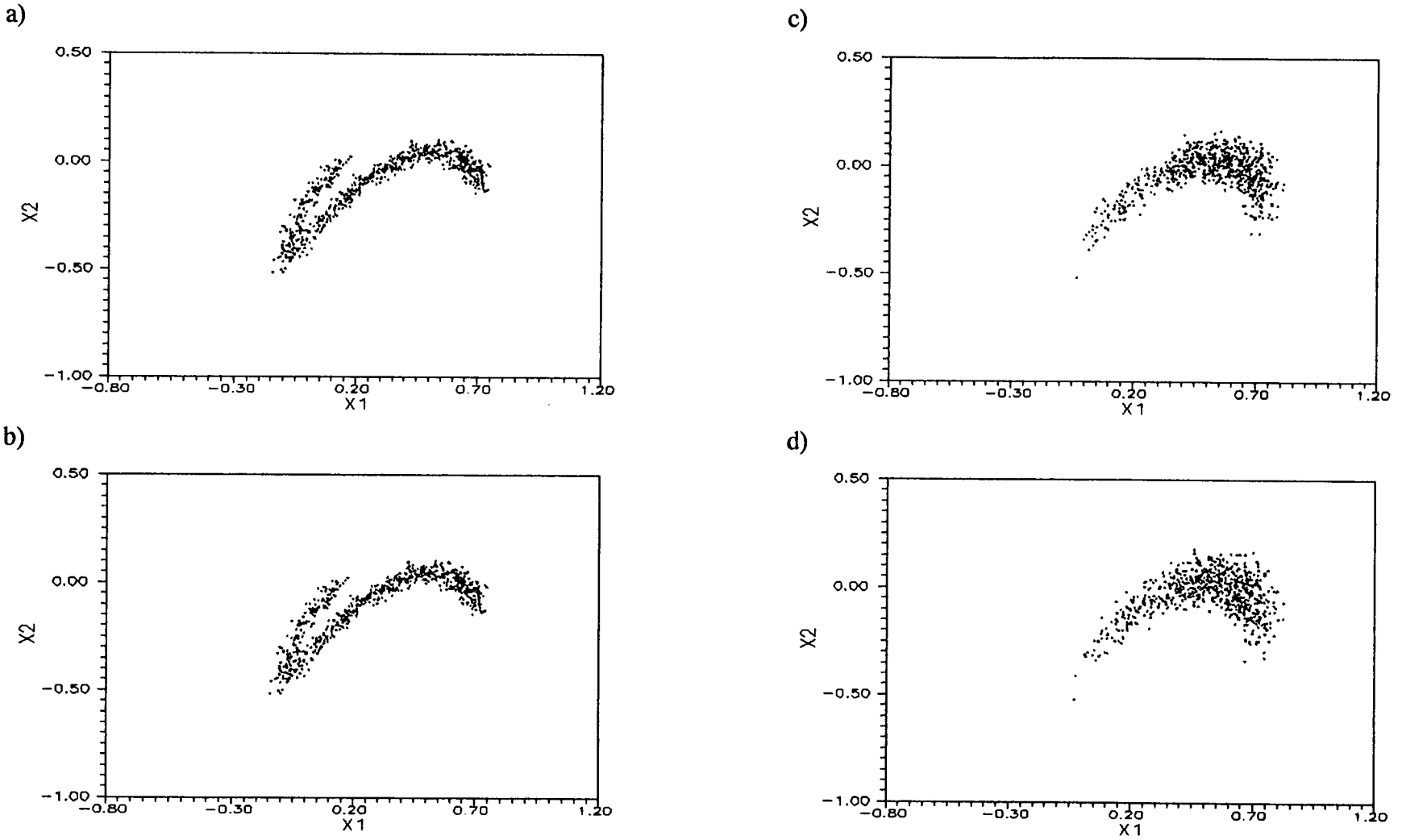

Figure 4.12 Mean Poincaré map (500 sample realizations for 700 cycles): σ^2 = a) 0.03, b) 0.05, c) 0.06 and d) 0.07; $(\alpha,\beta,\gamma,\delta,\mu,A,\omega)=(4.0,0.0,0.001,0.01,1.0,20.0,0.32)$

response with weak stability. Possible chaotic response may be embedded in a time history that appears random and undetectable by existing data analysis techniques. Hence, advanced (time series) analysis techniques need to be developed in future research to identify the existence of possible embedded chaotic response.

4.2 Narrow-Band Random Waves

As described in Chapter 2, a narrow-band wave spectrum can be approximated by a sinusoidal function with additive white noise. Figures 4.13a and b show the spectra of two narrow-band excitations together with their corresponding sinusoidal plus white-noise approximations. Note that for the case of Fig.4.13a, the spectra of the narrow-band process and its corresponding sinusoidal plus white-noise approximation are practically indistinguishable. In both cases, noisy chaotic system responses are observed (Figs.4.14a and d; Figs.4.14b and e). Figures 4.14a-c and d-f show chaotic attractors (on Poincaré maps) of response subjected to narrow-band excitations and their white-noise approximations, respectively. The fractal structure of the chaotic response is preserved for both excitations when the bandwidth is very narrow (Figs.4.14a, b, d, and e), and the responses behave in the same chaotic fashion. When the bandwidth increases, the approximation of the spectrum is not as accurate (Fig.4.13b). However, the responses from both cases still behave in a similar fashion (Figs.4.14c and f). Therefore, the sinusoidal function with white noise is an appropriate approximation to narrow-band spectra. With this simple approximation, the Markov process can be employed explicitly, and the resulting PDF of the response is can be computed directly.

Comparisons of the PDF obtained from the PIS procedure with numerical simulations is presented next.

With various noise intensity, the probabilistic properties of the response can be examined on the Poincaré section. Figures 4.15a-c show the response distribution on the Poincaré map of the chaotic system response subjected to a narrow-band excitation. These figures are normalized histogram plots of the occurrence of the Poincaré points in the phase space. With the sinusoidal plus white-noise approximation, the resulting steady-state JPDF's with various noise intensities computed from the PIS procedure are shown in Figs.4.15d-f. For both cases, the noisy chaotic responses exhibit similar probabilistic signatures. Obscurity of the imprint of chaotic attractor is observed when degree of randomness is high.

4.3 JONSWAP Random Waves

Probabilistic properties of the moored structural response subjected to random waves with a JONSWAP spectrum are examined in this section. As discussed in Chapter 2, a filtered white noise process provides a relatively good approximation to the JONSWAP spectrum. With linear filter approximation, the FPE is applied and solved for the PDF of the response using the PIS procedure, and the results are compared with those from numerical simulations. The resulting stationary-state PDF is identified as an invariant measure of the response, and the corresponding engineering applications (e.g., extreme values problems) are investigated.

Figure 4.16a shows the JPDF of a sample system response subjected to the approximated JONSWAP random waves (filtered-white-noise). Figure 4.16b shows a

a)

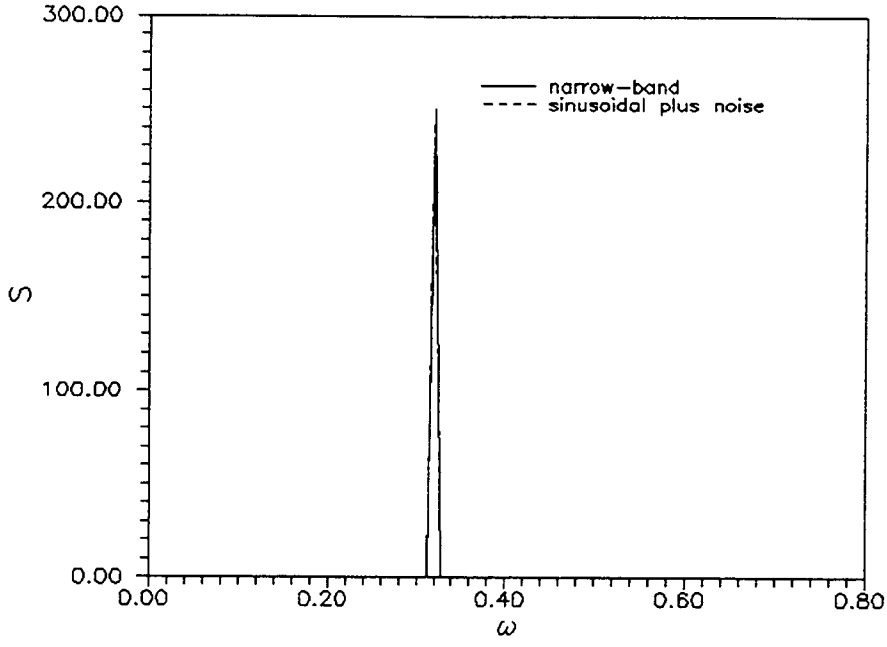

b)

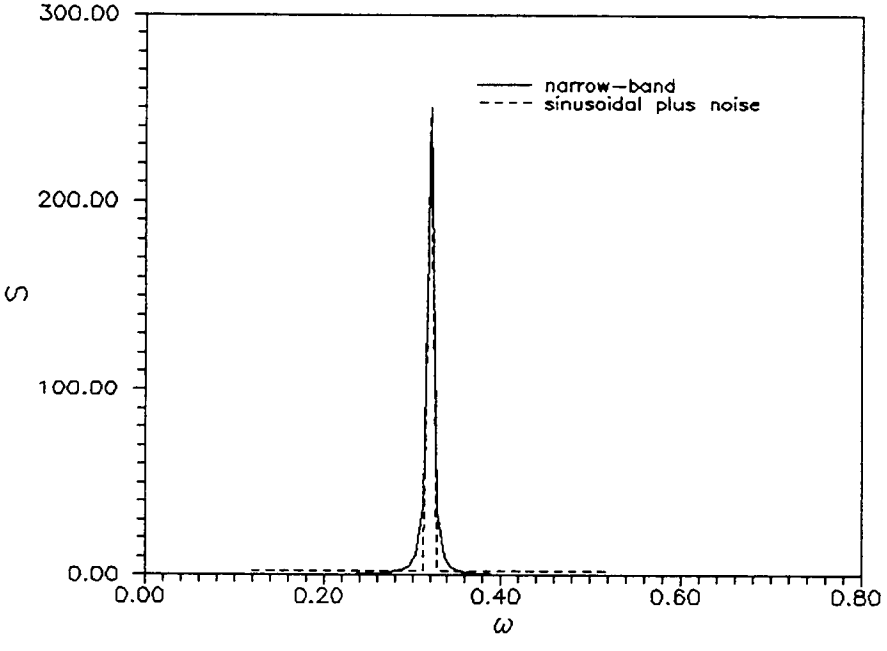

Figure 4.13 Approximation of sinusoidal plus noise to narrow-band spectra: a) $\beta_n = 0.0012$, $\sigma^2 = 0.03^2$; b) $\beta_n = 0.0416$, $\sigma^2 = 1.0^2$

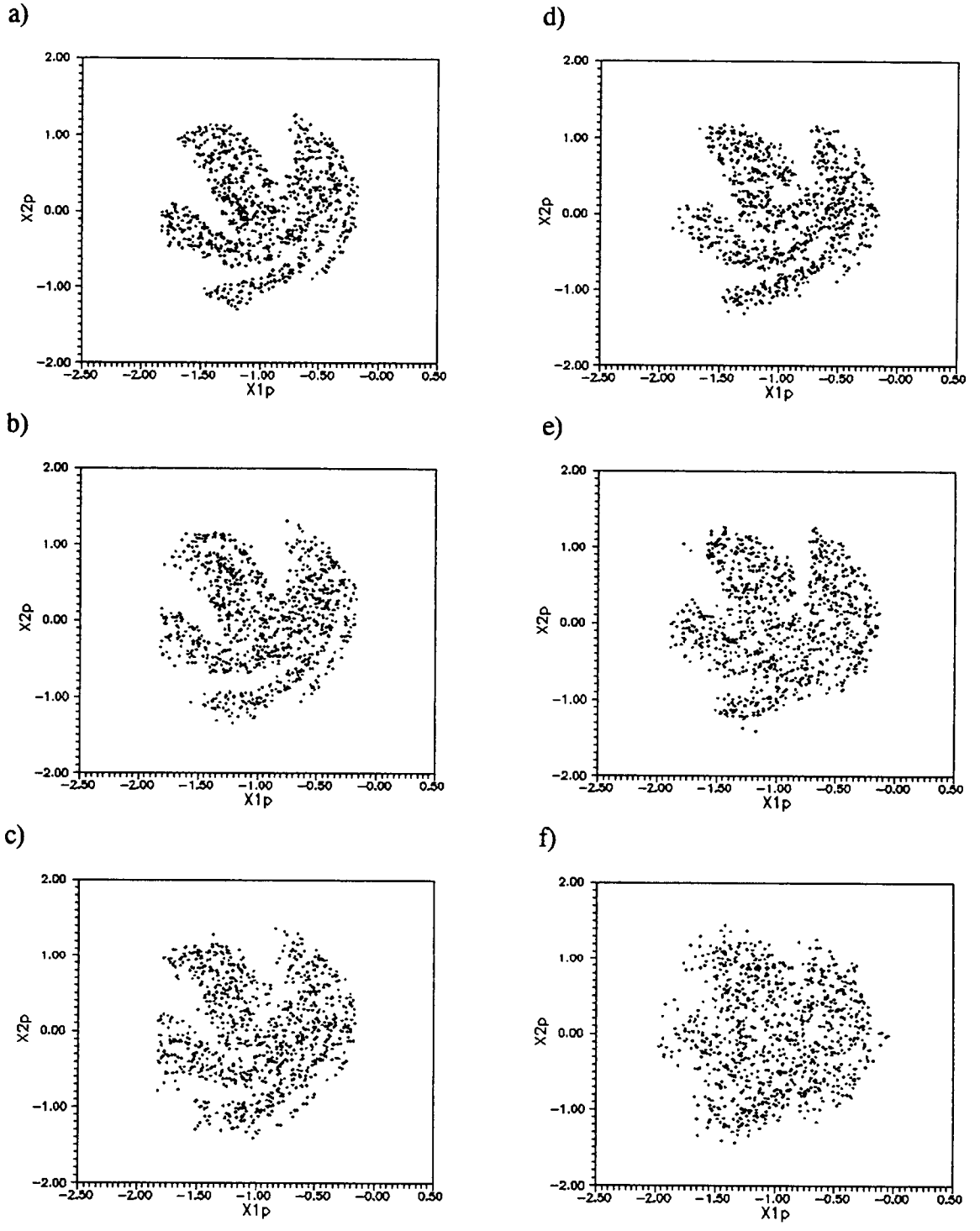

Figure 4.14 Responses to narrow-band random waves with increasing bandwidth, a)-c); responses to corresponding sinusoidal plus noise approximations, d)-f); β_n = a) 0.0012, b) 0.0039, c) 0.0077 and σ^2 = d) 0.03^2, e) 0.05^2, f) 0.07^2; $(\alpha,\beta,\gamma^*,\mu,A,\omega)=(4.0,0.0,0.01,1.0,2.0,0.32)$

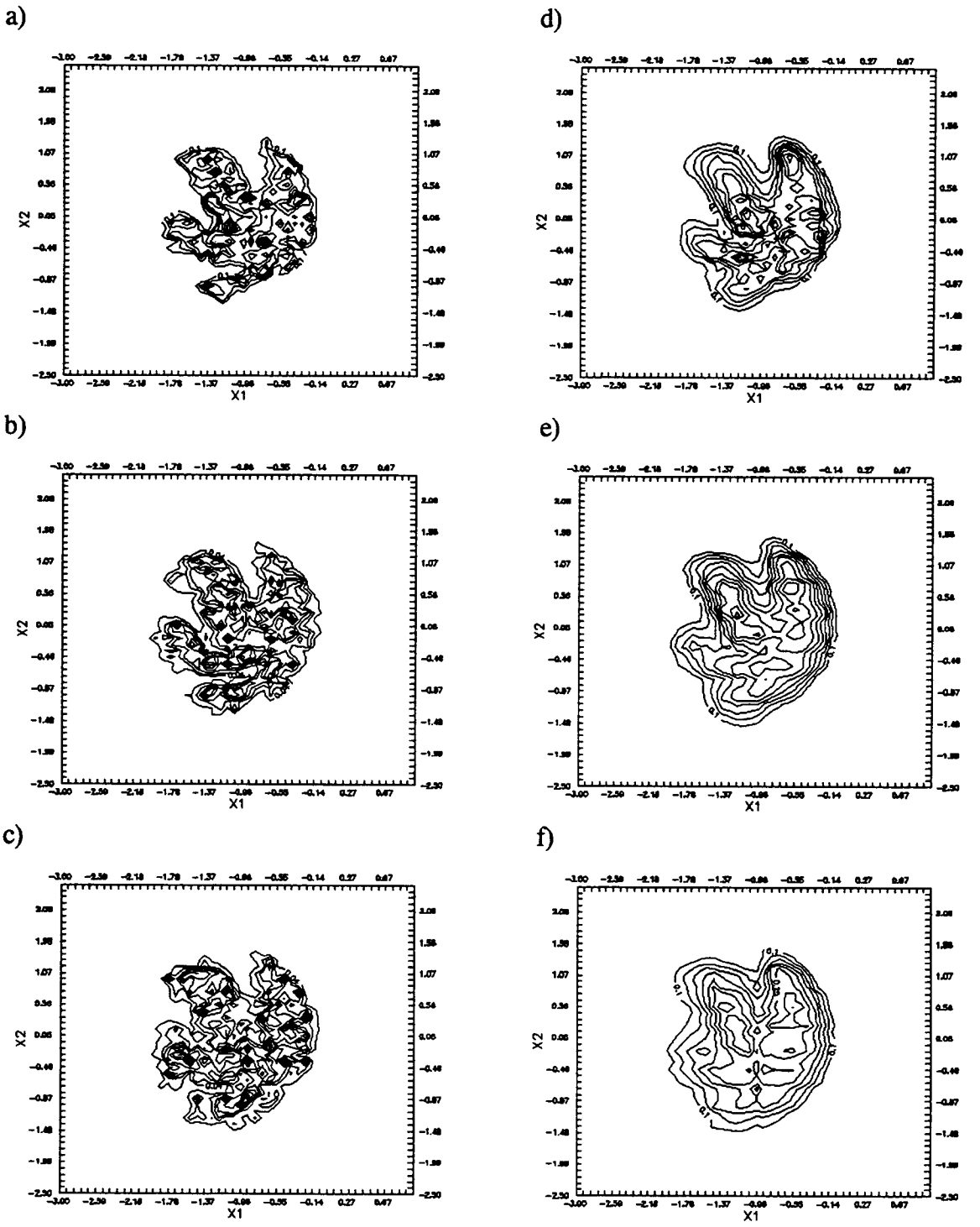

Figure 4.15 JPDF's of responses subjected to narrow-band random waves, a)-c); JPDF's of responses subjected to corresponding sinusoidal plus noise approximations, d)-f); κ = d) 0.001, e) 0.003 and f) 0.005; $(\alpha,\beta,\gamma^*,\mu,a,\omega)$=(4.0,0.0,0.01,1.0,2.0,0.32)

comparison of the computed MPDF's of the responses subjected to the filtered white-noise and simulation results from the JONSWAP excitations. Good agreement is observed in general. Thus, the filtered white-noise approximation with the Markov process approach provides a good analytical means to study nonlinear structural system response to JONSWAP random wave excitations.

It is noted that, although with low probability, the response may result in large excursions (Fig.4.16b), which can cause severe damages to the system. An invariant measure of the system behavior will be introduced and the associated maximum response distribution can be investigated in the following section.

4.4 Distribution of Maximum Response

An invariant measure for all possible dynamical systems (deterministic, random and chaotic) can be obtained by taking the average of the steady-state PDF over a suitable large duration to form a time-averaged PDF (Ruelle, 1989; Jung and Hänggi, 1990; Yim and Lin, 1992c). This time-averaged PDF is used as a tool to evaluate the distribution of maximum response amplitude in this study. The invariant measure is in general expressed as

$$P_{av}(X) = \frac{1}{t_n}\int_0^{t_n} P(X,t)\,dt \tag{4.1}$$

This measure is invariant for arbitrary time shifts, f_t, i.e.

$$P_{av}(X) = P_{av}(f_t(X)) \tag{4.2}$$

The invariant measure on the displacement response, x_1, is given by

$$P_{av}(x_1) = \int_{-\infty}^{\infty} P_{av}(x_1, x_2) dx_2 \tag{4.3}$$

The accuracy of the time-averaged PDF obtained from the Markov process approach has been demonstrated by comparing with the analytical solution (Lin and Yim, 1994). With this measure, the distribution of large excursions in the response subjected to various bandwidth random waves are computed and examined.

As discussed in Chapter 2, bandwidth controlling parameter β_n governs the degree of randomness in the filtered white noise. With the filter white-noise approximation to the JONSWAP waves, and considering β_n as a band-width parameter (with spectral peak fixed), spectra with various bandwidths may result (Fig.4.17b).

By applying the Markov process approach and taking the average of the resulting steady-state PDF over a long duration of time, the time-averaged density is obtained (Fig.4.18a). In this study, the mean up-crossing frequency is evaluated based on the Rice's formula (Lin, 1967; Naess and Johnsen, 1991) and the assumption of statistically independent large-amplitude up-crossings, which leads to Poisson distributed crossing events, is adopted. Accordingly, asymptotic approximation of the probability of response amplitude exceeding a specified (high) level during a given duration can be calculated.

The mean up-crossing frequency of the response is

$$\mu_{x_1}^{+}(x_d) = \int_0^{\infty} x_2 P_{av}(x_d, x_2) dx_2 \tag{4.4}$$

and the asymptotic approximation of the probability exceeding a specific (high) level x_d during time τ_n is given by

$$P_F(x_d, \tau_n) = 1 - \exp[-\mu_{x_1}^{+}(x_d)\tau_n] \tag{4.5}$$

Figure 4.18a shows that, with the spectral peak fixed, the time-averaged MPDF has a slightly larger spreading for the case with larger bandwidth. The corresponding distribution of large amplitude responses are shown in Fig.4.18b. For the case with larger spectral bandwidth, the probability of large excursions is elevated. These results may be further incorporated with the first passage time problem and used in extreme structural design.

a)

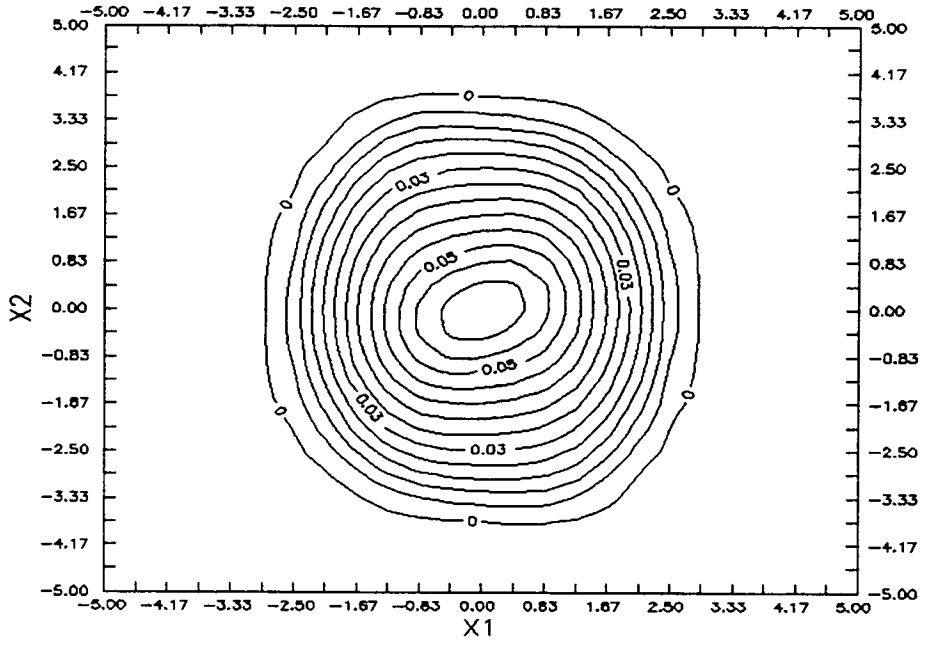

b)

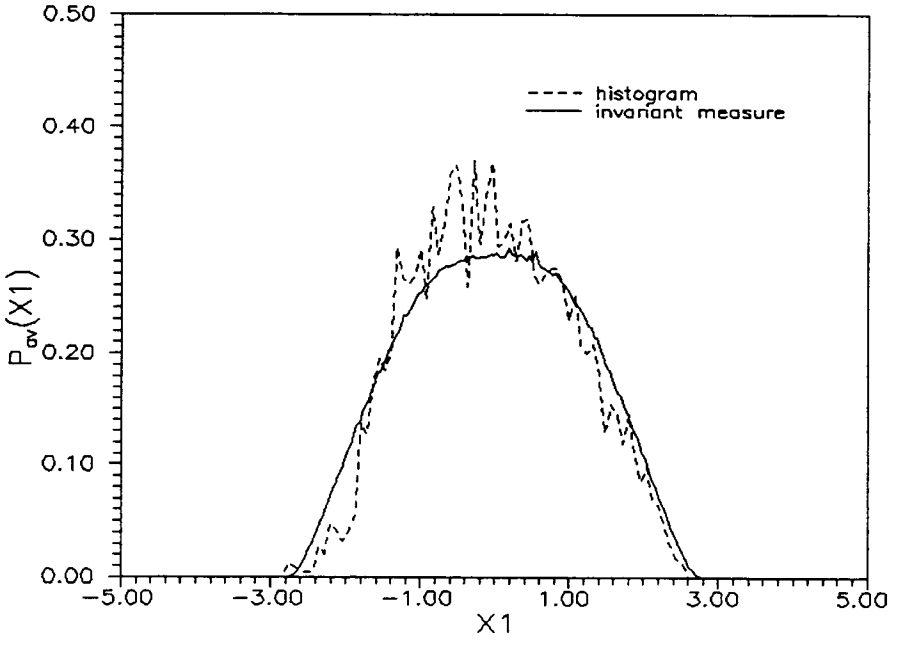

Figure 4.16 PDF's of response subjected to approximated JONSWAP random waves: a) contour map of JPDF; b) comparison with system response subjected to JONSWAP random waves (simulation, dashed line; approximation, solid line); $(\alpha,\beta,\gamma^*,\mu,\beta_n f_0,\kappa)=(4.0,0.0,0.01,1.0,0.413,0.32,0.6)$

a)

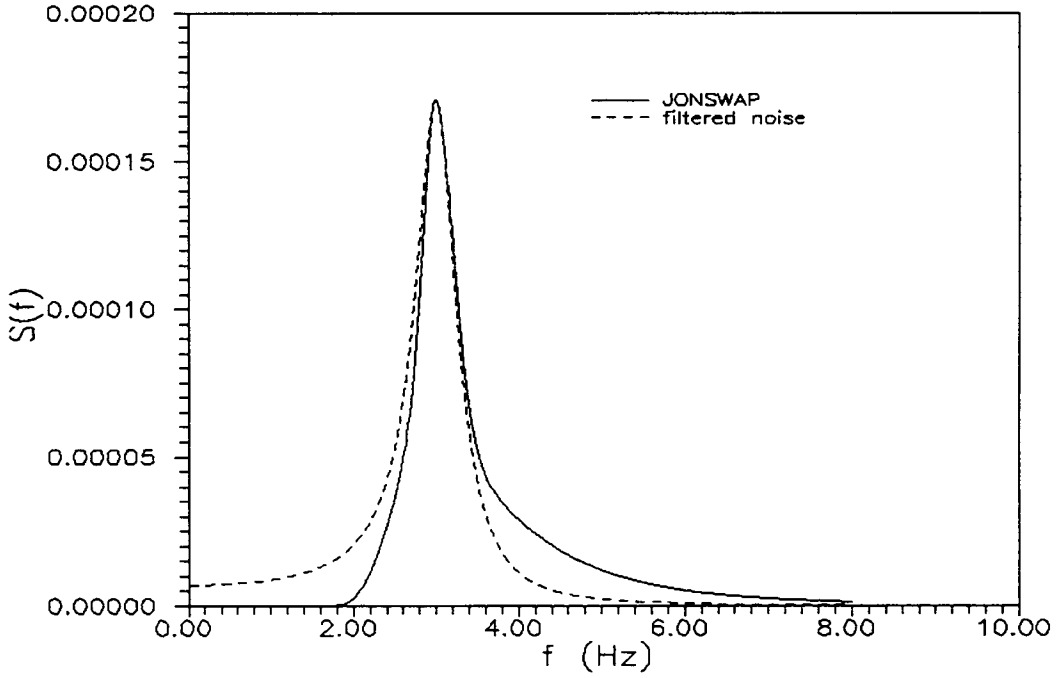

b)

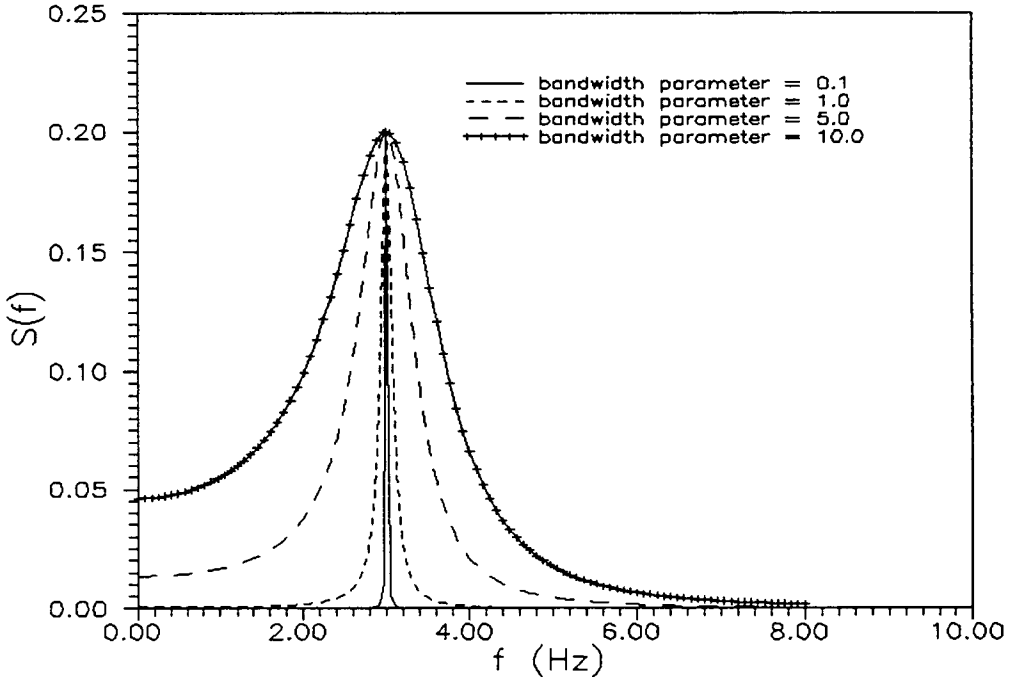

Figure 4.17 JONSWAP spectrum vs. filtered noise: a) comparison; b) filtered noise with various bandwidths

a)

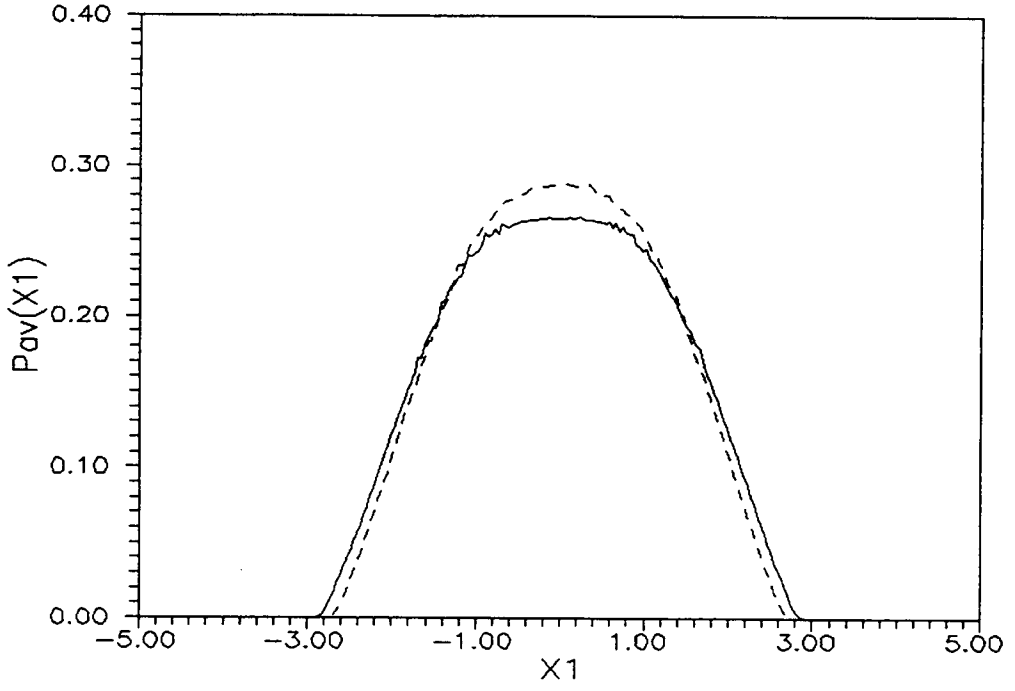

b)

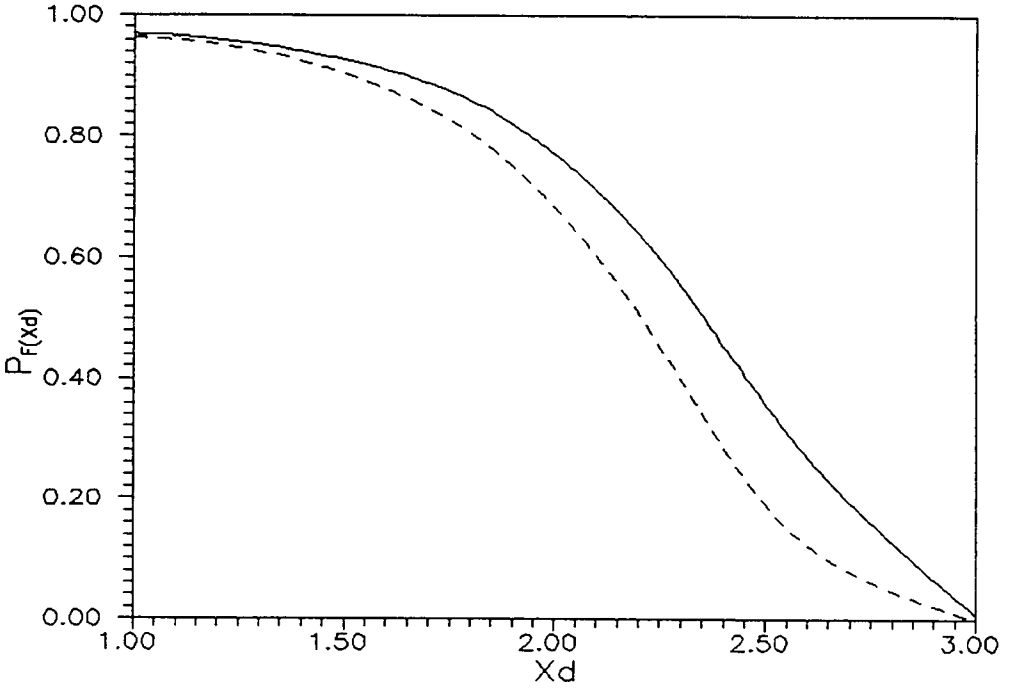

Figure 4.18 Response under filtered white noise with various bandwidths (β_n=0.6 and 1.0): a) corresponding invariant measures, and b) probability of large excursions; solid - β_n=1.0; dashed - β_n=0.6; T_n=20.0; $(\alpha,\beta,\gamma^*,\mu)$= (4.0,0.0,0.1,1.0)

5. PRELIMINARY EXPERIMENTAL OBSERVATIONS

An experiment has been conducted at the OSU Wave Research Laboratory on the nonlinear response behavior of a submerged moored spherical body (Yim *et al.*, 1993). Results from this experiment are employed in this study to qualitatively validate the analytical predictions and to guide additional future analysis of the moored structural system models. Excitations considered in the experiment include monochromatic and random waves. However, because of the presence of uncontrollable noise (at least a low level) in the wave flume is inevitable, the incident waves are also considered from a stochastic perspective for both regular and irregular waves, and the experimental observations are interpreted accordingly.

5.1 Experiment Overview

The experimental model consists of a submerged moored spherical sphere excited by oscillating regular and irregular waves in a closed wave flume. Configurations tested include both SDOF and MDOF moored structural systems with geometrically nonlinear and two or four mooring points. Excitations considered include periodic, periodic with band-limited white noise and narrow-band random waves (Yim *et al.*, 1993). Definition sketches of the SDOF and MDOF models are shown in Figs.5.1a-b and 5.2a-b. System parameters of the experimental models are designed to emulate the equations of motion described in Chapter 2.

Damping mechanism includes a linear structural component associated with the system connections and contact points of the instrumentation. In the SDOF model, due

a)

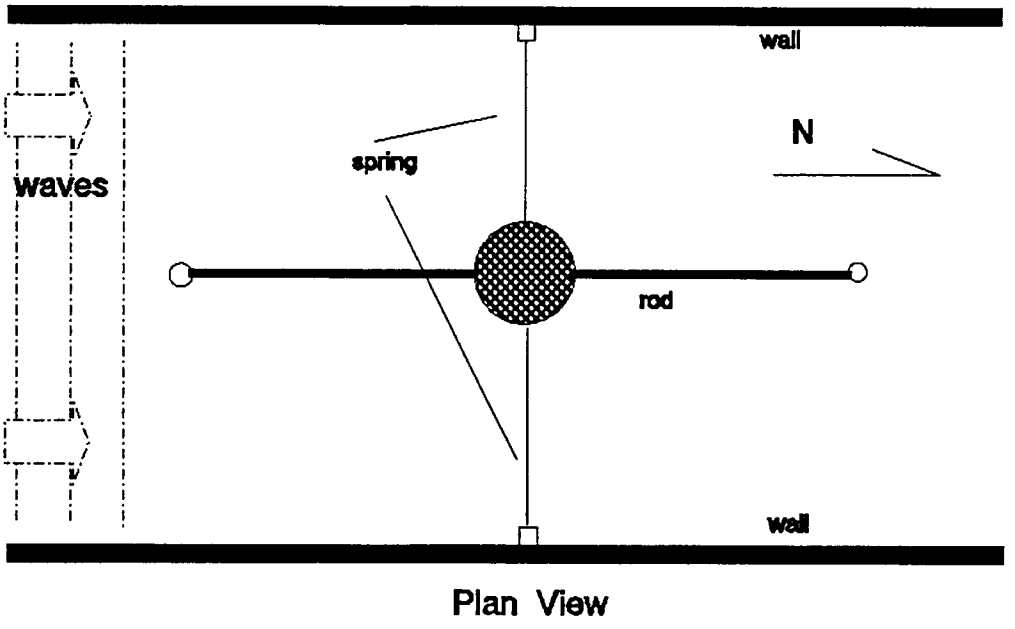

b)

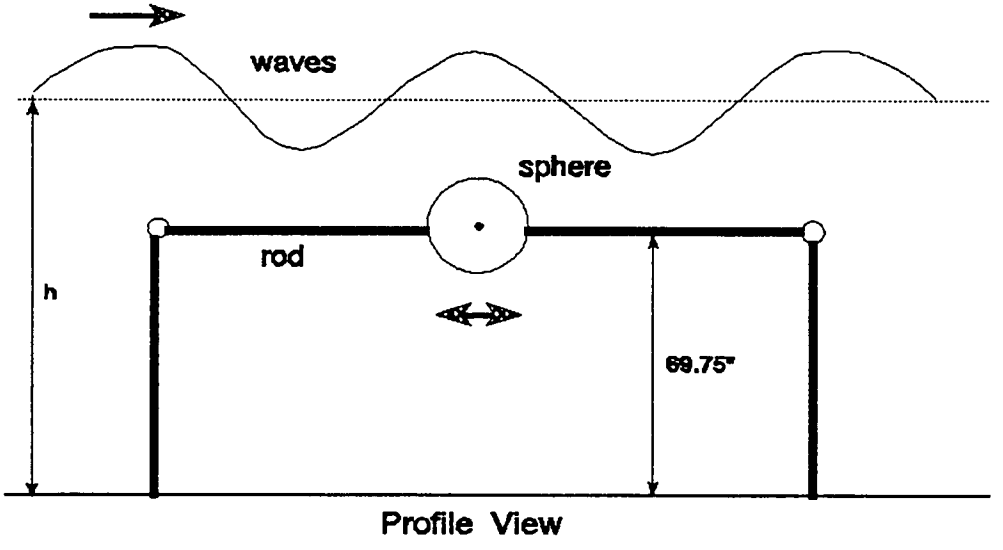

Figure 5.1 SDOF model (top and side views)

a)

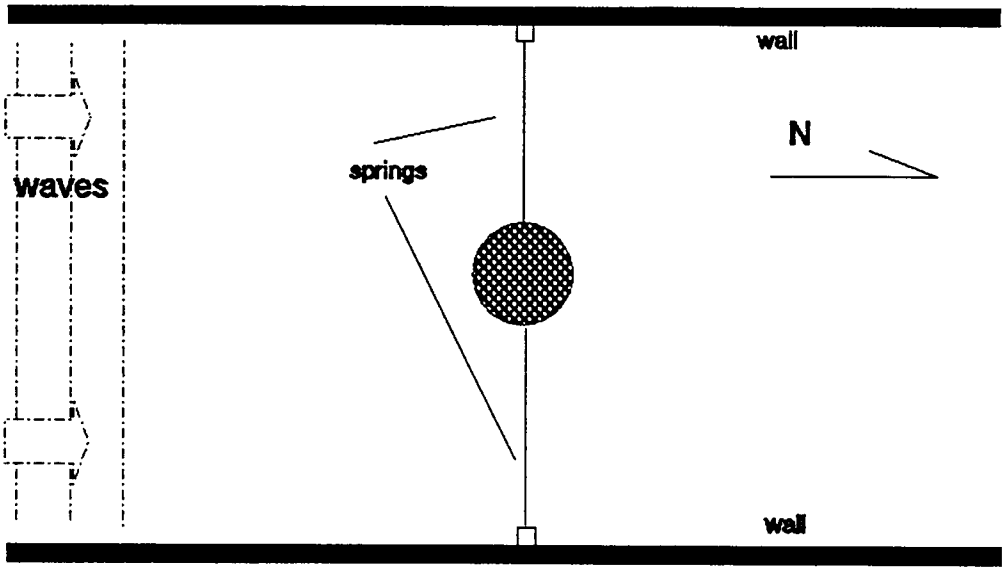

b)

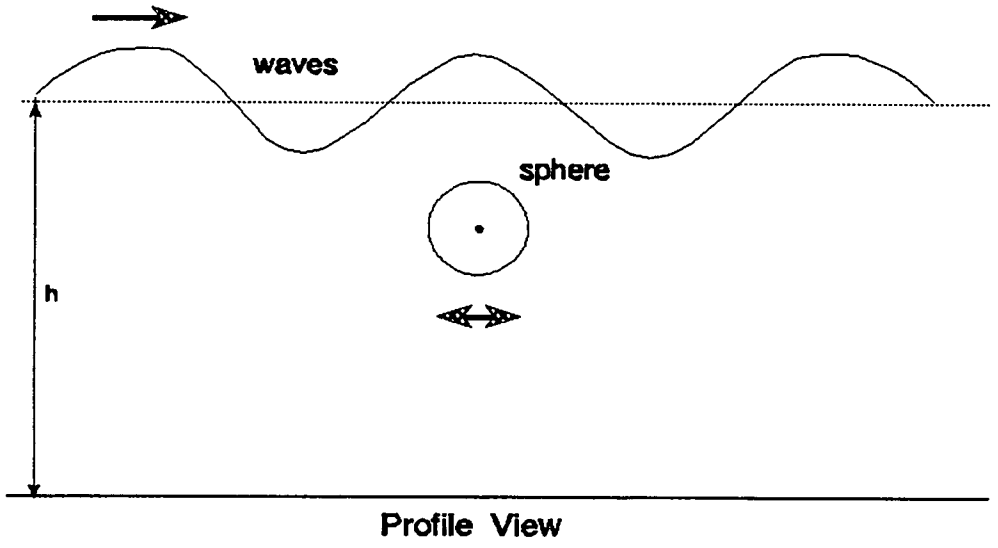

Figure 5.2 MDOF model (top and side views)

to the presence of a central rod (used to prevent vertical and side motions, Fig.5.1), the damping mechanism also include a time dependent coulomb friction component originating from the lift force (in the x_3 direction) and combined drag/lift moment (in the x_5 direction). Variability in the friction force results from changing contact area and normal force due to the oscillatory nature of the hydrodynamic drag/lift forces (Yim *et al.*, 1993).

Exciting forces include coupled fluid-structure interaction drag and inertial terms. The drag/lift is quadratic in nature whereas the inertial components consist of a linear O(1) temporal term and O(ϵ) nonlinear convective terms which may become increasingly important in the moored structural response near resonance (Gottlieb and Yim, 1992). The nonlinear field described above may be further complicated by re-reflections and a return flow driven by mass transport in the upper part of the water column (Mei *et al.*, 1972). Consequently, even monochromatic input waves will result in a non-stationary exciting force (e.g., Priestly, 1988). Random waves of white noise nature and those with a narrow-band TMA spectral shape (Hughes, 1984) were formulated in Chapter 2 with a peak frequency chosen from the monochromatic test sequence.

Some of the disturbances in the wave flume, (e.g., reflections, return current and measurement errors, see Yim *et al.*, 1993) are considered in this study. The resulting deviations between the designed and measured inputs will be classified as "random perturbations" for further investigation.

5.2 Damping Force

Damping mechanism which dissipates energy in the moored structural system includes quadratic hydrodynamic drag effect (Morrison type) and structural damping. In this study, an equivalent linear damping force, including both structural and hydrodynamic components, is estimated by free vibration tests in still water. Linearization of the Morison equation is performed by constructing an equivalent linear damping mechanism which dissipates the same amount of energy within one period of motion as that of the nonlinear drag force. This linear damping force will be used in the analysis of the model tests under various wave excitations (Yim *et al.*, 1993).

5.3 Analysis Techniques

Displacements of the sphere are measured by attached string-pots for both the SDOF and the MDOF models. Biases in the measurement are analyzed independently and then removed from the dynamic response analysis. For the MDOF model, the moored structural response is determined in a planar (2-D) motion so that only surge, heave and pitch motions are taken into account. Conversion from experimental measurements to the physical displacements (surge, heave and pitch) are discussed in detail in a later section. Techniques used to identify the characteristics of the structural response include time domain analysis of time history and phase plane diagrams, frequency domain analysis of spectral density, and probability domain analysis of marginal amplitude PDF (Yim *et al.*, 1993).

Figures 5.3a-c, 5.4a-c, 5.5a-c and 5.6a-c show typical deterministic harmonic, sub-harmonic, super-harmonic, and chaotic response represented by time history, energy

spectrum and amplitude marginal PDF of simulated responses of the nonlinear system. Corresponding typical stochastic (with random noise) harmonic, sub-harmonic, super-harmonic, and chaotic response are shown in Figs.5.3d-f, 5.4d-f, 5.5d-f and 5.6d-f, respectively. The figures demonstrate that the presence of random noise induces randomness in the nonlinear responses. They also show spreading of energy over a wide range of frequencies, and smoothing of the MPDF.

5.4 Moored Structural Models

Moored structural models considered in this study include both SDOF and MDOF models. System configuration, sphere response and exciting wave field of each model are described in this section.

5.4.1 SDOF Model

In the SDOF model, only surge motion is allowed. All other movements (including heave and pitch) are restrained by the rigid rod placed through the center of the sphere. The structural configuration of the SDOF tests consisted of a neutrally buoyant sphere supported by rod with guyed masts six feet above the bottom of the wave flume (Fig.5.7). Elastic springs (20 lb/ft) were connected to the sphere via smooth cables to provide a restoring force. An initial restoring force of 25 lbs is selected to enhance nonlinear phenomena.

The surge motion of the sphere is measured by two attached string pots (Fig.5.7). The string pots are attached to the sphere on opposite sides to offset the force caused by the tensions in the strings. Two additional string pots are used to measure the elongation

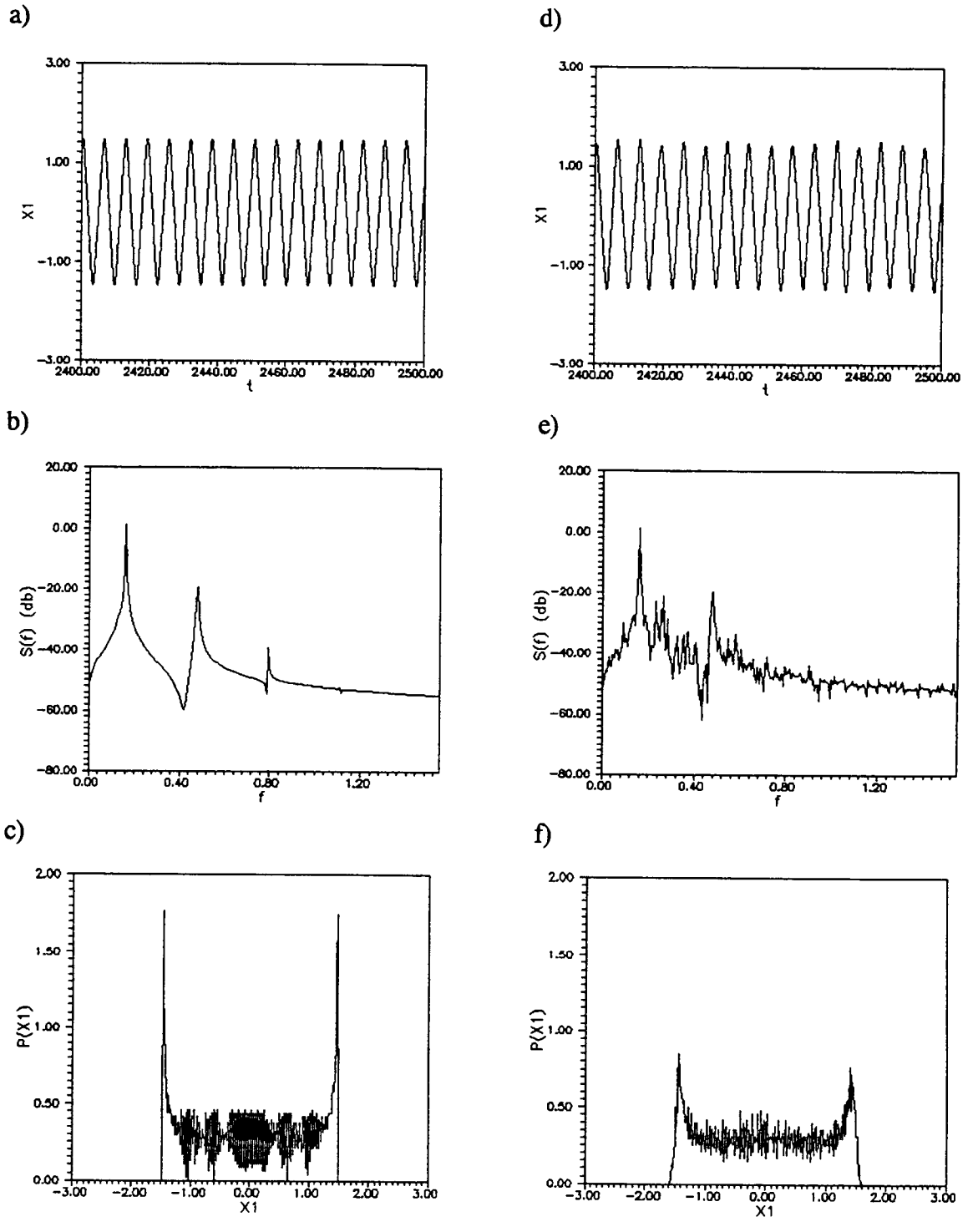

Figure 5.3 Deterministic and stochastic (σ=0.15) harmonic responses: deterministic (a-c) and stochastic (d-f) with a) and d) time histories; b) and e) spectral density functions; c) and f) marginal PDF's

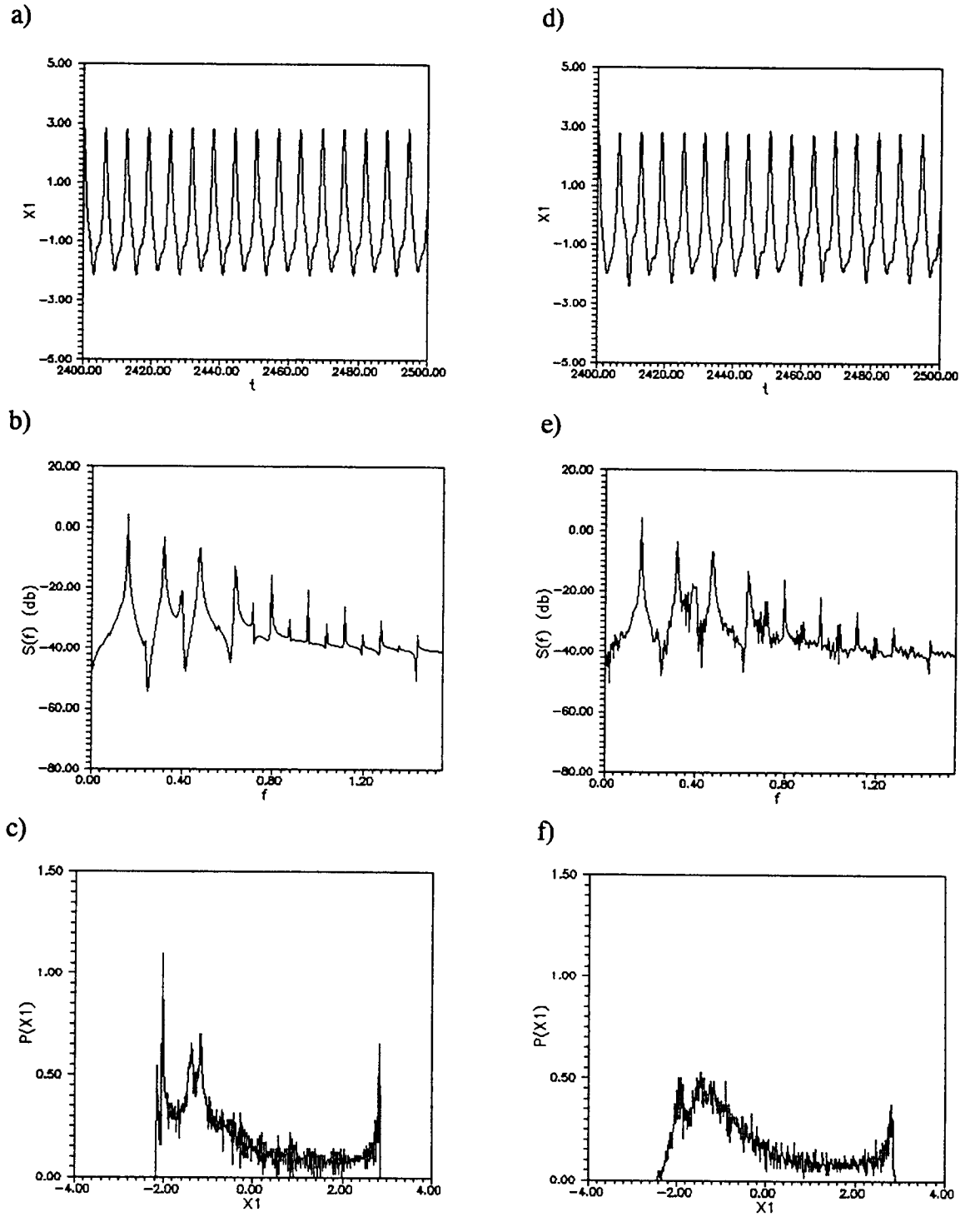

Figure 5.4 Deterministic and stochastic (σ=0.15) sub-harmonic responses: deterministic (a-c) and stochastic (d-f) with a) and d) time histories; b) and c) spectral density functions; c) and f) marginal PDF's

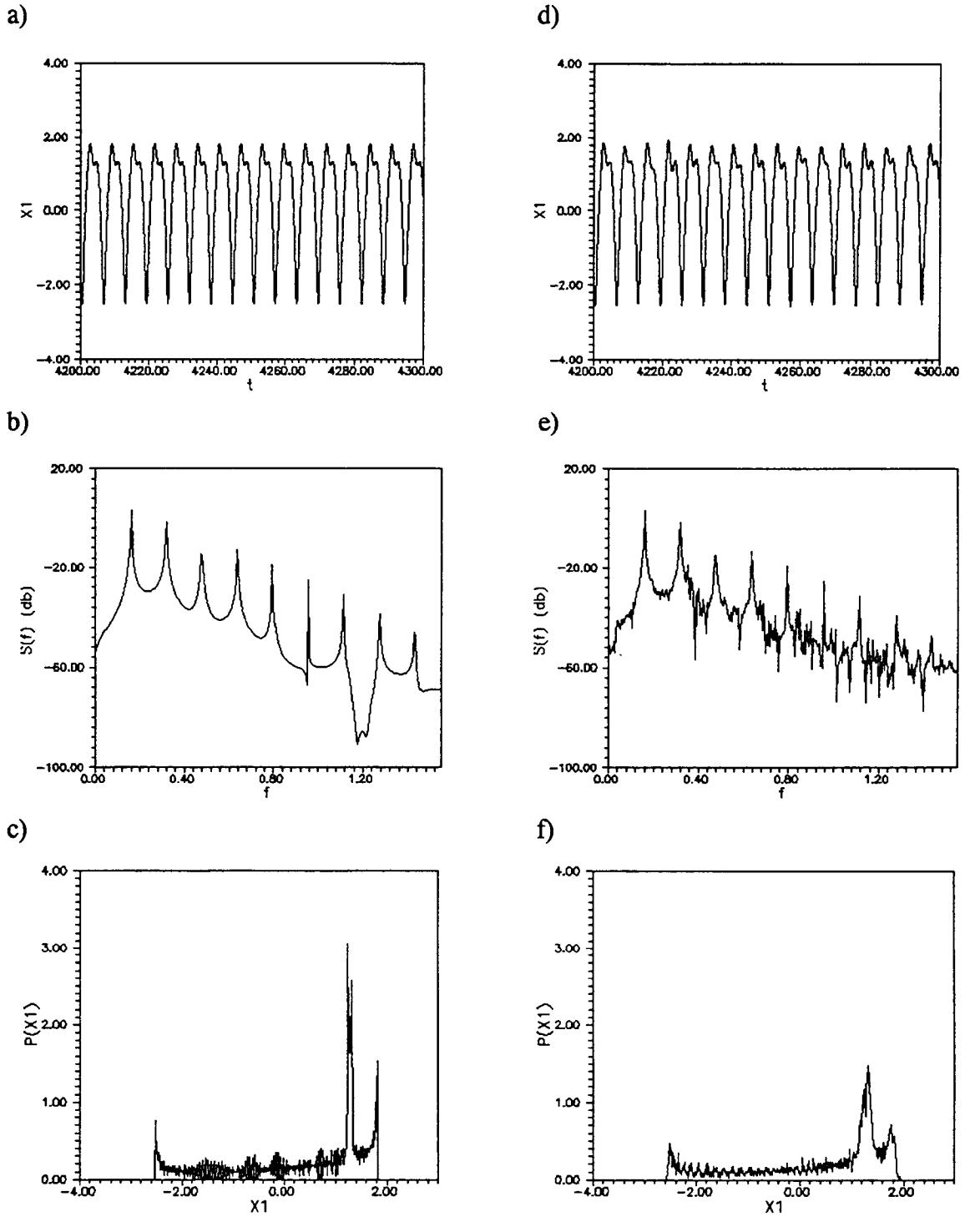

Figure 5.5 Deterministic and stochastic (σ=0.15) super-harmonic responses: deterministic (a-c) and stochastic (d-f) with a) and d) time histories; b) and e) spectral density functions; c) and f) marginal PDF's

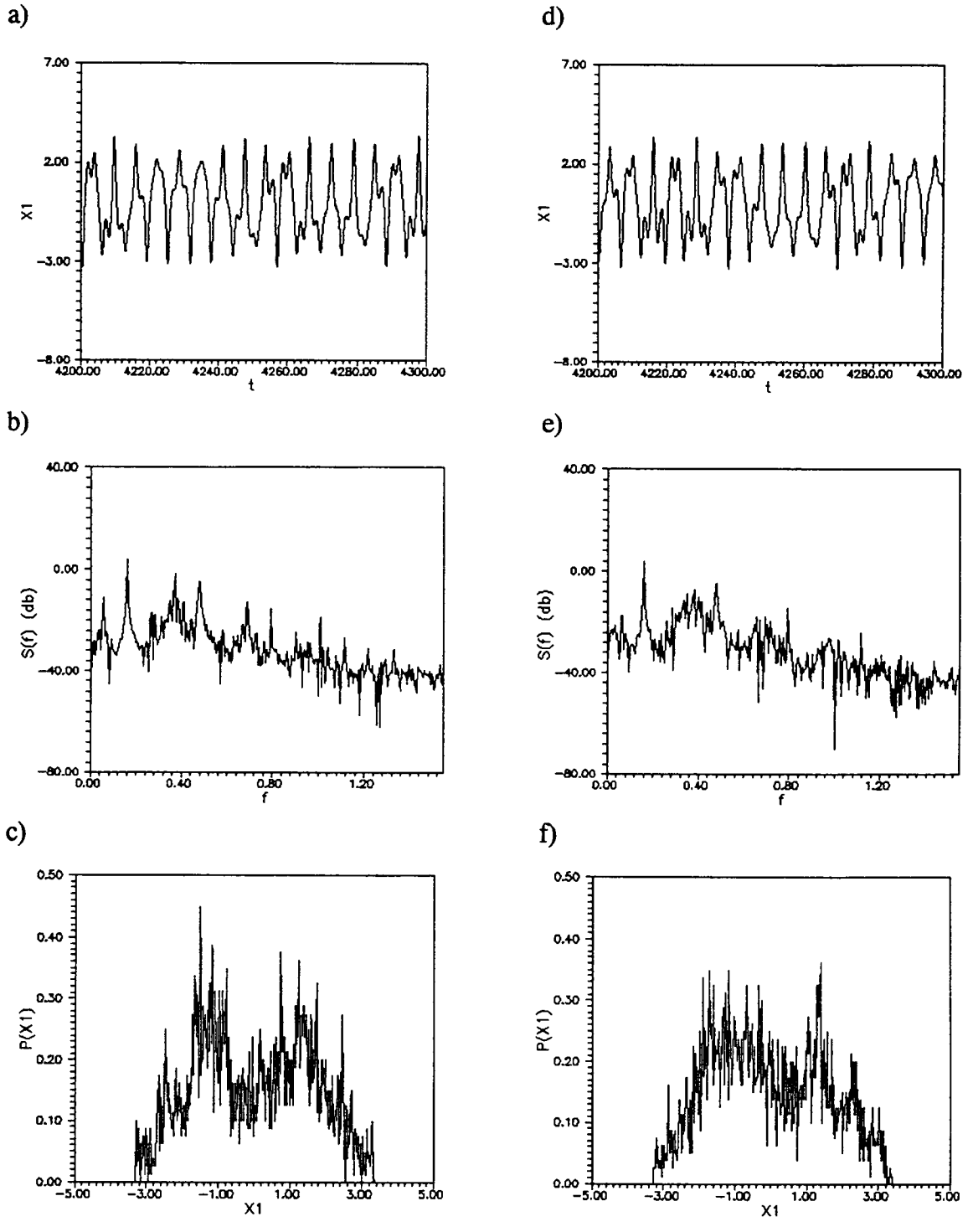

Figure 5.6 Deterministic and stochastic (σ=0.25) chaotic responses: deterministic (a-c) and stochastic (d-f) with a) and d) time histories; b) and e) spectral density functions; c) and f) marginal PDF's

a)

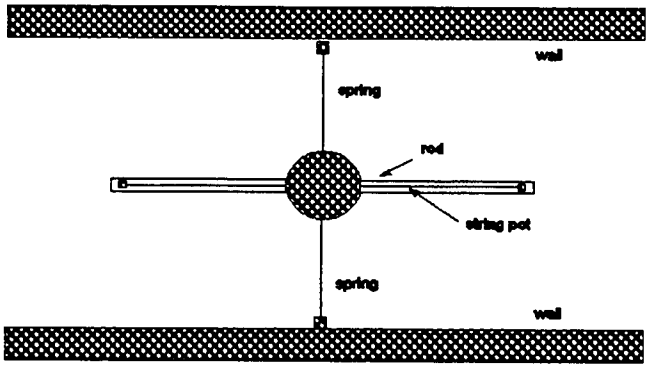

Plan View

b)

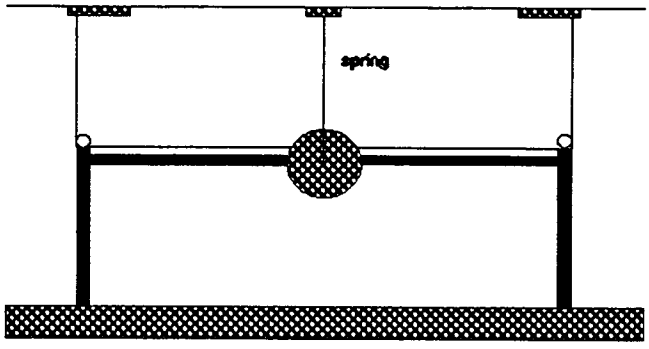

Profile View

c)

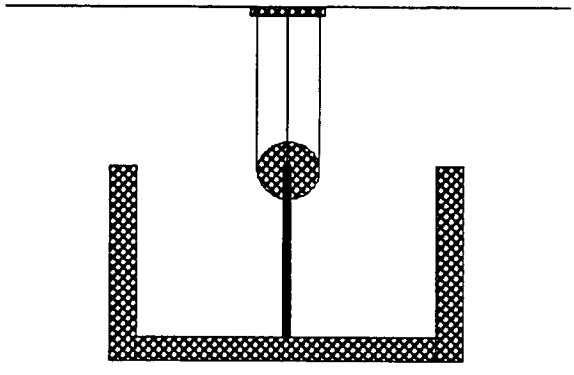

Front View

Figure 5.7 SDOF model (plan, profile and front views)

of the springs which could be used to computed the restoring force. As a redundancy in the measurements, string gauges are also employed to directly measure the tension in the springs.

Considering the inevitable presence of noise disturbance in the wave flume, deviations in actual wave excitations compared to analytical prescription are approximated as weak additive random noise.

5.4.1.1 Monochromatic Waves

Equations of motions for the SDOF moored structural model subjected to monochromatic regular waves with additive random perturbations are given by

$$\begin{aligned} \dot{x}_1 &= x_2 \\ \dot{x}_2 &= -R(x_1) - \gamma x_2 + F_D^d(x_2, t) + F_I^d(t) + \nu(t) \end{aligned} \tag{5.1}$$

where $\nu(t)$ represents a zero-mean and delta-correlated white noise.

5.4.1.2 Narrow-Band Random Waves

The response behavior of the sphere subjected to narrow-band random waves is examined experimentally. To preserve some deterministic properties of the system response, the spectral bandwidth is kept narrow throughout the study. The spectral properties of the narrow-band random waves are characterized by the TMA (Texel, Marsen and Arsloe) spectrum. It was chosen to model realistic shallow water wave conditions. In addition, the TMA spectrum is a built-in function of the wave-maker at the OSU Wave Research Laboratory. The TMA spectrum can be expressed as (Yim *et al.*, 1993)

$$E_{TMA}(f,h) = \alpha g^2 f^{-5}(2\pi)^{-4}\phi(2\pi f,h)\exp\left[-\frac{5}{4}(\frac{f}{f_p})^{-4}\right] \times\gamma\exp\left[\frac{-(\frac{f}{f_p}-1)^2}{2\sigma^2}\right] \tag{5.2}$$

with

$$\phi(2\pi f,h) = \begin{cases} \frac{1}{2}\omega_h^2, & \text{for} \quad \omega_h \le 1 \\ 1-\frac{1}{2}(2-\omega_h)^2, & \text{for} \quad \omega_h > 1 \end{cases} \tag{5.3}$$

$$\omega_h = 2\pi f(\frac{h}{g})^{\frac{1}{2}}$$

and

$$\sigma = \begin{cases} 0.07 & \text{for} \quad f \le f_p \\ 0.09 & \text{for} \quad f > f_p \end{cases} \tag{5.4}$$

where f_p is the peak frequency, and α and γ are the shape parameters.

As described in Chapter 2, narrow-band random waves can be approximated by a filtered white noise so that the Markov process approach can be employed and the corresponding predictions compared with the experimental observations. A sample TMA spectrum is compared with filtered white noise in Fig.5.8, and reasonably good agreement is observed.

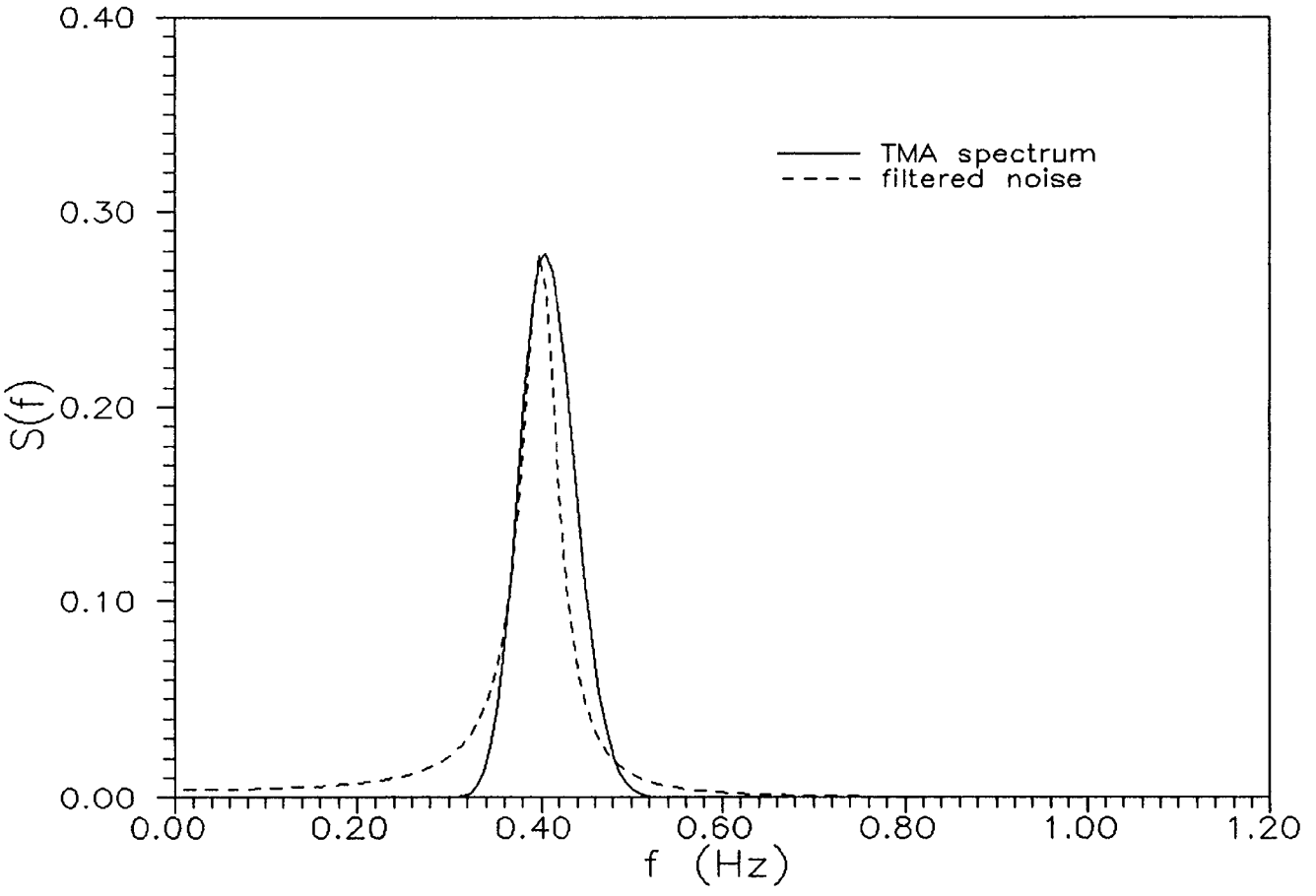

Figure 5.8 TMA spectrum vs. filtered white noise

5.4.2 MDOF Model

To study the influence of the heave and possibly pitch responses on the nonlinear behavior of the MDOF structural system, the central rod was removed. Springs with stiffness of 20 lb/ft were used to support the nearly neutrally buoyant sphere and provide a restoring force. The initial restoring force was set at 25 lbs. The configuration of the MDOF model is shown in Fig.5.9.

Motions of the sphere were measured by eight attached string pods (Fig.5.9). Symmetry of the configuration (Fig.5.2) with respect to the x_1 axis indicates that the sphere motion may be enclosed in the x_1 and x_3 plane (surge, heave and pitch). Small difference between two measurements on the string-pots on the top indicate a negligible side motion (Fig.5.10). Surge (x_1) and heave (x_3) motions are thus converted from the measurements based on the 2-D motion approximation.

The geometrical relationships between surge and heave motions, and the measurements are illustrated in Fig.5.11. Because of the large excursion in the moored structural response, linear transformation is not applicable. Based on the configuration, only the measurements of the two string-pots at the top, the string-pot in the south, and the string-pot in the north are needed for the conversion (Fig.5.9). Note that readings of the two string-pots at the top are averaged to reduce measurement errors.

Distances between the location of the sphere and the string pots at the top, in the south and in the north are denoted by l_1, l_2 and l_3, respectively, and their deformed lengths are denoted by l_1', l_2' and l_3' (Fig.5.11). Pitch motion is observed to be insignificant (negligible) compared surge and heave. Based on this assumption,

displacements in surge (x_1) and heave (x_3) can be computed from the deformed and un-deformed lengths

$$x_1 \cong \frac{1}{2(l_2+l_3)}(2l_2\Delta l_2+\Delta l_2^2-2l_3\Delta l_3-\Delta l_3^2)$$
$$x_3 \cong l_1-\sqrt{l_1^2-(x_1^2-2l_1\Delta l_1-\Delta l_1^2)} \tag{5.5}$$

where Δ denotes the reading on the string pot. Similar characteristics are demonstrated in sample measurements (Figs.5.12a and b) and their converted surge and heave displacements (Figs.5.12c and d).

5.5 Structural Response

System parameters for various wave excitation tests are determined based on the stability analysis of the deterministic moored structural system subjected to regular waves (Gottlieb, 1991). Parameter space may be modified due to the presence of friction between the sphere and the rod in the SDOF model, and large body hydrodynamic effects of the wave-structure system. However, the deterministic analytic predictions on response instability are used as baseline reference for the experimental study.

5.5.1 Monochromatic Waves

Figures 5.13 shows the time history of a sample structural response under steady-state monochromatic wave excitation. It can be observed that the structural response initially visits a harmonic (period-1) attractor in the first 80 seconds, and then shifts to and stays in a sub-harmonic (period-2) attractor.

a)

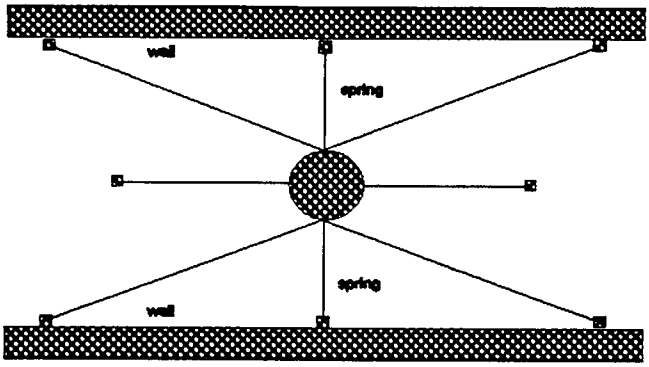

Plan View

b)

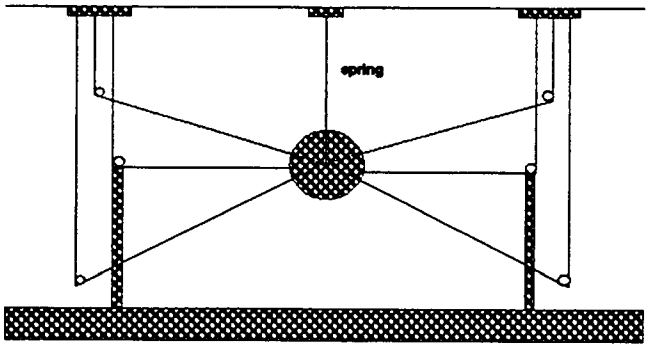

Profile View

c)

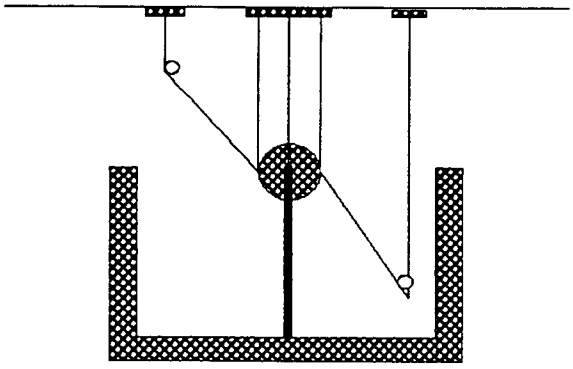

Front View

Figure 5.9 MDOF model (plan, profile and front views)

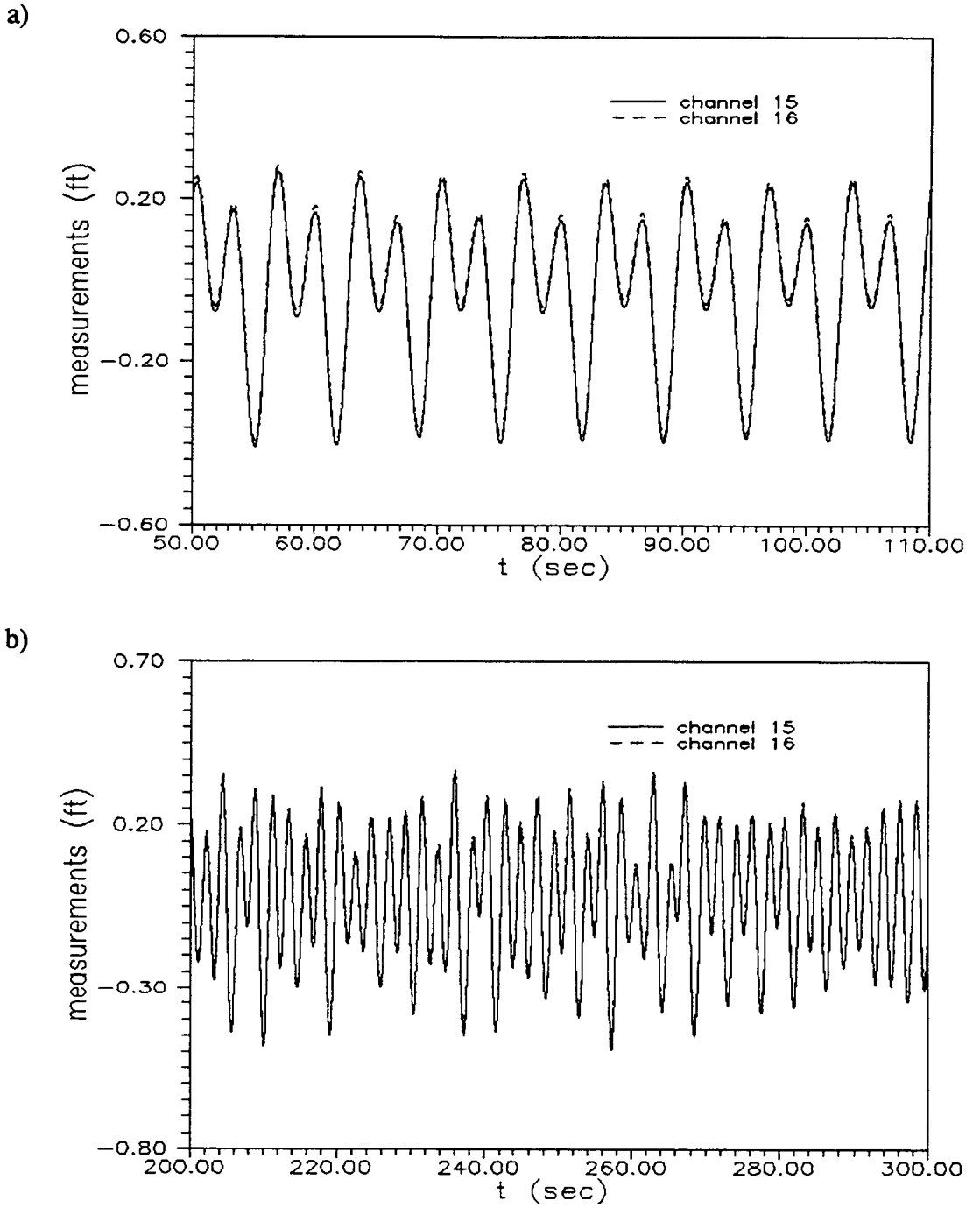

Figure 5.10 Measurements of structural response (MDOF, 2-D motion): a) run E5; b) run E9

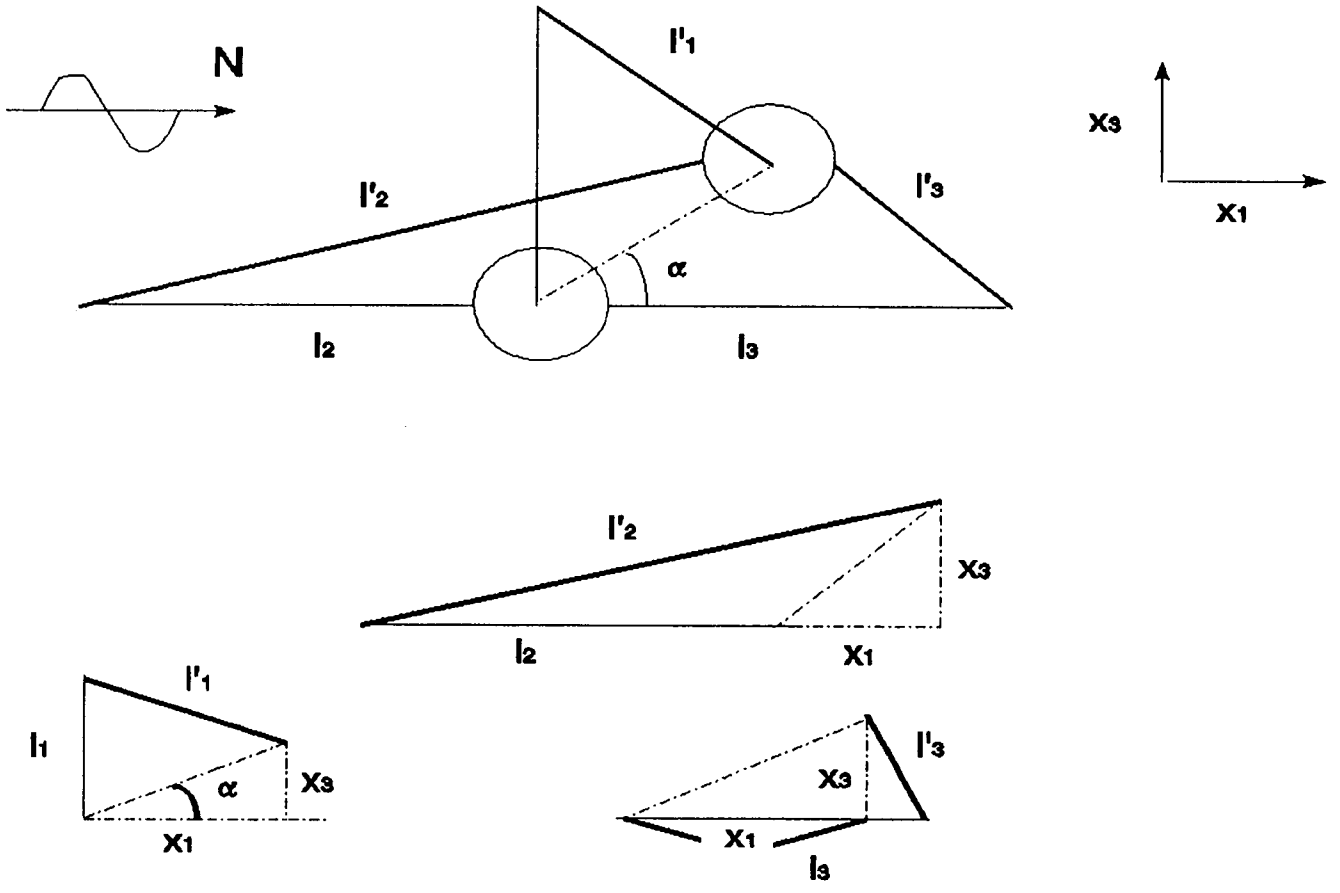

Figure 5.11 Geometric relationships between displacements and measurements

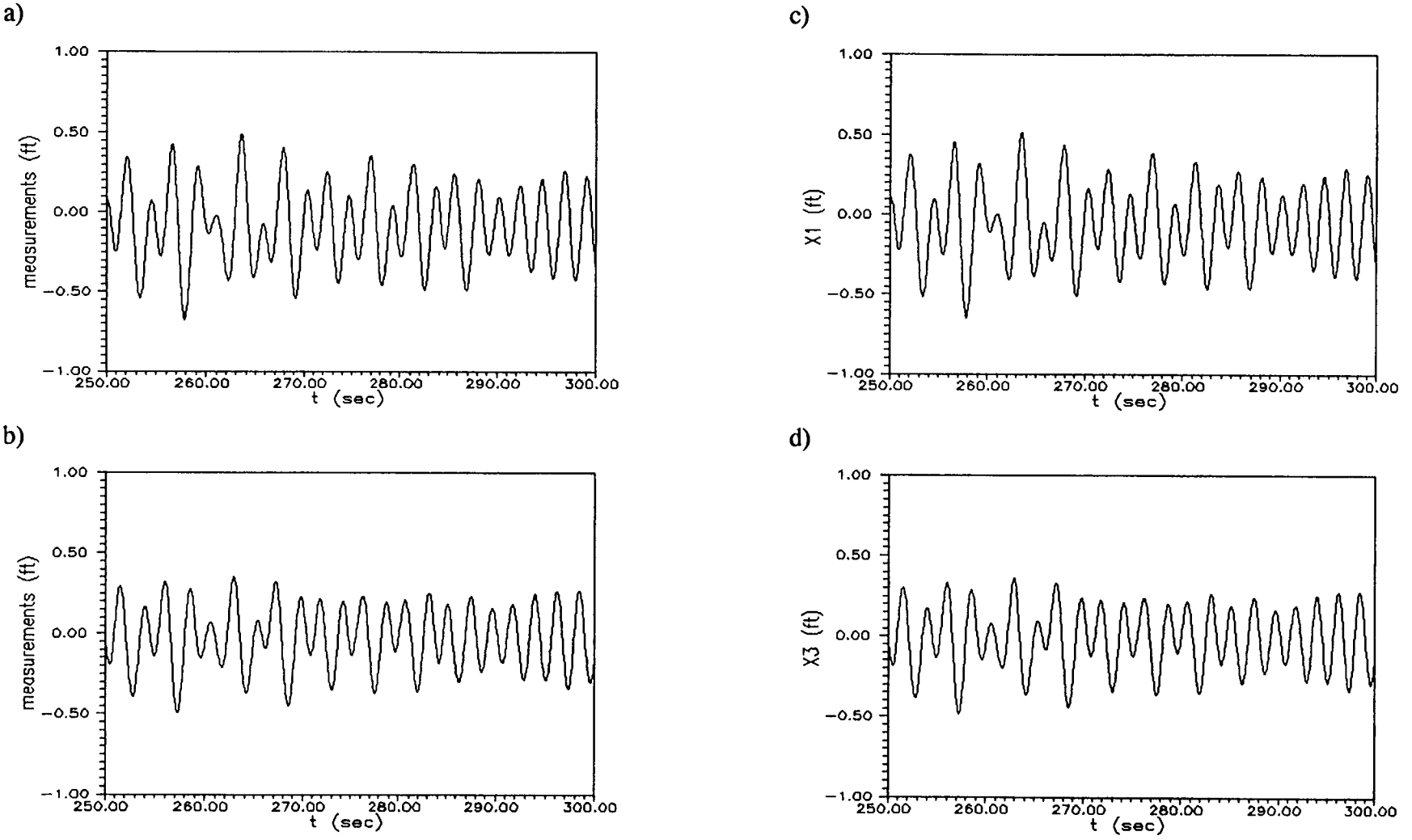

Figure 5.12 Displacements conversion (run E9): measurements from a) channel 11, b) channel 15; displacements of c) surge and d) heave motions

The transition observed may be explained by the analytical predictions developed in the previous Chapters. As demonstrated (see Fig.4.4), when the noise intensity is relatively low, the domains of attraction of coexisting response attractors are not well bridged. Response trajectories stay in the stronger attractor with low probability of returning to the other attractor. Considering the presence of inevitable (low intensity) noise in the wave flume as random perturbations to the monochromatic waves, the structural response is then induced from the weaker (harmonic) attractor to the stronger (sub-harmonic) attractor (Figs.5.13a-c).

Thus the transition observed confirms the analytic predictions of co-existing attractors, and reaffirms the need to include noise effects for the analysis of designated "deterministic" systems.

5.5.2 Monochromatic Waves with Random Noise

Noise effects on highly nonlinear phenomena, e.g., coexisting responses, can be demonstrated by fixing the monochromatic wave parameters and varying the additive noise intensity. Figures 5.14 and 5.15 show sample time histories of randomly perturbed monochromatic waves and their corresponding structural response, respectively. Because of the presence of randomness in the wave excitation, both harmonic and sub-harmonic characteristics are present in the structural response.

The combined response characteristics observed can also be explained by the analytical predictions. When the additive noise intensity is moderate, κ=0.003 for example, the attraction domains of the coexisting response are well-bridged. The steady-state PDF indicates an oscillatory shift between coexisting response attractors in an

ensemble sense (Fig.4.4b). Therefore, due to the presence of additive noise, the experimental response drift back and forth between the coexisting harmonic and sub-harmonic attractors, and the combined characteristics are observed (Figs.5.14 and 15).

According to the analytical predictions confirmed by experimental observations, the presence of random noise may facilitate a global description of the system behavior in the phase space. The possibility of finding chaos experimentally may increase with the presence of a moderate-intensity noise. As indicated in the analytical prediction, the strength of the chaotic attractor of the system response is weak. Thus, in the presence of noise with a very low intensity, co-existing chaotic and other periodic attractors may result in the concentration of the PDF in the region the stronger attractors (periodic responses). A co-existing weak chaotic attractor will be difficult to observe because of its a low probability (or frequency) of occurrence under noisy excitations.

For a given noise intensity, as demonstrated in Figs.4.7b and d, a chaotic response may be the only attractor in the phase space. However, if the noise intensity fluctuates (a likely scenario over the duration of a "steady-state" model test), noise-induced transitions between different attractors in the neighborhood may lead the system response from the (weak) chaotic state to the neighboring stronger periodic states (Figs.4.6a-d). Under the noise-induced bridging effects of the different response states (corresponding to slightly different parameter values) and co-existing attractors (of a constant parameter set), the nonlinear response may drift in and out of several attractors. Hence, a chaotic response may be embedded in a time history which appears to possess combined (periodic and random-like) response characteristics. More advanced data

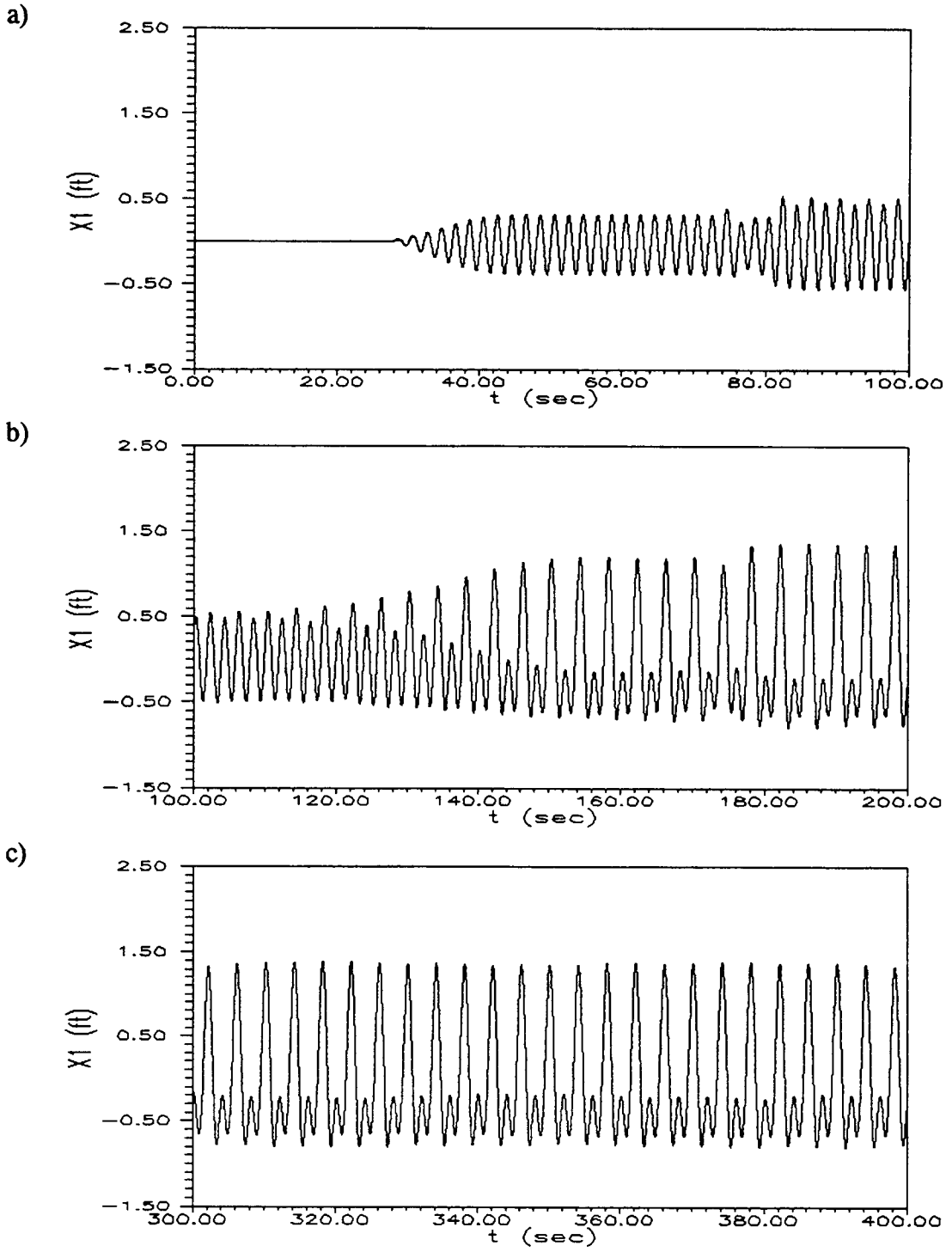

Figure 5.13 Transition of system response from harmonic to sub-harmonic (subjected to designed deterministic monochromatic excitation, channel 11 of run D2)

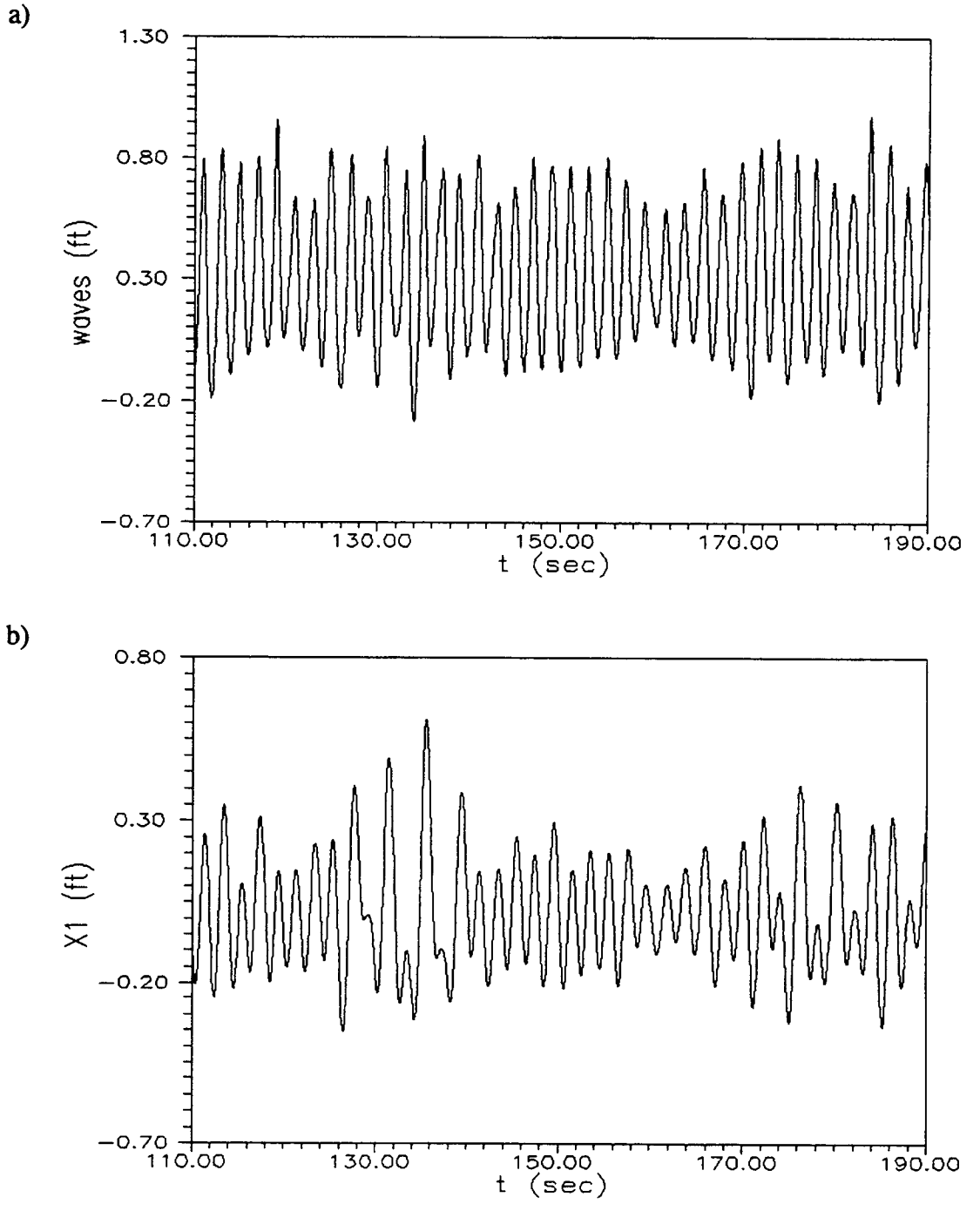

Figure 5.14 Oscillations between harmonic and sub-harmonic responses (run D7): a) wave profile (channel 3); b) structural response (channel 11)

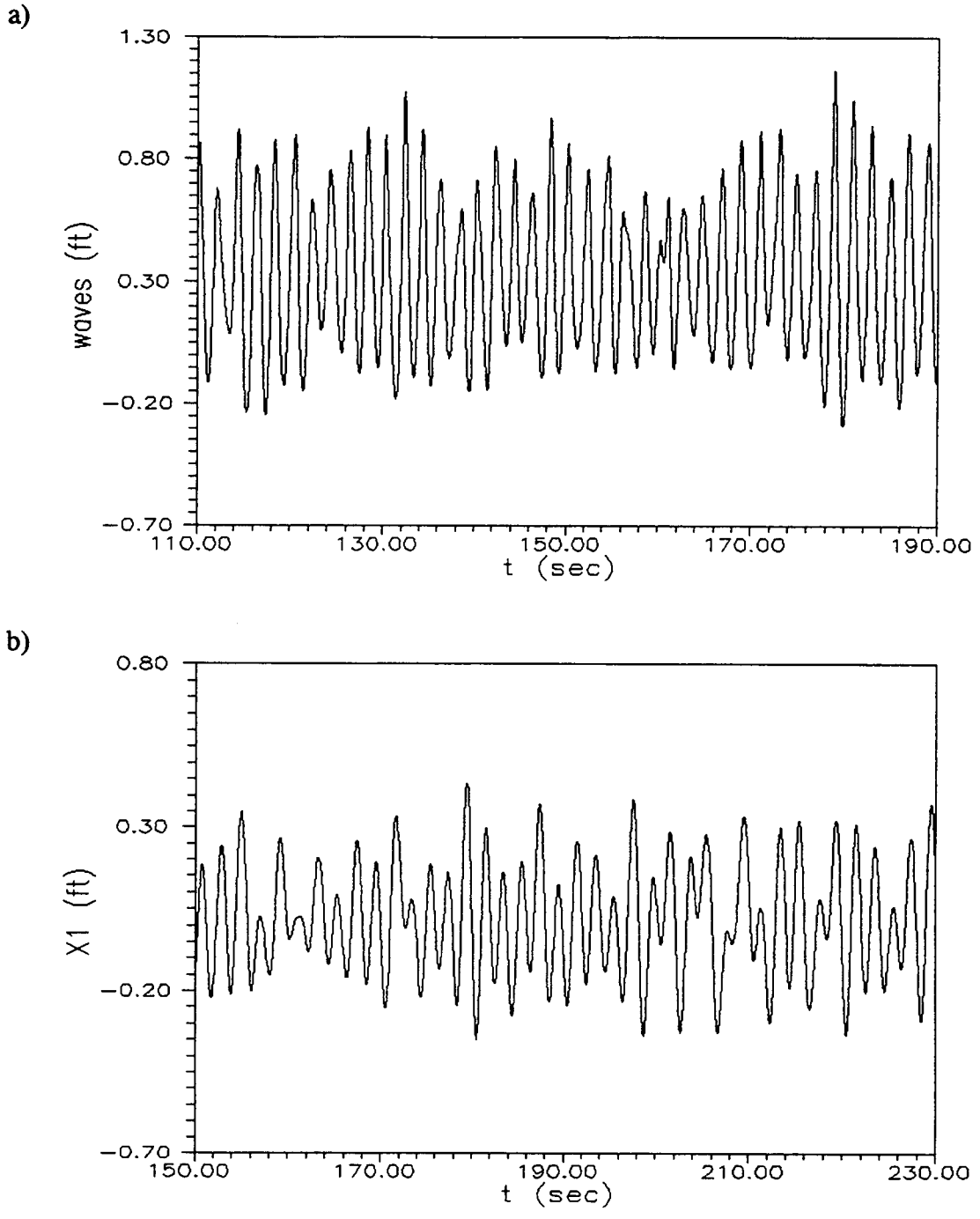

Figure 5.15 Oscillations between harmonic and sub-harmonic responses (run D8): a) wave profile (channel 3); b) structural response (channel 11)

analysis techniques are necessary to identify the existence of the embedded chaotic attractor within a complex measured time history. Selection of the length and the segment of experimental time history for analysis could be essential for the identification of chaotic response.

5.5.3 Narrow-Band Random Waves

The behavior of the structural response under TMA random wave excitations was also experimentally examined. A sample test of the TMA random waves and its corresponding structural response are demonstrated via time histories (Figs.5.16a and d), MPDF's (Figs.5.16b and e) and spectral densities (Figs.5.16c and f). The response MPDF in Fig.5.16e does not appear bi-modal (Davies and Liu, 1990). However, the associated two-peak spectral density shows a signature of the existence of sub-harmonics, or the coexistence of harmonics and sub-harmonics.

Experimental chaotic moored structural response have not been identified in the designed deterministic search runs. Several areas of improvement of the analytical model may be needed in order to better predict the experimental test results:

(1) The experimental system may be much more complex than the associated analysis model. In this case, an improved analytical moored structural model is needed to accurately predict the experiment behavior to identify the chaotic domain.

(2) The sphere may be large compared to the water depth such that the wave field has been altered by its presence and small body theory may no longer adequate.

(3) The elastic force might be more linear than expected due to the high pre-tension chosen.

(4) The (linear) wave theory used to derive the wave loading may not be sufficiently accurate and a more sophisticated wave theory may needed.

(5) Additional energy dissipation due to the friction between the rod and sphere for the SDOF model, and the instrument-induced friction in both SDOF and MDOF models may have eliminated some of the chaotic attractors because, as discussed, a weak chaotic attractor can not survive heavy damping.

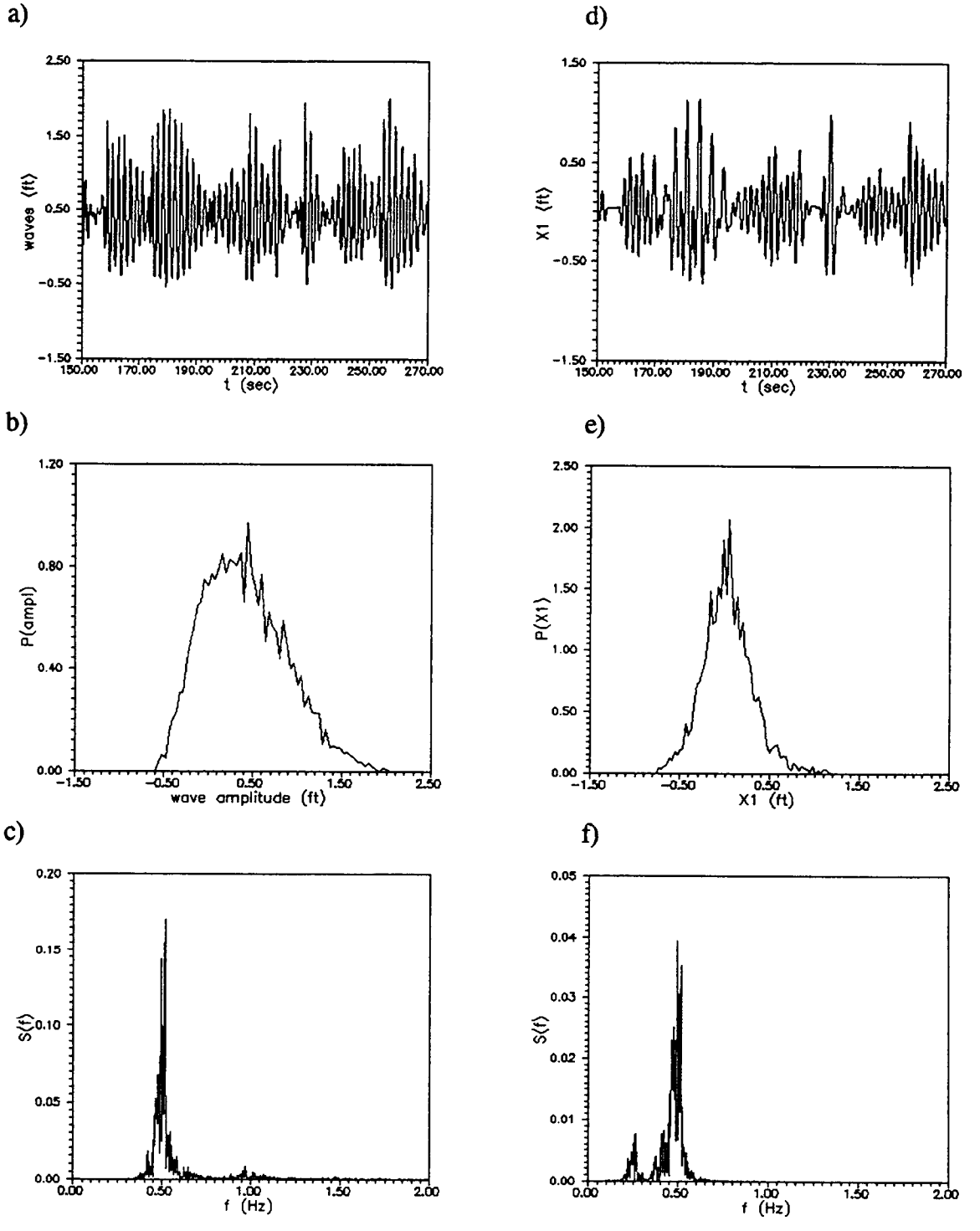

Figure 5.16 Narrow-band random wave profile (channel 3): a) time history, b) PDF and c) spectral density; and corresponding response (channel 11): a) time history, b) PDF and c) spectral density (run D18)

6. SUMMARY, CONCLUDING REMARKS AND FUTURE RESEARCH

6.1 Summary

The multi-point moored structural system considered is formulated as a two-degree-of-freedom (2DOF, surge and heave) submerged rigid body, hydrodynamically damped and excited nonlinear oscillator. The elastic mooring cables are taut and the resulting restoring force is geometrically nonlinear. The excitation force is computed by taking into account both nonlinear drag and inertia effects on a submerged axis-symmetric small body.

Inevitable random perturbations in the wave excitation are approximated as an additive Gaussian white noise. Very narrow-band random wave excitations are approximated as a sinusoidal function with additive noise. An arbitrary random waves (JONSWAP) is approximated as a filtered Gaussian white noise.

Homoclinic connections are found near the primary resonance in the averaged system associated to the moored structural system. The random noise is projected onto the averaged system and its influence over the generalized stochastic Melnikov criterion is examined. Via a mean square representation, the noise effects on the boundary of possible chaotic domain is qualitatively demonstrated.

With a white noise approximation to the randomness of various wave excitations, stochastic analysis of system response is conducted using a Markov process approach. The corresponding Fokker-Planck equation is derived based on the Markov assumption and is semi-analytically solved using a path integral solution procedure. Incorporating a higher order scheme (Runge-Kutta fourth order in this study) in the numerical

evaluation of the path integral solution procedure, weak chaotic response attractor can be depicted by the steady-state probability density function. The evolution of probability density function is demonstrated by repeated sampling of the probability density function. Time domain simulation (with Runge-Kutta fourth order integration scheme and Shinozuka's noise) is also employed to confirm the analytical predictions. For the system response subjected to JONSWAP random waves, the probability of large excursions in the response is estimated using the stationary probability density function as an invariant measure.

Experimental data of the behavior of a submerged spherical body (SDOF and 2DOF) is employed to confirm the analytical investigations. The excitations considered in the experiment include both monochromatic and random waves. Deviations between the designed and measured excitations are classified as random perturbations.

6.2 Concluding Remarks

Noise-induced transitions among nonlinear response attractors and states are demonstrated analytically and confirmed experimentally, and the results are summarized as follows:

(1) Taking into account the presence of random noise, the generalized Melnikov criterion is derived to identify possible chaotic domains. Results indicate that the presence of low intensity noise perturbations expedites possible occurrence of chaotic response.

(2) The Markov process approach is employed and a semi-analytical procedure is developed to solve for the transient and steady-state probability density functions

of the system response. Co-existing response attractors can be depicted by the associated steady-state joint probability density function, which also provides a global information of system behavior.

(3) Noise intensity is a controlling parameter of transition between co-existing response attractors. When the noise intensity is low, the response trajectories stay in the stronger attractor with low probability of exiting to the other attractor. The system response exhibits mainly the characteristics of the stronger attractor. When the noise intensity is moderate, the domains of co-existing attractors are bridged and the system response exhibits combined characteristics of coexisting attractors. When the noise intensity is strong, the domain of the co-existing attractors are further bridged and smoothed, and the system response appears random.

(4) Narrow-band random wave excitations can be approximated by a sinusoidal function with background white noise, and good agreement is observed via the response on the Poincaré maps.

(5) The JONSWAP random wave excitations are approximated by linearly filtered white noise, and good agreement is shown via steady probability density functions. Using a time-averaged probability density function as an invariant measure, probability of large excursion in nonlinear response is estimated and found to be elevated with increasing spectral bandwidth.

(6) Experimental observations confirm that noise effects should be taken into account for the analysis and design of deterministic systems. With a low intensity noise

present, transition of the response from the weaker attractor to the co-existing stronger attractor is experimentally observed. With moderate noise intensity, oscillations of the response between coexisting response attractors are also demonstrated. Both experimental observations confirm the analytical predictions.

6.3 Future Research

This study represents a first step in the stochastic analysis of nonlinear moored structural systems. The analytical predictions are confirmed by the associated experimental observations in general. However, this study provides only preliminary results. Improved models and analyses beyond the present work will be conducted in the immediate future.

6.3.1 Analysis Procedure

Because of the complexity of the nonlinear stochastic moored structural response behavior, the probability domain analysis in this study is focused on the SDOF model. An extended and systematic technique shall be developed to analyze nonlinear stochastic behavior of MDOF moored structural systems. Possible expansions of the semi-analytical path integral solution procedure applied to MDOF model needs to be examined. On the other hand, a non-grid, selective sampling Monte-Carlo simulation method has been developed by Kloeden and Platen (1992), which enables computation of numerical solution of high dimensional systems. The solutions from the Monte-Carlo method and the expanded path integral solution procedure shall be compared. Advanced

methods to perform response characteristics (first passage time, extreme value distribution and fatigue life) estimations shall be included in future studies.

In this study, random perturbations in the system are approximated by additive white noise to the deterministic periodic excitation or as filtered narrow-band noise to apply the Markov process approach explicitly. The results provide a preliminary understanding of the random perturbation effects on nonlinear responses. Relationships between these two types of models shall be examined. In addition, more realistic noise models shall be considered and incorporated in the analysis, and its effects on nonlinear responses shall also be considered.

A linearly filtered white noise is employed in this study for a proper fit to the JONSWAP random wave excitation. Inaccurate prediction of response behavior may occur in low frequency range. A more advanced (nonlinear) filter shall be derived for a better fit and to approximate more general random wave spectra (including broad-band). The analytical results shall be quantitatively compared with the experimental data, including field data if available.

6.3.2 Experimental Data Analysis

System parameters of the experiment need to be identified for further comparison with the analytical predictions. The parameters can be identified using a nonlinear system identification method (Bendat, 1990), and the applicability of which shall be examined with experimental data.

So far, no steady-state chaotic response has been identified from the experimental data. However, as demonstrated in the analytical predictions, co-existing response

attractors are bridged due to the presence of random noise. Thus a combinations of various responses (periodic, chaotic or random) may be exhibited in a time history. Current time domain analysis techniques, e.g., phase plane, first return map and Lyapunov exponent, have not be successful to identify the existence of (transient) chaotic response. Advanced analysis techniques need to be employed or developed to identify the existence of transient chaotic response. Yamamoto and Hughson (1993) developed a technique which uses an ordinary FFT-based cross-spectral method to estimate the random phase shift between the original and re-normalized time series, and can extract fractal components from a given time series in the frequency domain. Eckhardt and Yao (1993) derived a formulation to estimate the local Lyapunov exponents of nonlinear time series by extending previously used short time Lyapunov exponents to a point-wise definition. Applicability of these time series analysis techniques to the experimental data shall be examined in the future.

BIBLIOGRAPHY

Anishchenko, V.S., Neiman, A.B., and Safanova, M.A. 1993. Stochastic Resonance in Chaotic Systems. *Journal of Statistical Physics* 70:183-196.

Arecchi, F.T., Badii, R., and Politi, A. 1985. Generalized Multistability and Noise-Induced Jumps in a Nonlinear Dynamical System. *Physical Review A* 32:403-408.

Bathe, K.J., and Wilson, E.L. 1979. *Numerical Methods in Finite Element Analysis.* New Jersey: Prentice Hall.

Bendat, J.S. 1990. *Nonlinear System Analysis & Identification from Random Data.* New York:Wiley Interscience.

Bernitsas, M.M., and Chung, J.S. 1990. Nonlinear Stability and Simulation of Two-Line ship: towing and mooring. Applied Ocean Research 11:153-166.

Bishop, S.R., and Virgin, L.N. 1988. The Onset of Chaotic Motions of a Moored Semi-Submersible. *Journal of Offshore Mechanics and Arctic Engineering* 110:205-209.

Bulsara, A.R., and Jacobs, E.W. 1990. Noise Effects in a Nonlinear Dynamic System: the rf Superconducting Quantum Interference Device. *Physical Review A* 42:4614-4621.

Bulsara, A.R., Schieve, W.C., and Jacobs, E.W. 1990. Homoclinic Chaos in Systems Perturbed by Weak Langevin Noise. *Physical Review A* 41:668-681.

Choi, H.S., and Lou, J.Y.K. 1991. Nonlinear Behavior of an Articular Loading Platform. *Applied Ocean Research* 13:63-74.

Crandall, S.H. 1962. Random Vibration of a Nonlinear System with a Set-Up Spring. *Journal of Applied Mechanics* ASME: 477-482.

Crandall, S.H. 1964. The Spectrum of Random Vibration of a Nonlinear Oscillator. *Trans. 11th Cong. Appl. Mech.*:239-243.

Crutchfield, J.P., Farmer, J.D., and Huberman, B.A. 1982. Fluctuations and Simple Chaotic Dynamics. *Physics Reports* 92:45-82.

Davies, H.G., and Liu, Q. 1990. The Response Envelope Probability Density Function of a Duffing Oscillator with Random Narrow-Band Excitation. *Journal of Sound and Vibration* 139:1-8.

Eckhardt, B., and Yao, D. 1993. Local Lyaponuv Exponents in Chaotic Systems. *Physica D* 65:100-108.

Falzarano, J., Shaw S.W., and Troesch, A.W. 1992. Application of global methods for analyzing dynamical systems to ship rolling motion and capsizing. *International Journal of Bifurcation and Chaos* 2:101-115.

Farmer, J.D., Ott, E., and Yorke, J.A. 1983. The Dimension of Chaotic Attractors. *Physica D* 7: 153-180.

Feder, J. 1989. *Fractals*. Plenum.

Frey, M., and Simiu, E. 1992. Equivalence between Motions with Noise-Induced Jumps and Chaos with Smale Horseshoes. *Proceeding of the Ninth Engineering Mechanics Conference ASCE:660-663.*

Fuller, A.T. 1970. Analysis of Nonlinear Stochastic Systems by Means of the Fokker-Planck Equation. *Nonlinear Stochastic Control Systems*. London:Taylor&Francis.

Gardiner, C.W. 1985. *Handbook of Stochastic Methods: for Physics, Chemistry and Natural Sciences*. Berlin Heidelberg:Springer-Verlag.

Gottlieb, O. 1991. *Nonlinear Oscillations, Bifurcation and Chaos in Ocean Mooring Systems*. Ph.D. Dissertation. Oregon State University.

Gottlieb, O., and Yim, S.C.S. 1992. Nonlinear Oscillations, Bifurcations and Chaos in a Multi-Point Mooring System with a Geometric Nonlinearity. *Applied Ocean Research* 14:241-257.

Gottlieb, O., and Yim, S.C.S. 1993. Drag-Induced Instability and Chaos in Mooring Systems. *Journal of Ocean Engineering* 29:569-599.

Graham, R. 1977. Path Integral Solution of General Diffusion Processes. *Zeitschrift für Physiks B* 26: 281-290.

Grassberger, P., and Procaccia, I. 1983. Measuring the strangeness of strange attractors. *Physica* 9:189-208.

Guckenheimer, J., and Holmes, P. 1983. *Nonlinear Oscillations, Dynamical Systems, and Bifurcations of Vector Fields*. New York:Springer-Verlag.

Haken, H. 1976. Generalized Onsager-Machlup Function and Classes of Path Integral Solutions of the Fokker-Planck Equation and the Master Equations. *Zeitschrift für Physiks B* 24:321-326.

Hayashi, C. 1964. *Nonlinear Oscillation in Physical Systems*. New York:McGraw-Hill.

Hogan, S.J. 1989. On the dynamics of rigid-block motion under harmonic forcing. *Proceedings of Royal Society London A* 425:441-476.

Hughes, S.A. 1984. *The TMA Sallow-Water Spectrum Description and Applications*, U.S. Army Engineering Waterways Experiment Station. Vicksburg.

Isaacson, M. 1979. Nonlinear Inertia Forces on Bodies. *Journal of Waterway, Port, Coastal and Ocean Division* ASCE 103:213-227.

Jordan, D.W., and Smith, P. 1987. *Nonlinear Ordinary Differential Equations*. 2nd ed. Oxford:Oxford University Press.

Jung, P., and Hänggi, P. 1990. Invariant Measure of a Driven Nonlinear Oscillator with External Noise. *Physical Review Letters* 65:3365-3368.

Just, W. 1989. Dynamics of the Stochastic Duffing Oscillator in Gaussian Approximation. *Physica D* 40:311-330.

Kapitaniak, T. 1988. *Chaos in Systems with Noise*. Singapore:World Scientific.

Kifer, Y. 1989. Attractors via Random Perturbations. *Communications in Mathematical Physics*:445-455.

Kloeden, P.E., and Platen, E. 1992. *Numerical Solution of Stochastic Differential Equations*. New York:Springer-Verlag.

Kunert, A., and Pfeiffer, F. 1991. Description of Chaotic Motion by an Invariant Distribution at the Example of the Driven Duffing Oscillator. *International Series of Numerical Mathematics* 97:225-230, Birkhäuser Verlag Basel.

Lasota, A., and Mackey, M.C. 1994. *Chaos, Fractals, and Noise*. 2nd Ed. New York: Springer-Verlag.

Lin, Y.K. 1967. *Probabilistic Theory of Structural Dynamics*, McGraw-Hill.

Lin, H., and Yim, S.C.S. 1994. Chaotic Roll Motion and Capsizing of Ships Under Periodic Excitation with Random Noise. *Journal of Applied Research* (in press).

Lyon, R.H. 1960. Equivalent Linearization of the Hard Spring Oscillator. *Journal of Acoustical Society of America* 32:1161-1162.

Mei, C.C., Liu, P., and Carter, T.G. 1972. *Mass Transport in Water Waves*. Report No. 146. MIT:Ralph Parson Laboratory.

Meirovitch, L. 1970. *Methods of Analytical Dynamics*. New York:McGraw Hill.

Melnikov, V.K. 1963. On the Stability of the Center for Time Periodic perturbations. *Trans. Moscow Math. Soc.* 12:1-56.

Meunier, C., and Verga, A.D. 1988. Noise and Bifurcations. *Journal of Statistical Physics* 50:345-375.

Moon, F. C. 1987. *Chaotic Vibrations: An Introduction for Applied Scientists and Engineers*. New York:John Wiley & Sons.

Naess, A., and Johnsen, J.M., Statistics of Nonlinear Dynamic Systems by Path Integrations. *Nonlinear Stochastic Mechanics*:401-409.

Nayfeh, A.H. 1973. *Perturbation Methods*. New York:Wiley.

Nayfeh, A.H., and Mook, D.T. 1979. *Nonlinear Oscillations*, New York:John Wiley & Sons.

Newland, D.E. 1984. *An Introduction to Random Vibrations and Spectral Analysis*. 2nd ed. Longman.

Nicolis, G., Nicolis, C., and Mckernan, D. 1993. Stochastic Resonance in Chaotic Dynamics. *Journal of Statistical Physics* 70:125-139.

Ochi, M. C. 1990. *Applied Probability & Stochastic Processes: in Engineering & Physical Sciences*. New York:John Wiley & Sons.

Papoulias, F.A. and Bernitsas, M.M. 1988. Autonomous Oscillations, Bifurcations and Chaotic Response of Moored Vessels. *Journal of Ship Research* 32:220-228.

Priestley, M.B. 1988. *Nonlinear and Nonstationary Time Series Analysis*. Academic Press.

Risken, H. 1984. *The Fokker-Planck Equation: Methods of Solution and Applications*. Berlin Heidelberg:Springer-Verlag.

Roberts, J.B., and Spanos, P.D. 1990. *Random Vibration and Statistical Linearization*. Chichester:Wiley.

Rubinstein, R.Y. 1981. *Simulation and the Monte Carlo Method*. New York:John Wiley & Sons.

Ruelle, D. 1989. *Chaotic Evolution and Strange Attractors: the Statistical Analysis of Time Series for Deterministic Nonlinear Systems*. Cambridge University Press.

Sanders, J.A., and Verhulst, F. 1985. *Averaging Methods in Nonlinear Dynamics*. New York: Springer-Verlag.

Sarpkaya, T., and Isaacson, M. 1983. *Mechanics of Wave Forces on Offshore Structures*. Van Nostrand Reinhold.

Sharma, S.D., Jiang, T., and Schellin, T.E. 1988. Dynamic Instability and Chaotic Motions of a Single-Point Moored Tanker. *Proceedings of 17th ONR Symposium on Naval Hydrodynamics*:543-563.

Shinozuka, M. 1977. Simulation of Multivariate and Multidimensional Random Processes. *Journal of the Acoustical Society of America* 49: 357-367.

Stratonovich, R.L. 1967. *Topics in the Theory of Random Noise*. I-II. Gordon & Breach.

Svensmark, H., and Samuelsen, M.R. 1987. Influence of Perturbations on Period-Doubling Bifurcation. *Physical Review A* 36:2413-2417.

Thompson, J.M.T. 1983. Complex Dynamics of Compliant Offshore Structures. *Proceedings of Royal Society London A* 387:407-427.

Thompson, J.M.T., Bokaian, A.R., and Ghaffari, R. 1984. Subharmonic and Chaotic Motions of Compliant Offshore Structures and Articulated Mooring Towers. ASME. *J. Energy Resource Tech.* 106:191-198.

Thompson, J.M.T., and Stewart, H.B. 1986. *Nonlinear Dynamics and Chaos*, Chichester:John Wiley & Sons.

Thompson, J.M.T., Rainey, R.C.T., and Soliman, M.S. 1990. Ship stability criteria based on chaotic transition from incursive fractals. *Phil. Trans. Roy. Soc. London* 332:149-167.

Virgin, L.N. 1987. The Nonlinear Rolling Response of a Vessel Including Chaotic Motions Leading to Capsize in Regular Seas. *Applied Ocean Research* 9:89-95.

Wehner, M.F., and Wolfer, W.G. 1983. Numerical Evaluation of Path-Integral Solutions to Fokker-Planck Equations. *Physical Review A* 27:2663-2670.

Wiesenfeld, K., and McNamara, B. 1985. Period-Doubling Systems as Small-Signal Amplifiers. *Physical Review Letters* 55:13-16.

Wiesenfeld, K., and McNamara, B. 1986. Small-Signal Amplification in Bifurcation Dynamical Systems. *Physical Review A* 33:629-642.

Wiggins, S. 1988. *Global Bifurcations and Chaos: Analytical Methods*. New York: Springer-Verlag.

Wiggins, S. 1990. *Introduction to Applied Nonlinear Dynamical Systems and Chaos*. New York:Springer-Verlag.

Wissel, C. 1979. Manifolds of Equivalent Path Integral Solutions of the Fokker-Planck Equation. *Zeitschrift für Physiks B* 35:185-191.

Witz, J.A., Ablett, C.B., and Harrison, J.H. 1989. Nonlinear Response of Semi-Submissibles with Nonlinear Restoring Moment Characteristics. *Applied Ocean Research* 11:153-166.

Wolf, A., Swift, J.B., Swinney, H.L., and Vastano, J.A. 1985. Determining Lyaponuv Exponents from a Time Series. *Physica D* 16: 285-317.

Wong, C.M., and Tso, W.K. 1989. Steady state rocking response of rigid blocks, Part II: Experiment. *Earthquake Engineering and Structural Dynamics* 18:107-120.

Yamamoto, Y., and Hughson R.L. 1993. Extracting Fractal Components from Time Series. *Physica D* 68:250-264.

Yang, C.Y., Cheng, A., and Roy, R.V. 1991. Chaotic and Stochastic Dynamics for a Nonlinear Structural System with Hysteresis and Degeneration. *International Journal of Probabilistic Eng. Mech.* 6:193-203.

Yim, S.C.S., and Lin, H. 1991a. Chaotic behavior and stability of free-standing offshore equipment. *Ocean Engineering* 18:225-250.

Yim, S.C.S., and Lin, H. 1991b. Nonlinear Impact and Chaotic Response of Slender Rocking Objects. *Journal of Engineering Mechanics* 117:2079-2100.

Yim, S.C.S., and Lin, H. 1992. Probabilistic Analysis of a Chaotic Dynamical System. *Applied Chaos*:219-241. New York:John Wiley & Sons.

Yim, S.C.S., Myrum, M.A., Gottlieb, O., Lin, H. and Shih, I-Ming. 1993. *Summary and Preliminary Analysis of Nonlinear Oscillations in a Submerged Mooring System Experiment*, Report No. OE-93-03, Office of Naval Research.